PhD degree in Molecular Medicine (curriculum in Molecular Oncology)

European School of Molecular Medicine (SEMM),

University of Milan and University of Naples "Federico II"

Settore disciplinare: Med/04

Fibroblast growth factor binding protein 1 (FGFBP1) contributes in the establishment and maintenance of the Blood Brain Barrier

Azzurra Cottarelli

IFOM, Milan

Matricola n.R09406

Supervisor: Prof.ssa Elisabetta Dejana

IFOM, Milan

Cosupervisor: Dr.ssa Maria Grazia Lampugnani

IFOM, Milan

Anno accademico 2013-2014

"Two roads diverged in a wood, and I—

I took the one less traveled by,

And that has made all the difference."

(Robert Frost - The road not taken)

TABLE OF CONTENTS

LIST OF ABBREVIATIONS

ABC: ATP-binding cassette

ADAM-TS: a disintegrin-like and metalloproteinase with thrombospondin motif

AJ: adherens junction

Alk: activin receptor-like kinase

AMT: adsorptive-mediated transcytosis

APC: adematous poliposis coli

Aqp4: aquaporin 4

β-TrCP: β-transducin repeat containing protein

BBB: blood brain barrier

BM: basament membrane

bMEC: brain murine endothelial cell

BMPR1A: bone morphogenetic protein receptor type 1

CAM: chorioallantoic membrane

Cer: cerberus

CK1: casein kinase 1

CNS: central nervous system

CSF: cerebrospinal fluid

CYP: cytochrome P450

DA: dorsal aorta

DAPI: 4',6-diamidino-2-phenylindole

Dkk: dickkopf

DLAV: dorsal longitudinal anastomotic vessel

Dll4: delta-like 4

dpc: days post coitum

dpn: days post natal

Dvl: dishevelled

EC: endothelial cell

ECGS: endothelial cell growth supplement

ECKO: endothelial cell-specific knock out

ECM: extracellular matrix

ESM-1: endothelial specific molecule 1

FCS: fetal calf serum

FGF: fibroblast growth factor

FGFBP1: fibroblast growth factor binding protein 1

FrzB: frizzled-related protein

Fw: forward

GFP: green fluorescent protein

GLUT1: glucose transporter 1

GOF: gain of function

GSK3β: glycogen synthase kinase 3 β

HBp17: heparin-binding protein 17 kDa

hpf: hours post fertilization

HSPG: heparan sulfate proteoglycan

HRP: horseradish peroxidase

Icam1: intercellular adhesion molecule 1

ICH: intracerebral hemorrhage

IF: immunofluorescence

IGFBP3: insulin growth factor binding protein 3

ISV: intersomitic vessel

LAM: leukocyte adhesion molecule

LEF: lymphocyte enhancer factor

LMP: low melting point

LRP: lipoprotein receptor-related protein

MMP: matrix metalloprotease

MO: morpholino

MS: multiple sclerosis

NC1: non-collagenous domain 1

NSDT-1: N-deacetylase/N-sulfotransferase 1

N-cadherin: neuronal cadherin

NVU: neurovascular unit

Plvap: plasmalemmal vesicle-associated protein

PDGF-B: platelet derived growth factor B

PDGFRβ: platelet derived growth factor receptor β

PFA: paraformaldehyde

qRT-PCR: quantitative reverse transcriptase polimerasi chain reaction

RMT: receptor-mediated transcytosis

RT: room temperature

Rv: reverse

SCC: squamous cell carcinoma

SLC: small solute carrier

Shh: sonic hedgehog

SNP: single nucleotide polymorphism

SVD: small vessel disease

TCF: T-cell factor

TEER: transendothelial electrical resistance

TGFβ: transforming growth factor β

TJ: tight junction

Vcam1: vascular cell adhesion molecule 1

VE-cadherin: vascular endothelial cadherin

VEGF: vascular endothelial growth factor

VEGFR: vascular endothelial growth factor receptor

vSMC: vascular smooth muscle cell

WB: western blot

WIF-1: Wnt inhibitory factor 1

WT: wild type

ZO: zonula occludens

ZONAB: ZO-1-associated nucleic acid-binding protein

FIGURE INDEX

INTRODUCTION

RESULTS

DISCUSSION

ABSTRACT

The Blood Brain Barrier (BBB) is a highly specialized vascular structure whose aim is to tightly regulate the permeability between the blood flow and the Central Nervous System (CNS). To this purpose, the ECs in the brain need to present some peculiar features: the presence of high-resistance tight junctions (TJs) to block paracellular permeability, the lack of fenestrations, and the expression of some specific transmembrane transporters to selectively allow the entrance of nutrients and the exit of toxic metabolites. The high level of specialization of the brain microvasculature is obtained as a result of the interaction of the endothelial compartment with the other components of the so-called NeuroVascular Unit (NVU), such as the Basement Membrane (BM), pericytes and astrocyte end-feet.

The canonical Wnt/β-catenin pathway, that is specifically activated in CNS vessels during development, regulates BBB initiation and maintenance. Moreover, inactivation of this pathway in vivo leads to angiogenic defects in the CNS and not in other vascular regions.

Affymetrix analysis previously performed in our group provided a list of genes whose transcription is selectively regulated upon Wnt3a stimulation in murine primary ECs isolated from brain (bMEC). One of the most upregulated transcripts is that of Fibroblast Growth Factor Binding Protein 1 (FGFBP1) gene.

FGFBP1 is a cargo protein that, after being secreted in the extracellular matrix (ECM), is able to non-covalently bind the FGF immobilized in the ECM and to

mobilize it, protecting it from degradation and presenting it to FGF tyrosine-kinase receptor on the cell membrane.

Given the capability of Wnt3a stimulation to selectively induce FGFBP1 expression in brain ECs, we hypothesized that this protein could be involved in the process of initiation and/or maturation of the BBB.

In this work, we demonstrate *in vivo* in the zebrafish model that FGFBP1 knock down by morpholino presents vascular abnormalities in the brain and in the trunk, together with cerebral hemorrhages and impaired permeability. Taking advantage of the endothelial-specific FGFBP1 knock out murine model, we further demonstrate that inhibition of endothelial FGFBP1 expression affects brain vascular development, causing vascular defects and increased BBB permeability and also influencing the number of pericytes and the composition of the BM. Finally, we show *in vitro* that FGFBP1 absence promotes a "tip-like" phenotype and an increase in the expression of Plvap in bMECs.

In conclusion, our work proposes a novel role for FGFBP1 in the maintenance of the properties of the BBB and in the regulation of the complex interactions of the endothelial compartment with the other components of the NVU.

1. INTRODUCTION

1.1 The Blood Brain Barrier (BBB)

The brain is the most complex organ of the human body, with a constant metabolic request of oxygen and nutrients corresponding to 20% of the whole metabolic reserves of the organism [1]. Moreover, the central nervous system (CNS) relies for its function on a complex series of chemical and electric signals to modulate cell-to-cell communication in a much broader and intricate network. Most of these signals require changes in the flux of ions across the neuronal membrane, generating a variation in the electric potential of the cell that in absence of stimuli is maintained stable by a basal ionic current. External factors, such as food intake and physical activity, can physiologically result in fluctuations of blood ionic composition, therefore affecting also the composition of the extracellular fluids bathing the neurons. To limit the extent of these fluctuations and to guarantee the required oxygen and nutrients supply, a strict homeostatic control is required [2]. In the CNS, this homeostatic regulation is provided by three different layers, acting as physical barriers to the passage of ions and other solutes from the blood to the cerebral parenchyma: a) the brain microvascular endothelium; b) the choroid plexus, the ependymal covering of the brain ventricles, responsible for the secretion of the cerebrospinal fluid (CSF); and c) the arachnoid epithelium, the middle layer of the meninges forming the outer lining of the CNS [3, 4] (Fig.1).

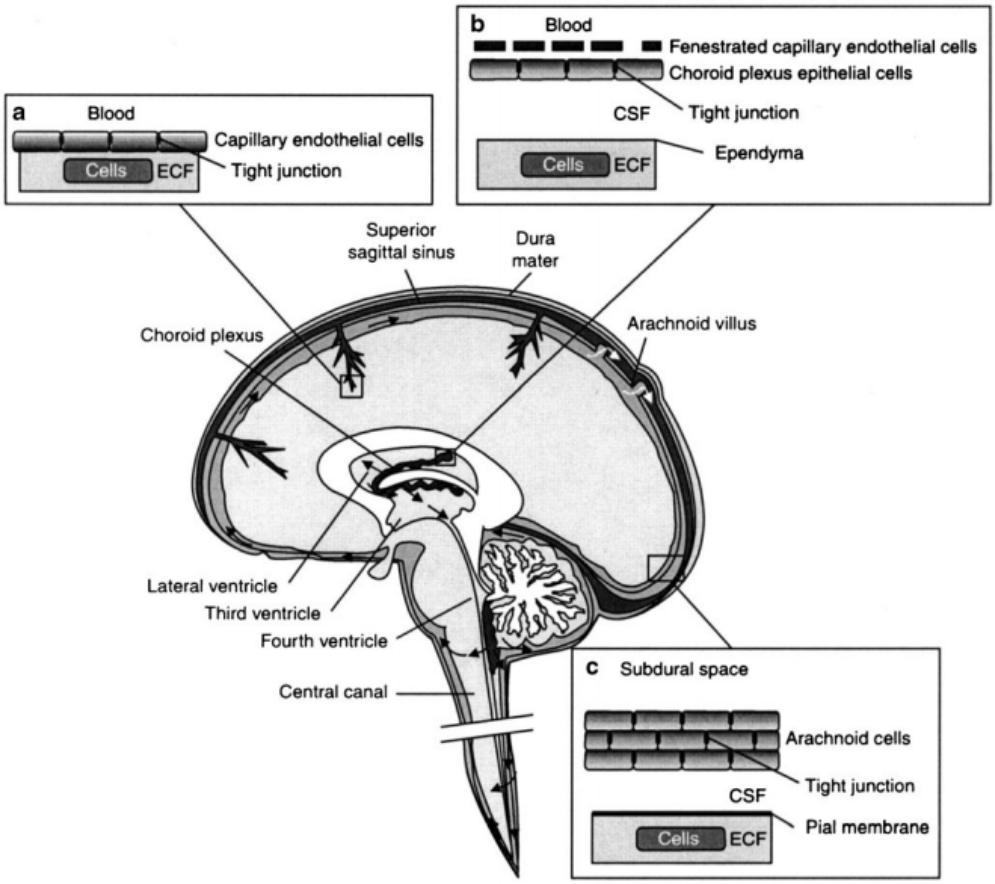

Figure 1. Barriers of the brain

Within the brain, three different barrier sites exist: a) the blood brain barrier (BBB), formed by the endothelial cells of the brain microvasculature; b) the blood-CSF barrier at the choroid plexus, formed by the epithelial cells of the plexus in the brain ventricle; and c) the arachnoid barrier, formed by the arachnoid cells in the subdural space. ECF: extracellular fluid; CSF: cerebrospinal fluid.

(Adapted from Abbott N.J., J Inherit Metab Dis 2013)

Of the three barriers, the endothelial layer (also referred to as blood brain barrier - BBB) is the major responsible for the homeostatic control of brain permeability and for the exchange of molecules between the blood flow and the CNS: indeed the BBB represents the broader interface between the vascular system and the nervous system, with an average surface of 12-20 m^2 in the human brain, and it ensures the

shortest diffusion distance between the blood and neurons (the average distance between a microvascular branch and a single neuron spans from 8 to 25 μm) [4].

Thanks to these features, the BBB stands in an optimal position to fulfill its main functions that are:

1) to regulate the traffic of solutes, allowing the entrance of nutrients from the blood and preventing the entrance of toxic molecules;

2) to maintain the ionic homeostasis necessary for a proper neuronal function;

3) to provide immune surveillance and to limit inflammation and cell damage [2].

To accomplish these tasks, the endothelial cells (ECs) in the brain need to present some important features: organization of high-resistance cell-to-cell tight junctions (TJs) to block the paracellular permeability, lack of fenestrations and very low rates of pinocytosis/transcytosis to limit the transcellular passage of molecules, expression of specialized transmembrane transporters to provide the brain parenchyma with nutrients and low expression of leukocyte adhesion molecules (LAMs) to avoid the passage of leukocytes from the blood flow to the brain tissue [5, 6].

1.1.1 Endothelial junctions

One of the most distinctive and extensively investigated features of the BBB is the presence of very strong and well-organized cell-to-cell endothelial junctions (Fig.2). Endothelial junctions are formed by two different types of structures, the tight junctions (TJs) and the adherens junctions (AJs), that are both composed by

transmembrane proteins tipically engaged in homophilic interactions and connected to the intracellular actin cytoskeleton [7].

The major components of the TJs are the claudins. More than 20 different claudins exist in mammals, but only few of them seem to be expressed by brain ECs [8]. Claudin 5 is the most abundant claudin in endothelial junctions; although claudin 5 is ubiquitously expressed along the vascular tree, it appears to play a specific role at the BBB: indeed, claudin 5 deficient mice die at birth due to BBB leakiness to small molecules [9]. Claudin 3 and claudin 12 have also been identified as specific components of the brain endothelial junctions, but their contribution to BBB physiology is still not clear [10, 11]. Together with the claudins, other transmembrane molecules, such as occludin and junctional adhesion molecules (JAMs), contribute to the formation of the TJ [12]. On the cytoplasmic side, these proteins are associated to other proteins, such as zonula occludens (ZO) proteins ZO-1 and ZO-2, cingulin and ZO-1-associated nucleic acid-binding protein (ZONAB), that link the TJs to the actin cytoskeleton, to the adherens junctions and to the polarity complexes [13].

Cell-to-cell adhesion at AJs is mediated by proteins belonging to the cadherin family: in particular, in the BBB (as in the rest of the vascular tree) the main cadherin present is the endothelial selective vascular endothelial cadherin (VE-cadherin), that form the AJs between endothelial cells, and the neuronal cadherin (N-cadherin), that mediates the EC-pericyte interaction [7, 14]. Intracellularly, these proteins bind to members of the catenin family, such as β-catenin, p120 and plakoglobin, that link them to actin-binding proteins, like α-catenin, finally

mediating the interaction between AJs and the cytoskeleton that is necessary to maintain the cell shape and polarity [7].

In the context of brain endothelium, the strict control of permeability is mainly operated by TJs, that can restrict the paracellular flux of small molecules and ions; however, AJs have an important role in TJ assembly, since it has been reported that VE-cadherin expression and clustering between neighboring cells is able to induce the upregulation of the TJ component claudin-5 [15].

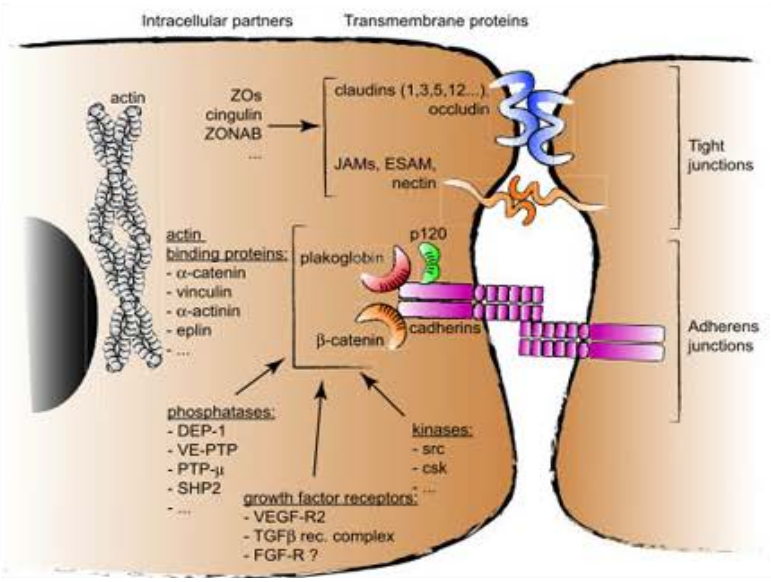

Figure 2. Tight Junctions and Adherens Junctions in Endothelial Cells

TJs are mainly formed by members of the claudin family (in the BBB endothelium, claudin-3, -5 and -12), associated to some intracellular partners like ZO proteins. AJs in the endothelium are formed by the transmembrane VE-cadherin, whose intracellular domain binds members of the catenin protein family, such as β-catenin, plakoglobin and p120, mediating the interaction with actin binding proteins such as α-catenin.

(Adapted from Dejana E. et al., Dev Cell 2009)

1.1.2 Molecular transport

At the level of the BBB endothelium, the passage of gaseous molecules, such as O_2 and CO_2, and of small lipophilic compounds occurs via passive diffusion through the lipidic layers of the cell membrane.

Transmembrane transporters belonging to the family of solute carrier (SLC) proteins are embedded in both apical and basal membranes of the ECs and are responsible for the influx of ions, glucose, aminoacids and other essential molecules, and for the efflux of waste products [16]. Among these carriers, of great relevance is the glucose transporter GLUT1, encoded by the *Slc2a1* gene, whose expression is induced by Wingless-Int (Wnt) signaling [17, 18] and whose deficiency leads to epilepsy [19].

In addition, members of another class of transmembrane proteins, the ATP-binding cassette (ABC) transporters, are mainly inserted in the apical membrane and act by regulating the efflux of toxic compounds potentially coming from the environment. This line of defense is completed by the presence of a series of metabolizing enzymes, mainly belonging to the cytochrome P450 family (CYPs), that are able to metabolize any toxic molecule that eventually escapes the efflux by the ABC transporters [20].

Larger molecules, such as peptides and proteins, gain access to the brain parenchyma mainly by vesicular mechanisms of transcytosis, both receptor-mediated (RMT) and adsorptive-mediated (AMT). The number of endocytic vesicles in the brain ECs is normally kept quite low by mechanisms that still need to be clarified; interestingly, the increase in transcytosis rates is the first change

occurring during brain hypoxia and one of the first hallmarks of endothelial damage during stroke, brain injury and other pathological conditions [4].

A diagram summarizing the possible routes of access across the BBB is reported in Figure 3.

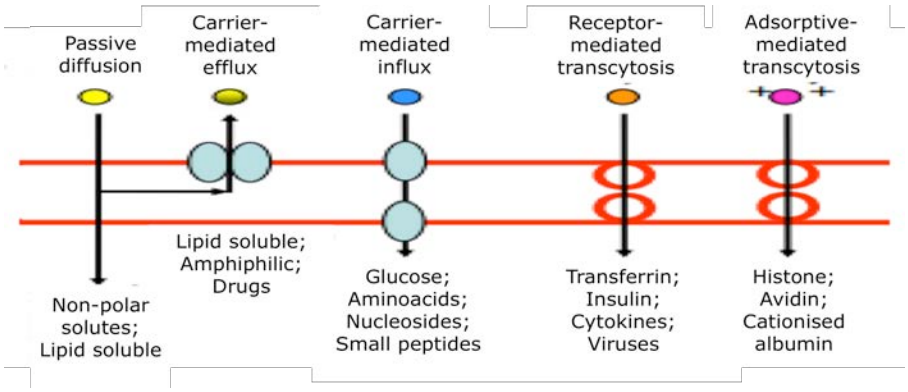

Figure 3. Routes for permeation and transport across the BBB

Non-polar solutes and small lipidic solutes may passively cross the endothelium and eventually be intercepted by active efflux carriers that will pump these solutes out of the EC. Small polar molecules, such as glucose and amino acids, can enter the CNS through specific influx carriers. Macromolecules like peptides and proteins are transported across the endothelium by receptor-mediated transcytosis (RMT), while the adsorptive-mediated transcytosis (AMT) is non-specifically induced by positively charged macromolecules.

(Adapted from Abbott N.J., J Inherit Metab Dis 2013)

1.1.3 Leukocyte adhesion

Leukocyte entry into tissues is a multistep process largely mediated by the expression on the endothelium of specific LAMs: molecules like E-selectin and P-selectin mediate the initial rolling adhesion of the leukocyte to the endothelium, while the subsequent firm adhesion step is mainly mediated by intercellular adhesion molecule 1 (Icam1) and vascular cell adhesion molecule 1 (Vcam1), allowing the final transmigration of the leukocyte [21]. While these molecules are

highly expressed in all peripheral vascular districts, their expression is very poor in the healthy CNS endothelium; however, during the inflammation processes that occur in the CNS when affected by diseases like stroke or multiple sclerosis (MS), the expression of these molecules can be upregulated [21, 22].

In addition to LAMs, also plasmalemmal vesicle-associated protein (Plvap), a protein already known to be involved in fenestrae formation and endocytic uptake, has been reported to be associated with leukocyte trafficking [23, 24]; as for LAMs, also Plvap expression is normally low in the brain ECs compared to peripheral ECs, while it is upregulated in the BBB in pathological conditions [25].

1.2 Cellular and extracellular components of the NeuroVascular Unit

Although most of the properties of the BBB are manifested within the endothelial compartment, the high level of specialization of the brain microvasculature is obtained as a result of the interaction of the ECs with other cell types (i.e. pericytes, astrocytes) and with the basement membrane (BM) [26]. Due to the strict interaction and interdependency of all these cellular and extracellular elements, they are often referred to as a whole anatomical and functional complex, named neurovascular unit (NVU) [27]. The different components of the NVU and their contribution to the BBB physiology are represented in Figure 4 and will be described in detail in the following sections.

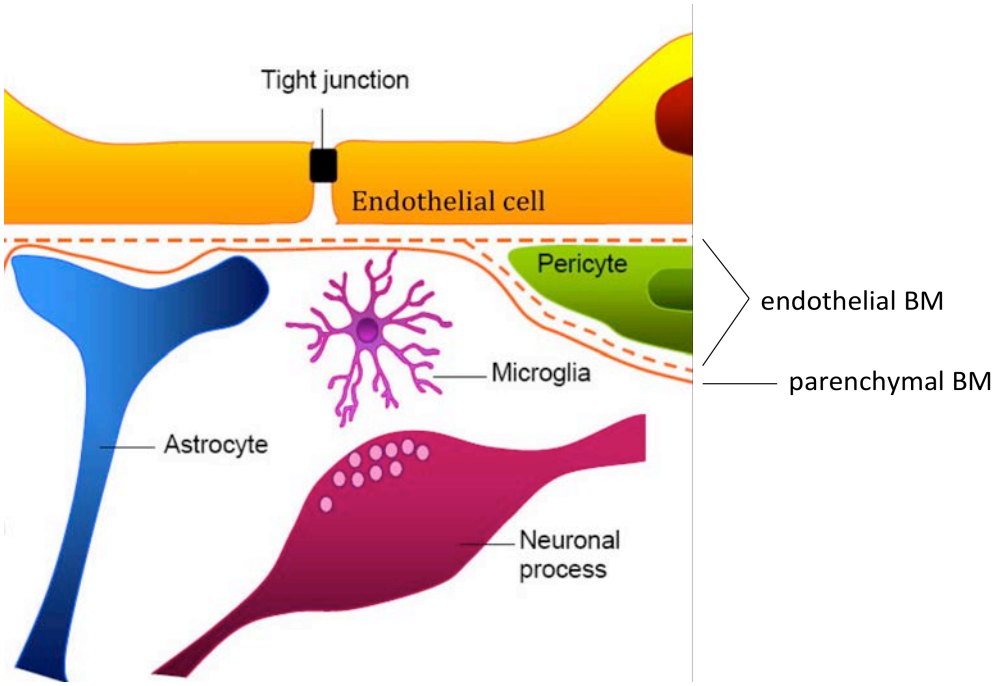

Figure 4. Organization of the neurovascular unit (NVU)

In the CNS, vessels forming the BBB interact with pericytes, astrocytes and the basal lamina to create an anatomically and functionally integrated platform named neurovascular unit (NVU).

(Adapted from Abbott NJ et al., Front. Pharmacol. Conference 2010)

1.2.1 Pericytes

The currently accepted definition of pericyte is "a cell embedded within the vascular BM" [28]. Pericytes are not to be confused with vascular smooth muscle cells (vSMCs): indeed, despite their similar perivascular location and the lack of univocal molecular markers to clearly distinguish the ones from the others, pericytes surround the endothelium around capillaries, while vSMCs surround mainly small arteries, arterioles and venules [29].

Pericytes have a quite rounded soma, generally located at the capillaries branching points, giving rise to primary processes extending in the length of the capillary; from the primary processes and perpendicularly to them, some secondary processes rise that partially encircle the vessel [29].

From an ultrastractural point of view, most of the endothelium-pericyte interface is separated by the BM, except at some points, where they can make contact in different ways: 1) through "peg-socket" contacts, where pericytes cytoplasmic protrusions, called "pegs", are inserted into endothelial invaginations, called "sockets" [30]; 2) through the "adhesion plaques", ultrastructurally similar to the AJ, where N-cadherin-based connections are formed [31]; 3) through gap-junction-like structures [32] (Fig.5).

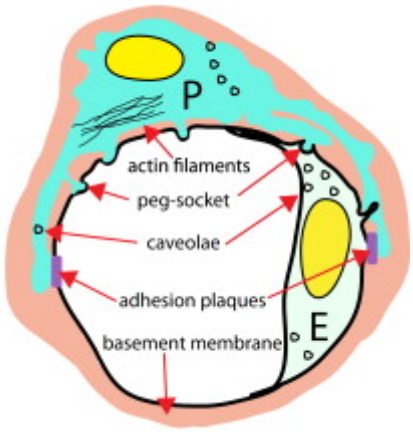

Figure 5. Pericyte ultrastructure

Pericytes (P) are ensheathed within the BM (pink), that they share with the endothelial cell (E). The BM is interrupted at some points, where the two cell types get directly in contact through the "peg-socket" contacts or through the adhesion plaques.

(Adapted from Armulik A. et al., Dev Cell 2011)

With a 1:1-3:1 ratio between ECs and pericytes, the CNS vasculature is the vascular district with the highest pericyte coverage [28, 33]. Pericytes enter the brain during angiogenesis at the same time as ECs, and the maturation of the two cell types is very strongly interdependent, since defects in the maturation of one cell type is able to cause defects in the other, and vice versa [34].

Pericyte development and their interaction with the ECs relies on several paracrine and juxtacrine signaling routes; only the main signaling pathways will be discussed below, but a more comprehensive description is schematically represented in Figure 6:

- Platelet Derived Growth Factor B (PDGF-B)/ Platelet Derived Growth Factor Receptor β (PDGFRβ):

  PDGF-B is released by ECs and binds to PDGFRβ on the pericyte surface. The knockout of *pdgfb* or *pdgfrb* genes are phenotipically identical and lead to perinatal lethality due to vascular abnormalities caused by mural cell deficiency [35, 36]. Different studies reported that PDGF-B is not uniformly expressed by the endothelium during angiogenesis: tip cells, the ECs guiding the sprouting by standing at the angiogenic leading front, express higher levels of PDGF-B compared to the stalk cells, the ECs that stand at the back of the tip cells. In this way, pericytes are immediately recruited to the angiogenic sprouts, lagging slightly behind the tip cell: as a consequence, pericyte recruitment to the nascent vessels is directly coupled to the angiogenic sprouting process [30].

  As soon as PDGF-B is secreted by the EC, it is bound to the extracellular matrix (ECM) thanks to its C-terminal retention motif with high affinity for heparan sulfate proteoglycans (HSPGs) and heparin [37-39]. Different studies demonstrated that the binding of PDGF-B to HSPGs is indispensable for a proper pericyte recruitment: indeed, mice with a targeted deletion of the retention motif ($pdgfb^{ret/ret}$) show hypoplasia and

partial detachment of pericytes [40], suggesting that PDGF-B needs to be presented as a matrix-bound factor to exert its function; moreover, a critical contribution is given by endothelium-derived HSPGs, since the global reduction of the enzyme N-sulfated heparin sulfate, due to the total knockout of N-deacetylase/N-sulfotransferase 1 (NSDT-1), causes a delay in pericyte recruitment and an impairment in their attachment to the vessel wall [38], while pericyte-specific deletion of heparin sulfates does not cause any similar defect [41].

- Angiopoietin-1 (Ang-1)/ Tyrosine kinase with immunoglobulin-like and EGF-like domains 2 (Tie-2):

  This pathway modulates endothelial maturation and stability and it goes in the opposite direction to PDGF-B/PDGFRβ pathway: indeed, Ang-1 is expressed by pericytes, while its receptor Tie-2 is mainly expressed by ECs [42-45]. Ang1 and Tie2 null mice die around midgestation because of cardiovascular defects and show lack of mural cells [46-48]; moreover, the overexpression of Tie-2 antagonist Ang-2 has been shown to cause pericyte loss [49].

  The published observations that *ang-1* conditional knockout does not affect pericyte recruitment [50] and that pericytes are normally recruited to Tie-2 negative endothelium in a mouse chimera of normal and Tie-2 null cells [51] suggest that Ang-1/Tie-2 signaling is required to stabilize the vasculature and to reduce vascular permeability, but not to recruit pericytes to the endothelium.

- Transforming Growth Factor β (TGFβ):

  TGFβ-mediated interaction between ECs and pericytes is bidirectional, since both cell types express both TGFβ ligand and its receptors [52].

  Both ECs and pericytes express two different type I TGFβ receptors, activin receptor-like kinase 1 (Alk-1) and Alk-5, that trigger different cellular effects. In mural cells, Alk-5 activation promotes mitotic and migratory quiescence by phosphorylation of Smad2/3, leading to pericyte differentiation; conversely, Alk-1 activation leads to Smad1/5 phosphorylation, promoting cell proliferation and migration and opposing pericyte differentiation [53-55]. On the other hand, in ECs a complex interplay between Alk-1 and Alk-5 exists, with Alk-1 inhibiting Alk-5 that, at the same time, is required for Alk-1 signaling [55, 56].

  Overall, Alk-5 and Alk-1 seem to have quite opposite actions, with the first promoting vascular stabilization and the latter opposing it. The net effect of TGFβ on ECs and pericytes may depend on the intensity and the duration of the signal and on the balance of Alk-1/5 expression levels; a plausible possibility is that Alk-1 signaling may be mainly active in the first phases of TGFβ stimulation, promoting cell proliferation and migration, while Alk-5 signaling may arise at later stages to induce cell differentiation and ECM production [29].

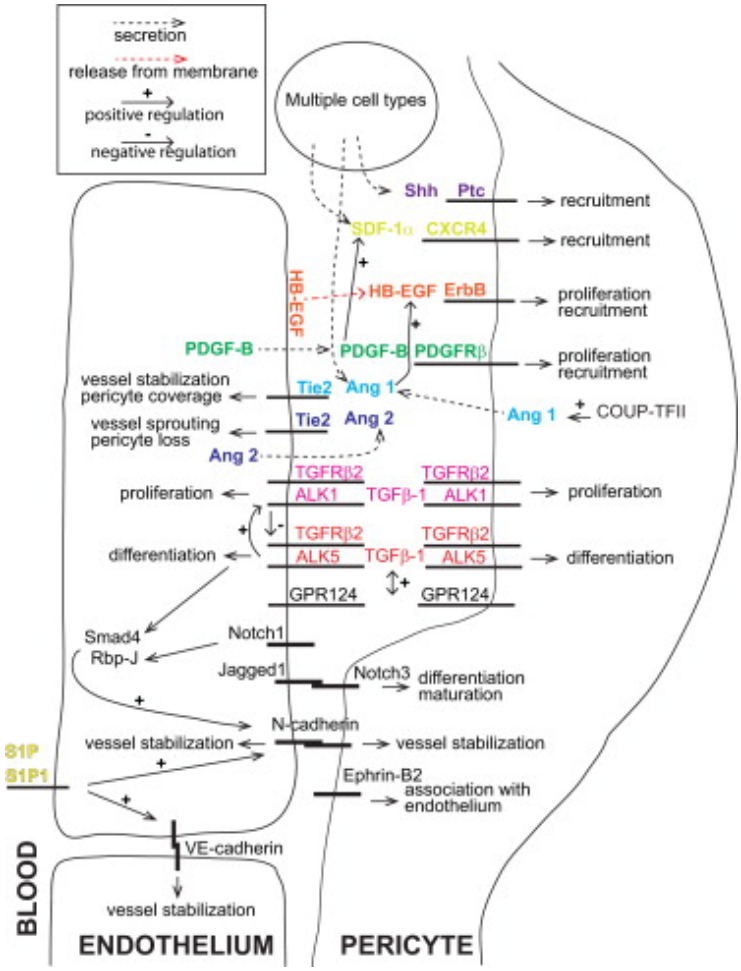

Figure 6. Molecular pathways regulating pericyte recruitment, differentiation and vascular stabilization

EC-pericytes interactions are mediated by several paracrine and juxtacrine signaling pathways, resulting in different effects on both cell types. Ligand-receptor pairs are indicated in the same color. In the case of N-cadherin and Notch-mediated interactions, the direct contact between the EC and the pericyte is required.

(Adapted from Armulik A. et al., Dev Cell 2011)

The role of pericytes in BBB development is under active investigation. Many in vitro studies suggest that pericyte may regulate the BBB at the level of endothelial junctions, by showing that the transendothelial electrical resistance (TEER) is increased in endothelial cell monolayers when cocultured with pericytes [57-60]. This theory was challenged by in vivo studies on pericyte-deficient murine models

[10, 61] that independently demonstrated that pericyte loss does not alter the endothelial molecular signature, but it increases the endothelial transcytosis rate, resulting in increased vessel permeability.

1.2.2 Astrocytes

Astrocytes are microglial CNS cells. They take part to the NVU by sending cellular processes that ensheath the abluminal side of BBB vessels: these processes, called astrocyte end-feet, are very rich of water channels, like aquaporin4 (Aqp4), and potassium channels, like Kir4.1, and they are anchored to the vascular BM via the distroglycan complex [62].

Astrocyte specification in the CNS takes place quite late during development, when neuronal differentiation and brain angiogenesis have already occurred (in mice this happens generally around birth) [63]; later on, during postnatal stages, the investment of BBB vessels with the astrocyte end-feet starts, and it is completed around two weeks after birth in mice [64].

Astrocytes are reported to be important regulators of the BBB properties; however, since they differentiate relatively late, most likely they do not act in the early induction phases of the BBB [65].

The current knowledge about the endothelium-astrocyte cross-talk and the astrocyte-derived signals regulating BBB physiology is relatively limited: the bone morphogenetic protein receptor type 1 (BMPR1A) expression and signaling in astrocytes has been reported to be necessary for the astrocyte end-feet to properly

invest the BBB vasculature [66]; in addition, also pericyte-derived signals have been shown to participate in the regulation of end-feet polarization [61].

In recent years, a role for astrocytes has been demonstrated also in regulating endothelial quiescence: Alvarez et al. showed that astrocyte-derived sonic hedgehog (Shh) is necessary for the maintenance of endothelial immune quiescence, an observation also sustained by the fact that Shh pathway is often found deregulated in MS patients [67].

Finally, some works suggested that astrocytes may regulate brain fluid transport at the NVU. While the lymphatic system provides clearance of interstitial fluids in the periphery, this does not happen in the brain since it completely lacks lymphatic vessels. Recently, a so-called "glymphatic" (derivative of glia and lymphatic) pathway was identified: this pathway takes advantage of the expression of Aqp4 on astrocytes, so that it can facilitate the drainage and the clearance of the interstitial fluids by exploiting astrocytic water channels [68].

1.2.3 Perivascular macrophages and microglia

Perivascular macrophages are blood-derived immune cells with phagocytic activity. They reside in the perivascular space surrounding arterioles and regulate the immune response and the leukocyte entry into the brain parenchyma [69, 70].

Microglial cells are actually misnamed small macrophages that reside in the brain and in the spinal cord. They are developmentally distinct from the perivascular macrophages, since they derive from the yolk sac, and they colonize the brain very early, before the CNS vascularization starts [71, 72]. Even though their function in

BBB development is still largely unknown, they are reported to have a role in maintaining vessel integrity and in facilitating damaged vessels repair [73].

1.2.4 Basement membrane

The abluminal side of vascular tubes in all different tissues is covered by the basal lamina, or basement membrane (BM), a layered cell-adherent ECM essential to maintain vessel integrity [74-76]. The BM protects the tissue from mechanical stress and provides an interface between the ECs and their environment, allowing the binding of secreted signal molecules, such as growth factors, and mediating their interaction with the vessels [74, 76]. The main BM components are fibronectin, type IV collagen, laminins, HSPGs (perlecan or agrin) and nidogens [77].

Laminins are large heterotrimeric glycoproteins formed by one α, one β and one γ chain; they have been shown to be able to self-assemble into large networks and to interact with cellular receptors, such as integrins, to transmit biological signals [78]. While laminins mainly account for the BM biological activity, collagen IV has been shown to be essential to confer structural stability to the vascular BM, although it is not required to initiate its assembly during development [79]; indeed, mutations in the human genes *Col4a1* and *Col4a2*, encoding for collagen IV α1 and α2 chains respectively, have been found to be associated with intracerebral hemorrhages (ICH) [80, 81].

In the CNS, vessels are surrounded by two different layers of BM, an inner endothelial BM (eBM) and an outer parenchymal BM (pBM), that differ for both

molecular composition and cellular origin: the first is deposited by ECs and pericytes and is characterized by the presence of α1 and α2 chains of collagen IV, α4 and α5 chains of laminin (combined with laminin β1 and γ1 to form laminin 411 and 511, respectively) and perlecan; the second is produced by astrocytes and is defined by the presence of α3 chain of collagen IV, α2 chain of laminin (combined with laminin β1 and γ1 to form laminin 211) and agrin. At the level of capillaries, the two different BM fuse to form a composite BM with characteristics intermediate between the endothelial BM and the parenchymal one [82].

ECs are known to be able to synthesize and secrete most of the matrix proteins involved in the BM formation; however, many published works demonstrated that pericytes can contribute to the eBM, also by secreting some BM components like laminin and collagen IV [83-85]. Beside the direct contribution of pericytes in the production of BM proteins, it has also been shown that an effective BM deposition is the result of the heterotypic interaction between ECs and pericytes: many groups contributed in showing, both *in vitro* and *in vivo,* that ECs-pericytes cross-talk increases the production of laminins α5 and β2, fibronectin, collagen IV α1 chain, nidogen-1 and perlecan [86-88].

Not only the different cell types forming the NVU contribute in the deposition of the BM, but also the BM composition can affect both the vessel angiogenic state and the differentiation of pericytes and astrocytes. In particular, recent works showed that the non-collagenous domain 1 (NC1) of collagen IV α1 chain is able to inhibit angiogenesis by binding matrix metalloprotease 2 (MMP-2) and preventing its activation, thus reducing ECs mobility [89], and that laminin α4 is able to

induce Delta-like 4 (Dll4)/Notch signaling, thus regulating the vascular density and tip-cell formation [90]. Finally, Yao and coworkers demonstrated that the loss of astrocytic laminins causes BBB breakdown by decreasing the expression of endothelial TJs proteins and of the astrocyte end-feet marker Aqp4 and by converting pericytes from a BBB-stabilizing resting state to a BBB-disrupting contractile state [91].

1.3 BBB development and specialization: the role of canonical Wnt/β-catenin pathway

Vascularization of the CNS starts between embryonic day 7.5 dpc and 8.5 dpc in mice, with the formation of a perineural vascular plexus by vasculogenesis. Later on, at around day 9.5 dpc, capillary sprouts invade the neuroepithelium by angiogenesis, branching from the pial surface to the periventricular zone [92, 93].

The acquisition of BBB features is a multi-step process, whose beginning coincides with the blood vessels ingression in the neural tube: it has been shown that, at day 12 dpc, brain ECs already express the TJ protein occludin and the glucose transporter GLUT1 [94, 95]. Nonetheless, at this stage the BBB still lacks an effective control of permeability, as shown by the fact that, at day 15 dpc, the fetal brain is permeable to horseradish peroxidase (HRP) [96, 97]. At late gestation and during early postnatal life, brain ECs start showing an increase in TJ organization and in efflux transporters expression, together with a decrease in the vesicular transport and in LAMs expression [94, 98]. All these developmental steps are mediated by molecular signals coming from the interaction with different cell

types: first, the neural progenitor cells induce the earliest "tight" properties, such as the appearance of immature TJs; then pericytes inhibit LAMs expression and suppress the transcytosis pathways; finally astrocytes definitively "seal" the barrier, inducing the expression of efflux transporters and cooperating with pericytes to stabilize the TJs [6, 65, 94] (Fig. 7).

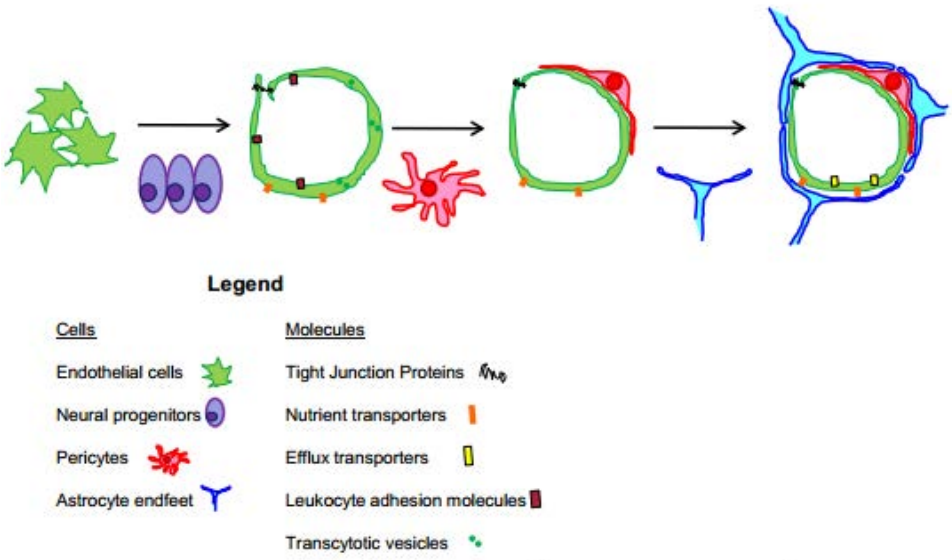

Figure 7 - Development of the BBB

The development of the BBB is a multistep process that requires the acquisition of specific proteins, including TJ molecules and specific nutrient transporters, whose expression is induced by neural progenitor cells. Pericytes recruitment allows strengthening of the endothelial barrier by regulating TJ structure, limiting transcytosis rate and inhibiting LAMs expression. Finally, astrocytes provide further regulation of the BBB functions.

(Adapted from Daneman R. et al., Nature 2010)

Many molecular pathways are involved in brain vascular development and in the BBB specification.

The vascular endothelial growth factor (VEGF) is the main growth factor to induce vasculogenic and angiogenic vascularization both in CNS and non-CNS tissues [99]. The abrogation of VEGF signaling pathway, by deleting either the ligand or

its receptor (VEGF receptor 2 – VEGFR2), cause early embryonic lethality due to compromised blood vessel formation [100, 101]. In embryo brain, VEGF is produced by cells in the subventricular ectoderm, so that sprouting vessels are directed along the VEGF gradient [102]; reductions of neural VEGF levels result in vascular malformations and abnormal vessel density in the retina and in the cerebral cortex [103].

While VEGF signaling supervises the initial vasculogenic and angiogenic phases of CNS and non-CNS vascular development, other molecular pathways have been shown to act specifically on brain vessel to establish the BBB.

The main pathway reported to be involved in CNS-specific vascularization is the canonical Wnt/β-catenin pathway.

Wnts are secreted glycoproteins produced by different cell types [104]; 19 different Wnt ligands exist in humans and mice, but the ones reported to activate the canonical β-catenin-mediated pathway are Wnt1, Wnt3a, Wnt7a/b and Wnt8 [11, 18, 105]. Reception and transduction of these signals relies on the binding of Wnt ligands to two different classes of cell-surface receptors: the seven-transmembrane G-protein-coupled receptors Frizzled, and the lipoprotein receptor-related proteins (LRPs), in particular LRP5/6 [106-110]. Some secreted molecules can interfere with Wnt signal activation, both by binding and antagonizing Wnt ligands, as in the case of Frizzled-related proteins (FrzB), Wnt-inhibitory factor 1 (WIF-1) and Cerberus (Cer), or by blocking Wnt access to LRP co-receptors and inducing LRP endocytosis, as in the case of Dickkopf (Dkk) proteins [111, 112]. In particular, Dkk-1 is one of the best characterized inhibitors of the canonical Wnt

pathway and is itself a Wnt/β-catenin target gene, thereby establishing a negative-feedback loop [113].

In the absence of Wnt, β-catenin is associated to a cytoplamic multimeric protein complex, called destruction complex, formed by Axin2, adenomatous poliposis coli (APC), casein kinase 1 (CK1) and glycogen synthase kinase 3β (GSK3β): CK1 phosphorylates β-catenin on Ser45, then GSK3β adds further phosphorylations on Ser33, Ser37 and Thr41[114]. These phosphorylations address β-catenin to ubiquitination by β-transducin repeat-containing protein (β-TrCP) and subsequent proteosomal degradation [105]. Deletions or point mutations of all the amino acid residues targeted by phophorylation result in β-catenin stabilization: for this reason, one of the genetic strategies used to create transgenic models with increased β-catenin stability is to conditionally delete the exon 3 of the gene, that encodes for all the phosphorylated residues [115].

In the presence of Wnt, a cascade of events starts that leads to inactivation of the destruction complex by the protein Dishevelled (Dvl) (with a mechanism still not well understood): β-catenin is therefore free to accumulate in the cytoplasm and is translocated to the nucleus, where it can serve as a transcriptional co-activator of the transcription factors T-cell factor(TCF)/lymphocyte enhancer factor (LEF), replacing the transcriptional co-repressor Groucho that was binding TCF/LEF before Wnt stimulation [113] (Fig. 8).

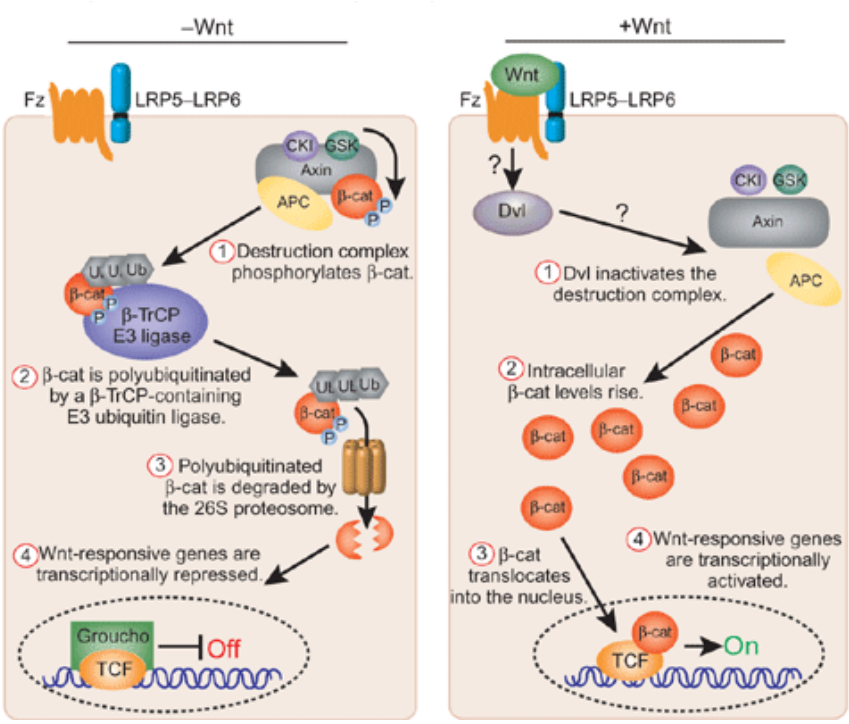

Figure 8. The canonical Wnt/β-catenin pathway

In the absence of Wnt ligands, β-catenin is sequestered in the cytoplasm by the destruction complex, phophorylated and addressed to proteosomal degradation. When Wnt is present, it binds to Frizzled receptor inducing the disassembly of the destruction complex, so that β-catenin is free to migrate to the nucleus and to act as a transcriptional co-activator of the transcription factors TCF/LEF.

(Adapted from Roberts D.M. et al., Nat Struct Mol Biol 2007)

In the last years, different groups independently (and almost simultaneously) demonstrated the influence of Wnt/β-catenin pathway on CNS vascularization and BBB development [11, 17, 18].

Brain angiogenesis is regulated by the canonical Wnt ligands Wnt7a and Wnt7b, that are produced by the neuroepithelial cells and act in a paracrine way on ECs in the CNS [17]. The genetic loss of function of canonical Wnt pathway, either by abrogating Wnt7a/b in the neuroepithelium or by inactivating β-catenin in the endothelium, lead to angiogenic defects and vascular hemorrhages [11, 17]:

however these defects are restricted to the CNS, confirming that Wnt/ β-catenin signaling is activated specifically in brain ECs and not in other vascular districts [18].

Beside inducing CNS angiogenesis, Wnt signaling (and in particular the canonical Wnt ligand Wnt3a) has also been demonstrated to upregulate the expression of BBB components, such as GLUT1 and Claudin-3, and to downregulate the expression of Plvap [11, 17, 18].

Finally, Liebner and coworkers showed that canonical Wnt signaling is active in ECs during brain angiogenesis, with a peak of activation during embryonic life (10.5 dpc – 15.5 dpc); then, starting from day 17.5 dpc, Wnt signaling decreases and finally it is maintained to very low level in the adult brain [11, 116].

All these observations underline that CNS vascularization and BBB development are two tightly coupled processes that occur simultaneously and under the control of the same signaling pathways. Whether canonical Wnt signaling can also intervene in the final steps of maturation of the NVU, for example by regulating the interaction of ECs with astrocytes and pericytes, is still to be determined [99].

1.4 Fibroblast Growth Factor Binding Protein 1 (FGFBP1)

The fibroblast growth factor (FGF) family consists of at least 23 structurally related members regulating a plethora of biological functions, including angiogenesis, embryonic development and cell migration, proliferation and differentiation [117]. In particular, FGF-1 (or acidic FGF – aFGF) and FGF-2 (or basic FGF – bFGF) are tightly bound to HSPGs in the ECM, which inhibits their biological activity [118].

Two different mechanisms have been proposed for FGFs release from the ECM: 1) an enzymatic cleavage of HSPGs by heparanase, or 2) the action of a carrier protein called FGF binding protein 1 (FGFBP1) [117].

FGFBP1 was first isolated in 1991 from the culture medium of human epidermoid carcinoma A431 cells and was initially designated as heparin-binding protein 17 kDa (HBp17) [119].

The primary structure of the protein consists of 234 amino acids. At the N-terminal there is a 33-residues signal sequence that addresses the protein to secretion, which is cleaved in the mature protein; an additional cleavage site prior to Met-168 confers the protein its apparent molecular weight of 17 kDa [119].

FGFBP1 is well conserved among different species, with the human protein showing 84, 57 and 49% amino acid identities with bovine, rat and mouse proteins, respectively [120, 121].

Mass spectrometry analysis of the protein isolated from bovine mammary gland secretion determined the presence of five disulfide bonds (Cys71-Cys88; Cys97-Cys130; Cys106-Cys142; Cys198-Cys234; Cys214-222) between all the ten Cys residues present in the bovine sequence; importantly, these residues are positionally conserved also in human and mouse proteins. The analysis of the bovine protein also revealed the presence of N- and O-glycosylation at Asn155 and Ser172, respectively, that may explain the discrepancies between the estimated and the observed molecular weight [121].

The domain of the human protein responsible for the interaction with heparin has been localized between residues Arg110 and Phe143 and is characterized by a high

content of basic amino acids [122]. Moreover, two additional heparin-binding consensus sequences have been localized: one is located at residues Lys163-Ser169, while the other, located at Lys25-His32, is positioned within the N-terminal signal sequence that is cleaved during the secretion process [123]. Finally, the FGF binding site has been described to be located at the C-terminal, between residues Lys193 and Cys234 [124] (Fig. 9).

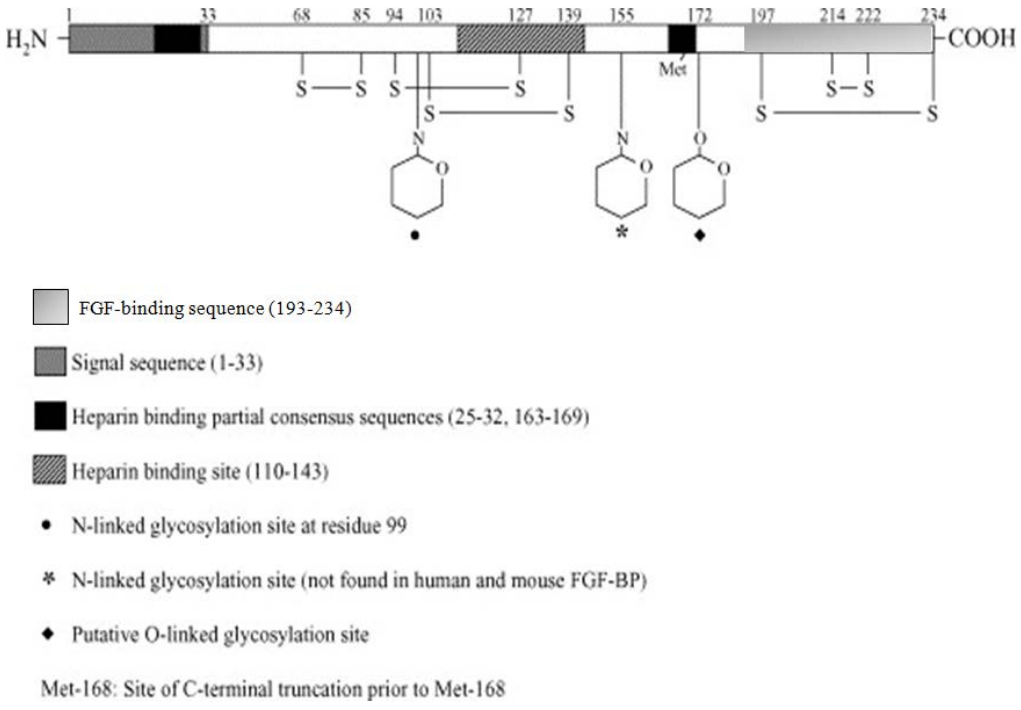

Figure 9. Structure of the human FGFBP1

The disulfide bonds are conserved among different species. The functional domains (N-terminal signal sequence, inner heparin-binding site and C-terminal binding site) and the glycosilation sites are reported in the figure.

(Adapted from Abuharbeid S. et al., Int J Biochem Cell Biol. 2006)

Immunohistochemical studies at different stages of mouse embryogenesis demonstrated that FGFBP1 is normally expressed in a broad spectrum of tissues during development and that its expression also correlates with the specific

developmental stage [125]; conversely, it was demonstrated that FGFBP1 is not expressed in most adult tissues [120, 126, 127].

Besides some studies on the physiological expression of FGFBP1, most of the research on the topic is focused on its role in tumor development: indeed, FGFBP1 was found to be highly expressed in cells and tissues from head and neck squamous cell carcinoma (SCC), invasive human breast cancer, some human colon cancer cell lines and tissues and prostate carcinoma cell lines [126-129]. Interestingly, FGFBP1 positive SCC showed the highest vascular density, suggesting that FGFBP1 could serve as an angiogenic switch in cancer [128].

The described mechanism of action of FGFBP1 involves FGFBP1 binding to FGF-2, that cause FGF-2 release from the ECM due to a reduction in its affinity to HSPGs [118] (Fig. 10). FGFBP1 interaction with FGF-2 is reported to be specific and dose-dependent, and it is inhibited by FGF-1, heparansulphate and heparinoids [130]. Many works demonstrated that this mechanism is able to positively modulate FGFs activity. The exogenous administration of FGFBP1 stimulates FGF-2-dependent growth of different tumor cell lines and promotes ECs growth and chemotaxis [118]. In addition, and further confirming the role of FGFBP1 in tumor angiogenesis, it has been shown that FGFBP1 addition can increase FGF-2-mediated blood vessel growth in a chicken chorioallantoic membrane (CAM) assay, and that early embryonic death due to hemorrhages and increased vascular leakage occur in a transgenic chicken model overexpressing FGFBP1[130, 131].

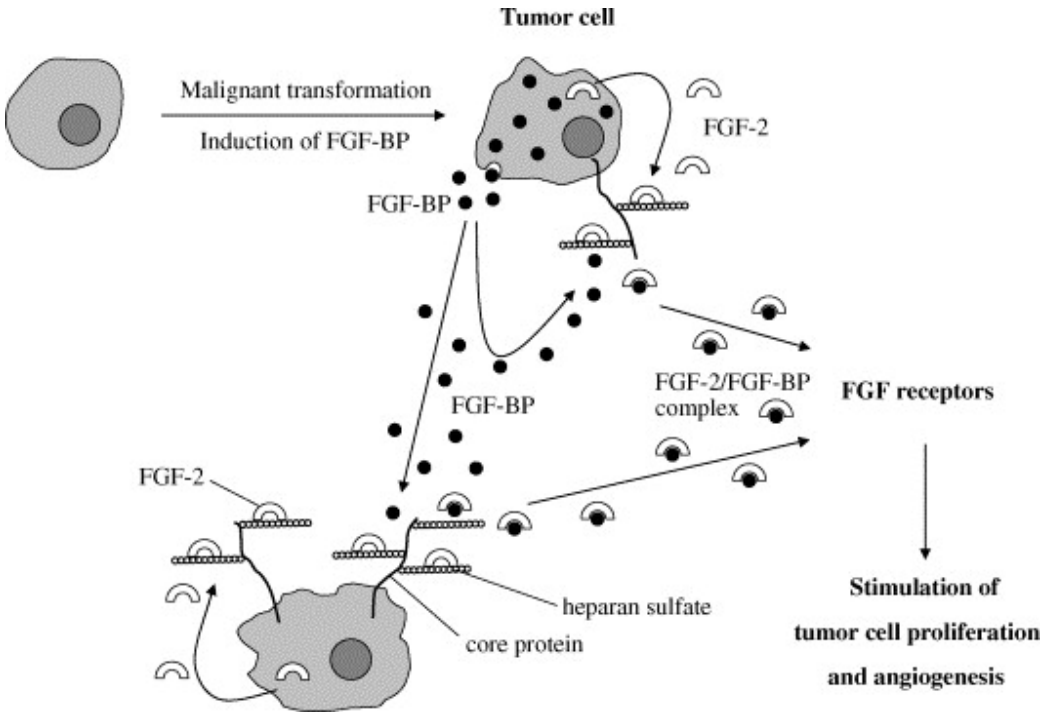

Figure 10. Mechanism of action of FGFBP1

Secreted FGFBP1 binds to immobilized FGF-2 and releases it from the HSPGs in the ECM. Solubilized FGF-2 is presented by FGFBP1 to its receptor and activates the downstream signaling.

(Adapted from Abuharbeid S. et al., Int J Biochem Cell Biol. 2006)

1.5 Aim of the work

The relevance of the canonical Wnt/β-catenin pathway in the determination of the BBB features in the CNS vasculature has been extensively investigated by our group and by others. In addition to this, our group also obtained data showing that FGFBP1, a protein known to be involved in physiological and pathological angiogenic processes and whose expression is strictly regulated during development, is upregulated by activation of Wnt/β-catenin signaling specifically in brain ECs.

Stemming from these observations, our works aims at elucidating a possible role for FGFBP1 in the development and/or in the maintenance of the BBB, in

particular trying to define both FGFBP1 effects on endothelium *per se* and its eventual relevance in regulating the cell-to-cell interactions occurring in the NVU.

2. MATERIALS AND METHODS

2.1 Sequence aligments and phylogenetic tree construction

FGFBP1 protein sequences in human, mouse and zebrafish were retrieved using BLAST, then aligned with ClustalW to determine the homology. The phylogenetic tree was constructed using ClustalW.

2.2 Animals

All animal procedures were approved by the Italian Ministry of Health and carried out in accordance with the guidelines established in the directive 2010/63/EU on the protection of animals used for scientific purposes.

The following zebrafish lines were used:

-AB, purchased from Zebrafish International Resource Center (ZIRC);

-Tg(fli1a:EGFP), kindly donated by Dr. B. Weinstein (National Institute of Child Health and Development, Bethesda, US)

-Tg(gata1a:dsRed), kindly provided by Dr. L. Zon (Harvard Medical School, Boston, US).

The following mouse strains were used:

- *FGFBP1*$^{flox/flox}$, generated by Taconic Artemis (Koeln, Germany) on a C57/Black6N background according to the knock-in procedures;

- *Cdh5(PAC)-CreERT2* (VEC-PAC) [132], kindly provided by Dr. R.H. Adams (University of Munster, Munster, Germany);

- *Rosa 26-Enhanced Yellow Fluorescent Protein* (R26-EYFP) [133], kindly donated by Dr. S. Casola (IFOM, Milan, Italy);

- β-cat$^{lox(ex3)/lox(ex3)}$ [134], generously provided by Dr. M. Taketo (Kyoto University, Kyoto, Japan).

- BAT-gal [135], kindly gifted by Dr. S. Piccolo (University of Padua, Padua, Italy).

For primary brain ECs (bMECs) preparation, C57Bl6 (Charles River) wild type animals were used.

2.3 Mouse genotyping

To determine the genotype of the mice, tail biopsies were collected and the genomic DNA was extracted by incubating the biopsies O/N at 56°C in a "tail buffer" made of 0.5 mg/ml Proteinase K (Sigma), 0.5% Triton X-100 in Gitschier Buffer 1X; then the Proteinase K was inactivated by keeping the sample at 95°C for 10 minutes. The genomic PCR was performed with specific primer pairs (reported in Table 1) to amplify the desired sequences and then loaded on a 1% agarose gel for amplicons detection.

PCR name		**Primers**	**Expected band**
LOXP1	Identifies the insertion of the 5′ LoxP sequence	*LOXP1 Fw:* TCCACCCTGTTTCAAGTTGG; *LOXP1 Rv:* GACCACCTGTTGGGAAAGG	*WT:* 210 bp *Tg:* 367 bp *Het:* 210 + 367 bp

PCR name		Primers	Expected band
LOXP2	Identifies the insertion of the 3′ LoxP sequence	*LOXP2 Fw:* GAACACAGGCTTAAGGATACACC *LOXP2 Rv:* AGAGTACAGATCTACCACTGCTTCC	*WT:* 209 bp *Tg:* 357 bp *Het:* 209 + 357 bp
FGFBP1	Identifies the presence of the recombined allele after tamoxifen injection	*LOXP1 Fw:* TCCACCCTGTTTCAAGTTGG; *FGFBP1:* AATGCTTACCAGGTCTCTGTCC *CTRL Fw:* GGATTCAGCACGTTGGACC *CTRL Rv:* CTTCATAGGTGGCTGTCTGG	*WT:* no ampl. *Tg:* 316 bp *CTRL:* 570 bp
VEC-CRE	Identifies the presence of Cdh5(PAC)-CreERT2 transgenic allele	*CRE A:* CCAAAATTTGCCTGCATTACCGGTCGATGC *CRE B:* ATCCAGGTTACGGATATAGT *CTRL Fw:* GGATTCAGCACGTTGGACC *CTRL Rv:* CTTCATAGGTGGCTGTCTGG	*WT:* no ampl. *Tg:* 1000 bp *CTRL:* 570 bp
R26-EYFP	Identifies the presence of Rosa26-EYFP transgenic allele	*R26-4982:* AAGACCGCGAAGAGTTTGTC *R26-316:* GGAGCGGGAGAAATGGATATG *R26-883:* AAAGTCGCTCTGAGTTGTTAT	*WT:* 600 bp *Tg:* 320 bp *Het:* 320 + 600 bp
Exon3/DEL	Identifies exon 3 deletion in β-cat$^{lox(ex3)/lox(ex3)}$ mice	*Exon3/DEL Fw:* GCTGCGTGGGACAATGGCTAC *Exon3/DEL Rv:* TGAGCCCTAGTCATTGCATAC	*WT: 690 bp Del: 490 bp*

Table 1. List of PCR reactions performed to determine mice genotypes

2.4 Preparation and culture of bMECs

Mouse brain microvascular fragments were processed as described previously [136, 137]. Capillary fragments were resuspended in culture medium composed of DMEM (GIBCO), 20% North American Fetal Calf Serum (FCS-NA) (HyClone), EC growth supplement (ECGS) (50 μg/ml; made in our lab from calf brain), heparin (100 μg/ml, from porcine intestinal mucosa; Sigma), glutamine (2 mM; Sigma), sodium pyruvate (1 mM; Sigma) and penicillin/streptomycin (100 units/l; Sigma), then seeded on wells coated with collagen I solution from rat tail (Sigma). ECs were selected for puromycin (4 μg/ml; Sigma) resistance for 2 days and grown in presence of either murine Wnt3a recombinant protein (100 ng/ml.; 315-20, Peprotech) or control vehicle (1%BSA in PBS). When required by the experiment, cells were treated with recombinant murine FGF-2 (100 ng/ml; 450-33, Peprotech). All cells were cultured at 37°C in a humidified atmosphere with 5% CO_2.

2.5 Morpholino microinjections

Morpholinos were injected at one cell-stage in the different strains and the phenotype was assayed between 48-72 hpf as described. The morpholinos were synthetized by GeneTools and dissolved in nuclease-free water; 5 nl of morpholino solution were injected in each egg. The sequences of the morpholinos used and the final concentrations are reported in Table 2. A p53 morpholino was coinjected in all the experiments to minimize the toxic effects. All morpholinos were injected at the highest concentration that did not cause embryo lethality.

Name	Sequence	Final concentration
MO-CTRL	CCTCTTACCTCAGTTACAATTTATA	0.15 mM
MO-Dkk1	AATTGTAGGATGTATTCCCTGGGTG	0.1 mM
MO-Fgfbp1a	CATGTCCTTCAGTCCTACAAATAGC	0.3 mM
MO-Fgfbp1b	CGCATCATGGCTGCATTGGAAATAC	0.2 mM
MO-p53	GCGCCATTGCTTTGCAAGAATTG	0.15 mM

Table 2. Nucleotidic sequences and final concentrations of the morpholinos used for in vivo knockdown experiments

2.6 Cell dissociation and sorting from zebrafish embryos

For cell dissociation and sorting experiments on zebrafish samples, 40 Tg(fli1a:eGFP) embryos at 72 hpf were used; in addition, the same number of AB (GFP negative) embryos was used as negative control. Embryos were put into 1.5 ml tubes (Eppendorf) and washed with PBS 1x twice (5 minutes each), then PBS was replaced with 1 ml of deyolking solution (NaCl 50 μM, KCl 2 μM, CaCl2 1 μM and NaHCO3 1 μM in distilled water) and pipetted with a 200 μl tip. Deyolked embryos were incubated at 28°C in 5 ml of protease solution (1 μM EDTA pH8, 0.25% Trypsin in PBS 1x) until embryos were completed dissociated, then 1 ml of stop solution (300 μl FBS plus 3 μl $CaCl_2$ 2M in PBS 1x) was added to block cell dissociation. The suspension was centrifuged at 3000 rpm for 3 minutes, the supernatant was discarded and the cell pellet was resuspended in suspension medium (1% FBS, $CaCl_2$ 0.08 μM in PBS 1x). Cells were sorted in two populations (GFP + and GFP -) with a Facsaria Cell Sorter (BD Biosciences) and immediately processed for mRNA extraction.

2.7 Semiquantitative RT-PCR

Total RNA from zebrafish embryos was extracted using Trizol (Qiagen) and then purified with RNeasy Kit (Qiagen) according to manufacturer's instruction. The desired amount of RNA (usually 1 μg) was retrotranscribed with random examers using the High Capacity cDNA Archive Kit (Applied Biosystems).

5 ng of cDNA were used as template for the RT-PCR reaction. The sequences of the primer pairs used to amplify the desired regions are reported in Table 3. The PCR conditions used for the amplification were: 94°C for 2 min, 35 cycles of 94°C for 40 sec, 57°C for 40 sec and 72°C for 1 min, then 72°C for 10 min. The samples were loaded on 1% agarose gel in TAE 1X for amplicons detection.

Fgfbp1a	*Forward*	GAAGGACATGTCTCTCCGCGGAA
	Reverse	GCTCAGCAGTCTCCACTCTGGATT
Fgfbp1b	*Forward*	ATGATGCGCGCGACAGGCATCGC
	Reverse	CATGAGCATTCATCATTCTCCAGC
β-actin	*Forward*	ACCTCATGAAGATCCTGACC
	Reverse	TAATCCACATCTGCTGCTGG

Table 3. Primers used for the amplification of the mRNAs of interest in semiquantitative RT-PCR experiments.

2.8 Whole-mount In Situ Hybridization

Whole-mount In Situ Hybridization (ISH) on zebrafish embryos at different stages was performed as previously described [138].

The full-coding sequence of Fgfbp1 cDNAs was cloned into *pCR2.1-TOPO* vector, using TOPO TA Cloning kit (Invitrogen); the sequence of the primers used are

reported in Table 4. cDNA-containing vectors were cut with *BamHI* and transcribed with T7 RNA Polimerase using a digoxigening-labebled NTPs mixture in order to obtain dig-labeled antisense RNA probes.

Fgfbp1a	*Forward*	CGGAATTCGCTATTTGTAGGACTGAAGGACATG
	Reverse	CGTCTAGAGCAGTCTCCACTCTGGATTACA
Fgfbp1b	*Forward*	CGGAATTCTATTTCCAATGCAGCCATGATGCGCGCG
	Reverse	CGTCTAGATTCATCATTCTCCAGCATCAAGAAGAG

Table 4. Primers used for Fgfbp1a and Fgfbp1b cloning into pCR2.1-TOPO vector

2.9 O-dianisidine staining

For histochemical staining of haemoglobin, embryos at 48 hpf were incubated with o-dianisidine stain solution (40% ethanol, 0.01 M sodium acetate, 0.65% H_2O_2, 0.6 mg/ml o-dianisidine Sigma) for 15 minutes and then washed in water.

2.10 In vivo permeability assays

72 hpf zebrafish embryos were anesthetized with 0.2% Tricaine (Sigma) and were positioned ventral side up in a 1% agarose injection mold. Using a microinjection device (Picospritzer III, Parker Instrumentation) fitted with a pulled glass capillary needle, 5nl of DAPI or rhodamine-labeled lysine-fixable 10kDa dextran (Invitrogen) were injected into the cardiac venous sinus. Embryos were returned to egg water to recover and then fixed in 4% paraformaldehyde (PFA) 40 minutes after the tracer injection.

For permeability assays in mice, the animals were injected intraperitoneally with a solution of Alexa555-Cadaverine (10 μg/g of body weight) (Invitrogen); 5 hours after the injection the animals were anesthetized with Avertin (250 μg/g of body weight) (Sigma), then perfused with PBS for 1 minutes and with 4% PFA for 5 minutes. After dissection, brain and eyes were fixed O/N in 4% PFA at 4°C, then washed twice in PBS.

2.11 Tamoxifen treatment

A stock solution of Tamoxifen (Sigma) was prepared by dissolving it in corn oil and 10% ethanol to reach a 10 mg/ml concentration. Tamoxifen working solutions were prepared immediately before the injection by diluting the mother solution 1:5 in corn oil. The solution was administered to newborns (0-1 dpn) by a single intragastric injection (35 μg/g of body weight). Control animals were injected with the same vehicle used to dissolve tamoxifen (corn oil plus 2% ethanol).

2.12 Immunofluorescence (IF) analysis of brains and retinas

For tissue IF analysis, brains and retinas were dissected from the mice and fixed in 4% PFA O/N at 4°C. Brains were embedded in 4% Low Melting Point (LMP) agarose in PBS and 100 μm sections were cut at the vibratome (1000 Plus, The Vibratome Company, St. Louis, MO, US). Both brain sections and retinas were incubated O/N at 4°C in a blocking solution (1% Fish Skin Gelatin, 0.5% Triton-X, 5% Normal Donkey Serum, 0.01% Thimerosal), then incubated O/N at 4°C with the primary antibodies diluted in an Ab buffer (1% Fish Skin Gelatin, 0.25%

Triton-X, 0.01% Thimerosal). The samples were washed three times with PBS + 0.25% Triton-X, then incubated for 4 hours at RT with the secondary antibodies diluted in Ab buffer, washed again with PBS + 0.25% Triton-X for three times and with PBS for two times. The samples were postfixed with 4% PFA at RT for 5 minutes, then washed in PBS for three times and finally mounted on glass slides with Vectashield with DAPI (Vector Labs). For ECM proteins staining, an initial step of unmasking was performed by preincubating floating sections in distilled water at 37°C for 5 minutes, incubating them in pepsin solution (1 mg/ml in 0.2% HCl) (Dako) at 37°C for 10 minutes and washing them with PBS once at 37°C (5 minutes) and three times at RT (10 minutes each).

Samples were observed at a confocal microscope (Leica) using 10x, 20x and 40x objectives. Acquired images were processed with ImageJ; only adjustments of brightness and contrast were applied in the preparation of the figures. For comparison purposes, different sample images of the same antigen were acquired under constant acquisition settings.

2.13 Transmission electron microscopy

Animals were anesthetized by intraperitoneal injection of Avertin 20mg/ml solution (about 0.5 mg/g of body weight). Mice were intracardiacally perfused with 1-2 ml of heparin 0.025% in PBS, followed by 20 minutes of perfusion with Fixative solution (2% PFA + 2.5% Glutaraldehyde in 0.2M Sodium Cacodylate) at a speed of 5 ml/min. Perfused animals were kept in a plastic bag for 90 minutes and then the brains were dissected and stored in Fixative solution until processing.

Brain samples were treated with 1% reduced osmium tetroxide, stained with 0.3% thiocarbohydrazide in 0.1 cacodylate buffer (pH 7.0), treated again with reduced osmium tetroxide for 30 minutes and then dehydrated using increasing ethanol concentrations. The samples were finally embedded in Epon resin and 60nm-thick sections were cut and observed at the electron microscope (Tecnai 20).

2.14 RNA interference

Three different Stealth RNAi Duplexes (Invitrogen) were used to knockdown FGFBP1 mRNA. The sequences of the siRNA used are reported in Table 5. Stealth RNAi siRNA Negative Control Med GC Duplex #3 (Invitrogen) was used as negative control in all the experiments. Transfection was performed using Lipofectamine 2000 (Invitrogen) following manufacturer's instruction.

	Name	**Sequence**
siFgfbp1#1	NM_008009_stealth_201	CCTCGTTAGGGAAGGCCCAGAATAA
siFgfbp1#2	NM_008009_stealth_235	CAGGACATCTAAATCTCTGACGCAT
siFgfbp1#3	NM_008009_stealth_406	CGACAAAGACCAGATCTACTGGAAA

Table 5. Nucleotidic sequences of the siRNAs used for in vitro FGFBP1 knockdown.

2.15 Affymetrix analysis

Total mRNA was extracted by primary bMECs, treated with either vehicle or recombinant Wnt3a and with either siCTRL or siFgfbp1#2, and analyzed using Affymetrix GeneChip arrays Gene ST 1.0 covering 29000 murine genes. For each condition, total mRNA extracts from three different experiments were analyzed to

measure biological variability. In order to identify the modulated genes, an initial filter was applied to select transcripts with at least a 2-fold change and with a statistical significance lower than 0.05.

2.16 Immunofluorescence (IF) analysis of cells

For cell IF analysis, cells were fixed and permeabilized in 1% PAF/0.1% Triton-X/0.1% NP40 for 30 minutes at RT or with ice-cold 100% methanol for 3 minutes. Fixed cells were incubated with blocking solution (PBS + 5% BSA + 5% Normal Donkey Serum) for at least 1 hour at RT and then with the primary antibody (diluted in PBS + 5% BSA) O/N at 4°C; after 3 washes in PBS + 1% BSA, the cells were incubated with the appropriate secondary antibody (diluted in PBS + 1% BSA) for 1 hour at RT, then washed in PBS, postfixed in 1% PFA for 3 minutes at RT, washed again and finally mounted in Vectashield with DAPI.

Samples were observed at a confocal microscope (Leica) using 20x, 40x and 63x objectives. Acquired images were processed with ImageJ; only adjustments of brightness and contrast were applied in the preparation of the figures. For comparison purposes, different sample images of the same antigen were acquired under constant acquisition settings.

2.17 Quantitative Real Time RT-PCR (qRT-PCR)

Total RNA from cultured cells was extracted with RNeasy Kit (Qiagen) following manufacturer's instructions. The desired amount of RNA (usually 500 ng) was retrotranscribed with random examers using the High Capacity cDNA Archive Kit

(Applied Biosystems). cDNA (5 ng) was amplified in triplicate with the TaqMan Gene Expression Assay (Applied Biosystems) and the I/Prism 7900 HT Thermocycler. For each sample, the expression level was first normalized to 18S housekeeping gene and then determined with the comparative threshold cycle (Ct) method as previously described.

2.18 Western blot analysis

Total proteins were extracted by solubilizing cells in boiling Laemli buffer. Lysates were incubated for 10 minutes at 100°C and then spinned for 5 minutes at 13000 rpm to discard cell debris. The supernatants were collected and the protein concentration was determined using a BCA Protein Assay Kit (Pierce) according to the manufacturer's instructions. Equal amounts of protein were loaded on gel and separated by SDS-PAGE, transferred to a Protran Nitrocellulose Hybridization Transfer Membrane 0,2 μm pore size and blocked for 1h at RT in TBS-T 1X containing 5% BSA. The membranes were then incubated for 1 hour at RT with primary antibodies diluted in TBS-T 1X containing 5% BSA. Membranes were rinsed at least three times in TBS-T 1X and then incubated for 1 hour at RT with secondary antibodies diluted in TBS-T 1X containing 5% BSA. After three washes, membranes were incubated with ECL for 1 min and exposed for the required time.

2.19 Antibodies and reagents

The following antibodies were used for IF: FGFBP1 (R&D AF1413, dil. 1:400), FGFBP1 (Bioss, bs-1768R, dil.1:150), GFP (Invitrogen, A-21311dil. 1:300), PECAM (Millipore MAB1398Z, dil. 1:200), VE-cadherin (BD, 550548, dil. 1:200),

podocalyxin (R&D, AF1556, dil. 1:200), GLUT1 (Thermo Scientific #RB-9052-P0, dil. 1:300), NG2 (Millipore AB5320, dil. 1:200), desmin (Abcam ab15200, dil. 1:200), PDGFRβ (R&D AF1042, dil. 1:200), laminin α2 (Abcam ab11576, dil. 1:200), collagen IV α1 chain (Chondrex #7070, dil. 1:200), collagen IV α2 chain (Chondrex #7071, dil. 1:200), aquaporin IV (Millipore AB3594, dil. 1:200), collagen IV (Serotec 2150-1470, dil. 1:200), appropriate secondary antibodies conjugated with Alexa 488, Alexa 555 and Alexa 647 (Invitrogen, dil. 1:200). Antibodies against laminin α4 and laminin α5 were kindly provided by Prof. Lydia Sorokin (Institute of Physiological Chemistry and Pathobiochemistry, Münster University, Germany).

To enhance FGFBP1 signal, the Tyramide Signal Amplification kit (TSA kit#12, Life Technologies) was used on vibratome sections.

The following primary antibodies were used for WB: total p42/44 MAPK (Cell Signaling, dil. 1:1000), phosphorylated p42/44 MAPK (Cell Signaling, dil. 1:1000).

2.20 Quantifications

In zebrafish experiments, at least 10 animals per group were analyzed. The number of ISVs and of ISVs-DLAV connections, the number of hemorrhages and the number of DAPI positive nuclei in the permeability assay were manually counted.

In mice experiments, at least 2 WT and 3 KO animals from the same litter were analyzed for each stage of development. At least 3 confocal z-projection (about 15 μm thickness) images were used for each quantification.

To quantify the vascular density, whole-mount retinas/brain sagittal sections were stained for PECAM; the images were thresholded and binarized and the percentage of PECAM-positive pixels was determined with ImageJ.

To quantify the vessel coverage by BM proteins (collagen IV, Col4a1, Col4a2, laminin α2, laminin α4, laminin α5), the images were thresholded and binarized; the respective binarized PECAM image was then used as selection mask and the percentage of BM/pericyte marker positive pixels within the selection was calculated using ImageJ.

To quantify the fluorescence intensity of Plvap and of BM/pericyte markers (as a measure of their expression), the respective binarized PECAM image was used as selection mask and the mean fluorescence intensity of BM/pericyte markers within the selection was determined using ImageJ.

The number of branching points and the number of PDGFRβ positive pericytes were manually counted.

All images acquisitions and all quantifications were carried out blind.

2.21 Statistical analysis

Data are presented as mean ± standard deviation. Statistical significance was determined by performing 2-tailed unpaired Student's t-test (Excel). A P value <0.05 was considered statistically significant.

3. RESULTS

3.1 Fgfbp1 expression is regulated by canonical Wnt/β-catenin pathway both in vitro and in vivo

3.1.1 Fgfbp1 expression is upregulated by Wnt3a treatment in primary brain ECs

In the perspective of better understanding the effect of the canonical Wnt pathway on brain microvasculature, we performed an Affymetrix screening to determine the modifications in the transcriptional program of murine primary brain ECs when treated with the canonical Wnt ligand Wnt3a. Among the genes that resulted to be modulated by Wnt pathway activation, one of the genes that showed the strongest upregulation was *Fgfbp1*, that in Wnt3a-treated cells was 2.646 fold higher than in control cells ($p<0.001$). As an internal control of an effective Wnt3a treatment, also the canonical Wnt/β-catenin target genes *Axin2* and *Slc2a1* resulted to be upregulated in Wnt3a-treated cells (*Axin2*: fold change = 2.781, p value <0.001; *Slc2a1*: fold change = 1.218; p value <0.005).

3.1.2 Fgfbp1 expression is upregulated in brain, but not lung, ECs in a murine model of β-catenin gain-of-function

To verify *in vivo* the effect of Wnt activity on FGFBP1 expression, we took advantage of a murine model of β-catenin gain of function ($\beta\text{-cat}^{lox(ex3)/wt}$). After crossing these mice with the transgenic strain (*Cdh5(PAC)-CreERT2*), where CRE recombinase is under the transcriptional control of the endothelial specific Cdh5

promoter, the recombinase is expressed only in ECs, where it targets for recombination the LoxP sites. Indeed, the CRE protein is fused to a tamoxifen-responsive ERT2 domain, that translocates the recombinase to the nucleus to induce the deletion only upon tamoxifen treatment. This approach allowed us to obtain an endothelial-specific β-catenin gain of function (GOF) model.

The recombination was induced in the progeny by injecting tamoxifen soon after birth (0 dpn) and ECs from brain and lungs were isolated at day 8 dpn. Real-Time PCR (qRT-PCR) analysis of Ffgbp1 gene expression showed that Fgfbp1 mRNA was significantly higher in brain ECs isolated from GOF mice compared to those isolated from WT mice ($p<0.05$), while it was not induced by β-catenin activity in the ECs isolated from the lung (Fig. 11a). The absence of Fgfbp1 induction in lung ECs isolated from GOF mice was not dependent on the eventual lack of activation of Wnt/β-catenin pathway in these cells, since the transcription of the canonical Wnt target gene Axin-2 was strongly upregulated in lung ECs isolated from GOF mice compared to those isolated from control animals (Fig. 11b).

Finally, in GOF 8 dpn pups Fgfbp1 levels are significantly higher in brain ECs compared to lung ECs ($p<0.001$) (Fig. 11a).

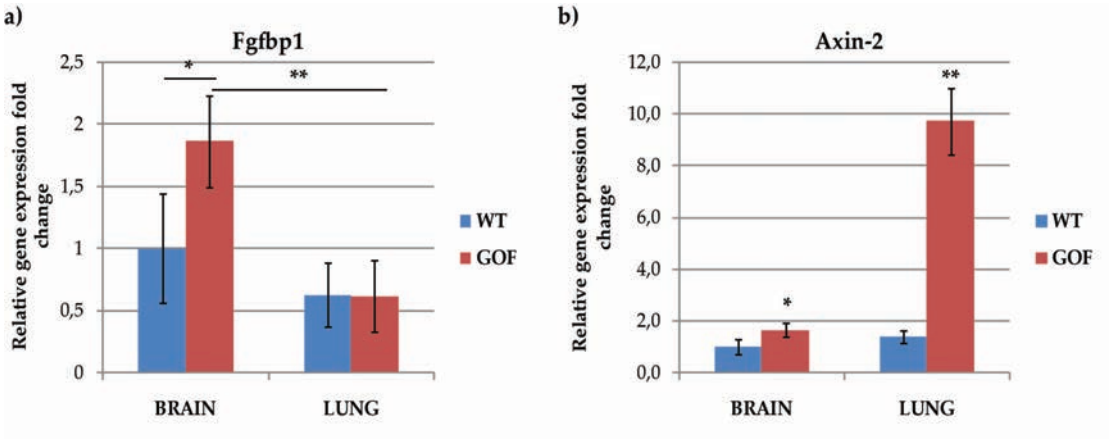

Figure 11. Analysis of Fgfbp1 and Axin-2 expression in lung and brain ECs in a β-catenin gain-of-function model

qRT-PCR analysis of **(a)** Fgfbp1 and **(b)** Axin-2 expression in ECs freshly isolated from the brain and the lungs of WT and β-cat$^{lox(ex3)/wt}$x Cdh5(PAC)-CreERT2 (GOF) 8 dpn pups. The levels of mRNA are normalized on 18S. Data are presented as mean ± standard deviation of the analyzed samples (WT: n=2; GOF: n=6). *: $p<0.05$; **:$p<0.001$.

Lastly, we confirmed that the expression of Fgfbp1 was lower in lung ECs compared to brain ECs also in older mice, as shown by the qRT-PCR analysis of Fgfbp1 mRNA levels in microvascular fragments isolated from the brain and the lung of 1 week old and 3 weeks old mice (Fig. 12).

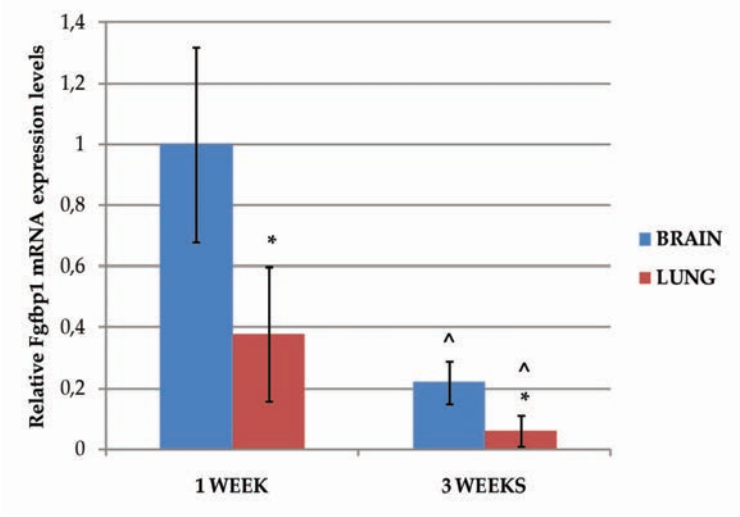

Figure 12. Analysis of Fgfbp1 expression in lung and brain ECs of 1 week old and 3 weeks old mice

qRT-PCR analysis of Fgfbp1 expression in ECs freshly isolated from the brain and the lungs of 1 week old and 3 weeks old WT mice. The levels of mRNA are normalized on 18S. Data are presented as mean ± standard deviation of the analyzed samples (WT: n=2; GOF: n=6). *: Lung vs. Brain: $p<0.05$. ^: 3 weeks vs. 1 week: $p<0.05$.

3.1.3 Fgfbp1 is upregulated by Wnt pathway activation in a zebrafish model

To further confirm these in vivo observations, we decided to analyze a second animal model: zebrafish. The preparatory bioinformatics analysis performed to search for FGFBP1 homologues in human, mouse and zebrafish showed that FGFBP1 belongs to a family of proteins, that includes three different members: FGFBP1, 2 and 3. Both FGFBP1 and 2 are present in zebrafish as two different paralogues: a and b. Despite a quite low total sequence homology of FGFBP1a and b with both human and mouse protein sequences (23% and 24% amino acid identities to human and mouse, respectively), the functional domains of the protein (the C-terminal FGF-binding domain and the intermediate heparin-binding domain) resulted to be very conserved among the three species. In

addition, FGFBP1b is the zebrafish paralogue with the highest homology with the murine and human proteins.

To study the effect of Wnt signaling activation on zebrafish Fgfbp1a and b expression, we took advantage of the transgenic line Tg(fli1a:EGFP), in which ECs are marked in green by the expression of GFP, that is driven by the endothelial-specific promoter fli1a. Tg(fli1a:EGFP) eggs were collected and injected with either a control or a Dkk1 morpholino to specifically enhance Wnt activity. Three days after the morpholino injection, embryos were disaggregated and cells were sorted for GFP fluorescence in order to obtain two subpopulations: GFP positive (GFP+, mainly endothelial) and GFP negative (GFP-, mainly non-endothelial). Total mRNA was extracted from sorted cells and analyzed by semiquantitative RT-PCR for the expression of Fgfbp1a, Fgfbp1b and Axin-2 (as an internal control of an effective Wnt activity enhancement by Dkk1 morpholino injection). As expected, Axin-2 was significantly increased upon MO-Dkk1 injection in both endothelial and non endothelial cells ($p<0.05$), indicating that the treatment effectively induced Wnt signaling activation. In ECs, both Fgfbp1a and b were significantly upregulated by Wnt activity ($p<0.05$); conversely, in non endothelial cells MO-Dkk1 injections resulted to be able to increase only Fgfbp1a mRNA levels ($p<0.05$), while Fgfbp1b was not significantly modulated. Finally, the analysis showed that already in basal conditions (i.e. in control-injected samples) Fgfbp1a expression was lower in non-endothelial cells compared to ECs, and vice versa Fgfbp1b was lower in ECs than in non-endothelial cells, suggesting a different cell specificity of the two paralogues (^: $p<0.05$) (Fig. 13).

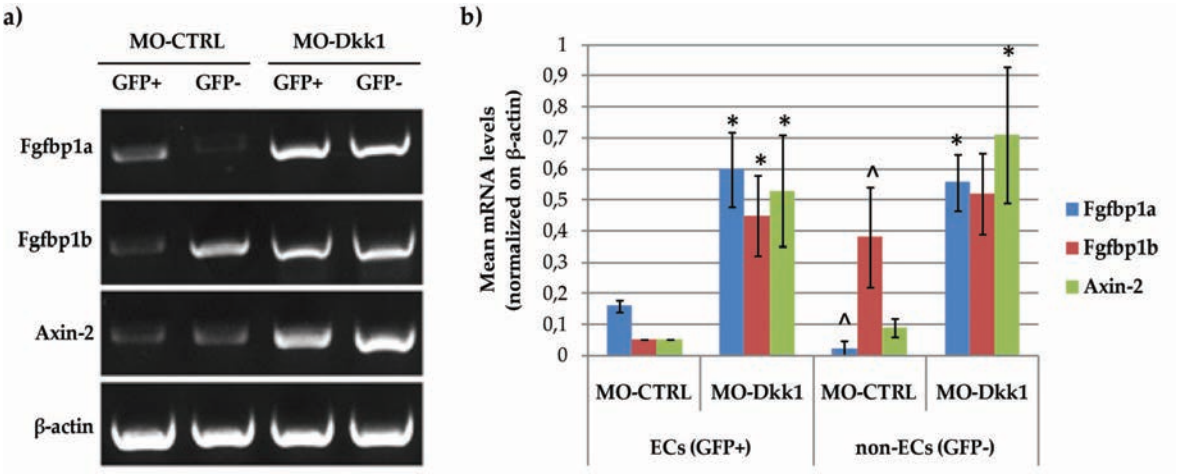

Figure 13. Analysis of Fgfbp1a and b expression upon Wnt signaling activation

(a) Semiquantitative RT-PCR analysis of GFP+ and GFP- cells isolated and sorted from Tg(fli1a:EGFP) 3 dpf zebrafish embryos after injection with either a control morpholino (MO-CTRL) or a Dkk1 morpholino (MO-Dkk1) and **(b)** its quantification. Data are presented as mean ± standard deviation of replicates of a representative experiment (n=2). *: ECs MO-Dkk1 vs. MO-CTRL; non ECs MO-Dkk1 vs. MO-CTRL: $p<0.05$. ^: MO-CTRL non-ECs vs. EC: $p<0.05$

3.2 Characterization of Fgfbp1 expression and function in the zebrafish model

3.2.1 Fgfbp1a and b are differentially expressed during zebrafish development

To evaluate Fgfbp1a and b expression during zebrafish development, we performed a semiquantitative RT-PCR on whole embryo mRNA extracts, with primer pairs specifically designed to amplify each of the two transcripts, at different embryonic stages: 2 hours post fertilization (hpf), 9 hpf, 24 hpf, 48 hpf and 72 hpf. The results showed that the two paralogues were differentially expressed during larvae development: Fgfbp1a was expressed at low levels already at 2 and 9 hpf, it was strongly upregulated at 24 and 48 hpf and it started decreasing at 72 hpf; Fgfbp1b was completely absent until 24 hpf, when it started

being expressed at low levels, and then gradually increased at later time points (Fig. 14).

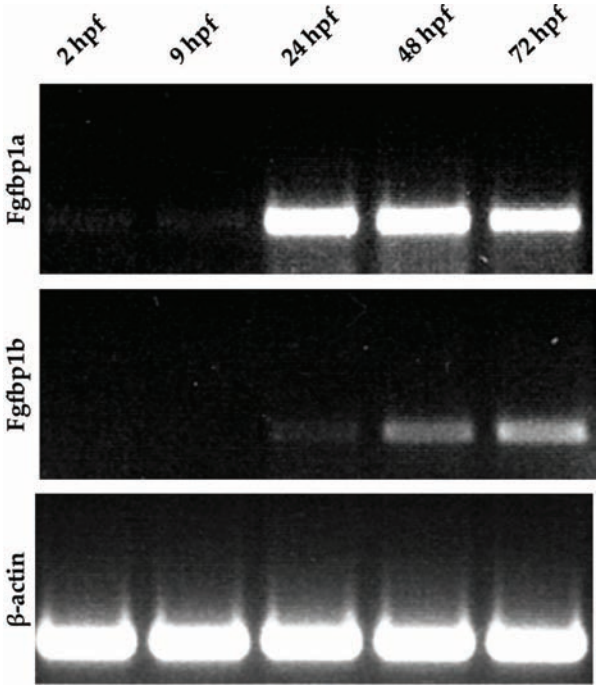

Figure 14. Kinetics of expression of Fgfbp1a and b in zebrafish during development
Representative image of a semiquantitative RT-PCR analysis of Fgfbp1a and b expression in whole embryo mRNA extracts at different developmental stages. β-actin was used as internal loading control.

To further investigate the expression pattern of Fgfbp1a and b in terms of spatial distribution, we performed an In Situ Hybridization (ISH) with antisense probes specific for each of the two transcripts. The ISH revealed an almost ubiquitous pattern of expression for both paralogues, confirming the reports in the literature about Fgfbp1 role during development of different tissues and organs. Observation at high magnification also revealed the presence in the brain of strongly positive structures with a topology very similar to that of the major brain vessels (Fig. 15, arrows). The same structures were also visible in 100 μm-thick

vibratome sections of 72 hpf larvae, where it was possible to distinguish also the vascular lumen of the major vessels (Fig. 15, arrowhead).

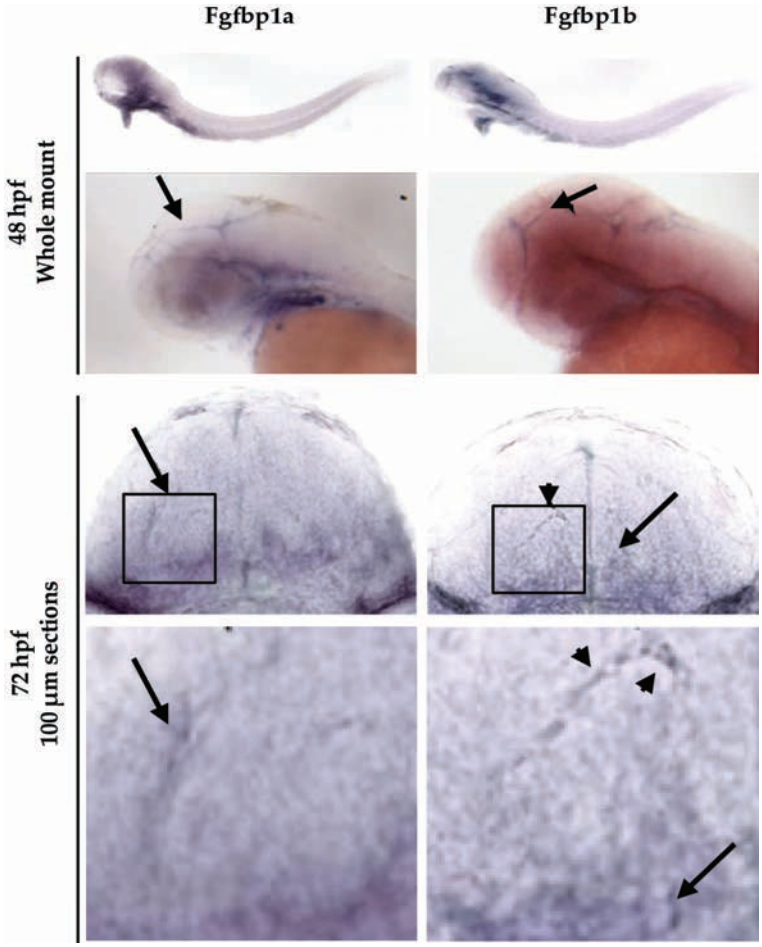

Figure 15. Localization of Fgfbp1a and b during zebrafish development

Representative image of an In Situ Hybridization (ISH) analysis of the expression of Fgfbp1a and b in zebrafish embryos at different developmental stages. Arrows indicate strongly stained structures with a vascular-like topology; the arrowhead indicates the vascular lumen of a major brain vessel.

3.2.2 Fgfbp1a and b knock down in vivo causes brain hemorrhages in zebrafish

To test the role of Fgfbp1a and b during zebrafish development, we decided to silence them using specific morpholinos. The designed morpholinos belong to the class of ATG-blocking morpholinos, meaning that they bind to ATG sequence of the mRNA and block its translation into protein (Fig. 16a). For this reason, to

check for the efficacy of the designed morpholinos in blocking their specific targets, we used two DNA constructs (one for Fgfbp1a and the other for Fgfbp1b) in which the morpholino target sequence is tagged with GFP: in presence of a specific and effective binding of the morpholinos to their respective target DNA construct, the GFP signal is expected to be switched off (Fig. 16b). We injected the DNA constructs in the fertilized eggs, alone or in combination with the respective morpholino, and subsequently analyzed GFP expression in 8 hpf embryos with a fluorescence microscope. As shown in Fig. 16c, GFP was clearly expressed when the construct was injected alone, but it was switched off when the construct and the morpholino were coinjected, indicating that each morpholino was effective in blocking its specific target sequence. Importantly, the turning off of the GFP was not an aspecific effect due to the coinjection of both construct and morpholino, since the eggs that received the morpholino together with the empty vector were clearly GFP positive.

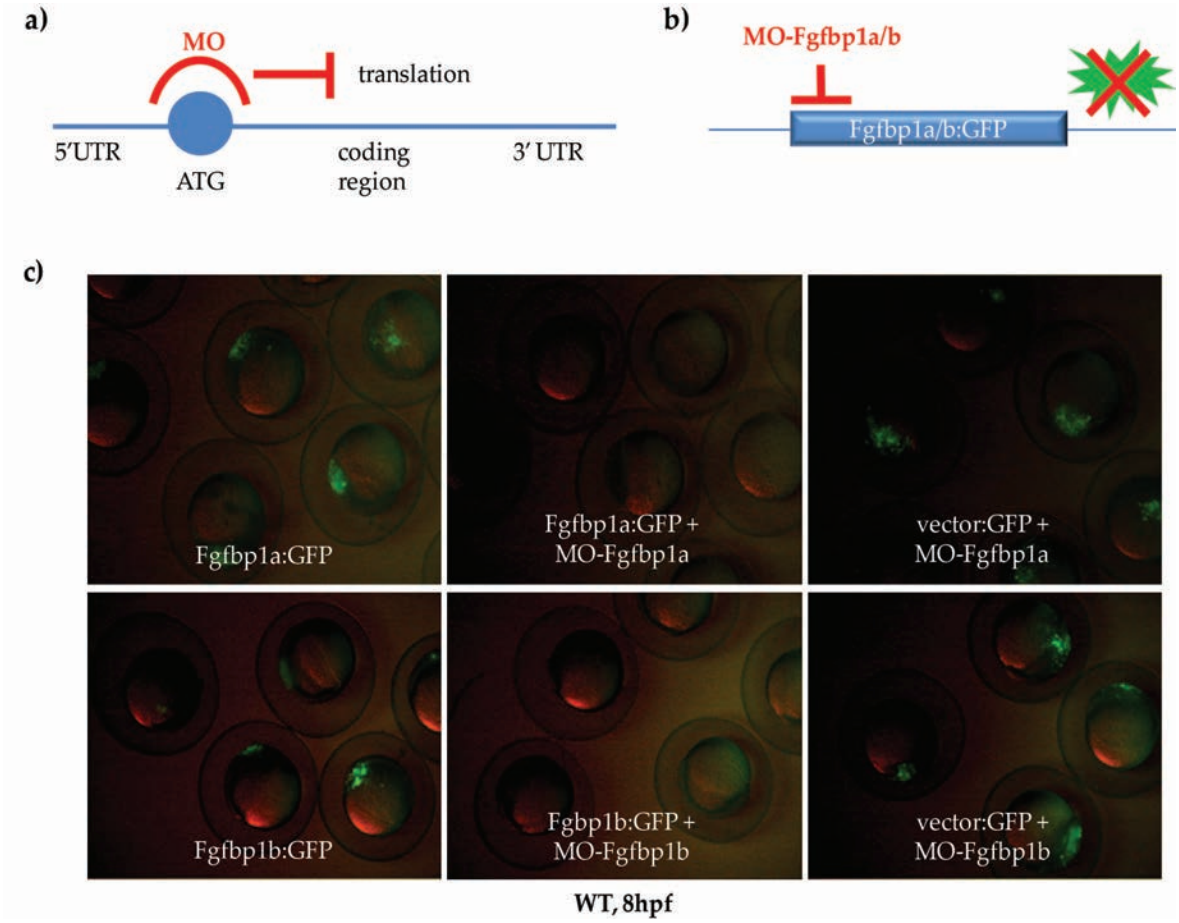

Figure 16. Design and testing of morpholinos targeting Fgfbp1a and b

(a) Mechanism of action of the designed ATG-blocking morpholinos. **(b)** Design of the constructs for the test of efficacy of the morpholinos. Two different DNA constructs, with either Fgfbp1a or b sequence fused to GFP, were designed in order to be coinjected with the respective morpholino. **(c)** Test of efficacy of the designed morpholinos. The DNA constructs were injected alone or in combination to the respective morpholino in order to check for the expression of GFP.

The morpholinos were injected into a wild type zebrafish strain to search for gross morphological alterations. The morphological analysis did not show any evident difference in size and overall development, but it displayed the presence of hemorrhagic events in both Fgfbp1a and Fgfbp1b morphants. In particular, more than half of the animals treated with MO-Fgfbp1a (51,65%; $p<0.001$) presented large hemorrhagic areas in the brain and 15,38% ($p<0.001$) of them presented small hemorrhages in other body regions; conversely, a much smaller, but still

statistically significant, proportion of MO-Fgfbp1b-injected animals (brain: 4,55%; other: 4,55%; $p<0.001$) displayed hemorrhages in the brain and in other regions. In addition, brain hemorrhages of Fgfbp1b morphants were much smaller compared to those of MO-Fgfbp1a-injected animals, and most of the time they were so small that they could not be detected by direct stereomicroscope observation but were revealed only after O-dianisidine staining to detect hemoglobin (Fig. 17).

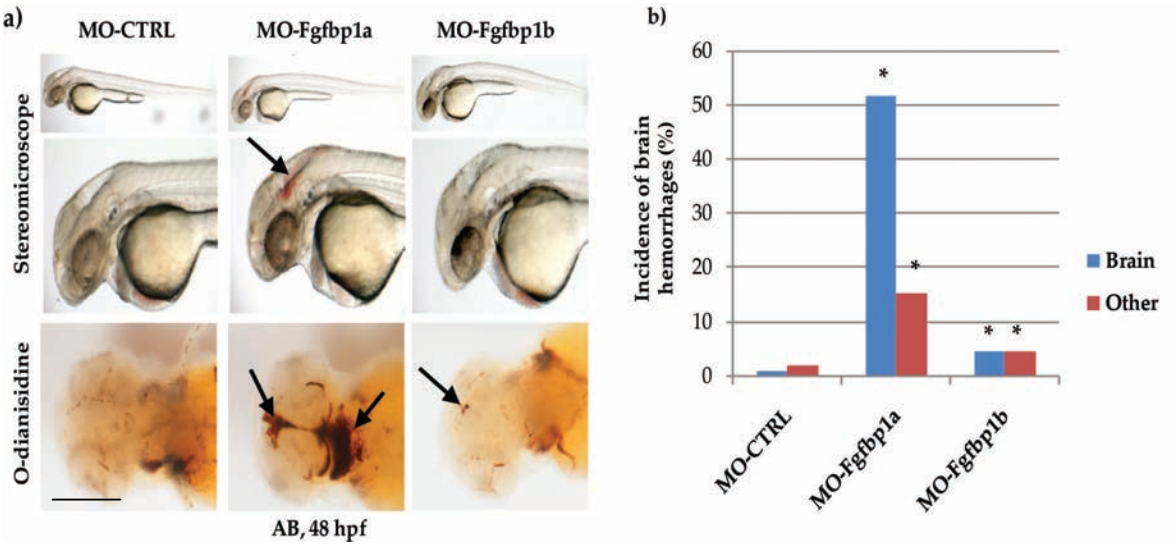

Figure 17. Quantification of the hemorrhagic phenotype in Fgfbp1a and b morphants

(a) Morphological observation and **(b)** hemorrhages quantification after injection of either MO-FGFBP1a or MO-FGFBP1b. All animals were injected at 1-cell stage and analyzed 48 hours later by simple stereomicroscope observation or by O-dianisidine staining. At least 40 animals were analyzed for each condition. Scale bar: 500 μm.

3.2.3 Fgfbp1a and b knock down in vivo causes defects in zebrafish vascular development

To determine whether the occurrence of the hemorrhages was due to vascular defects, we took advantage again of Tg(fli1a:eGFP) line to visualize blood vessels morphology after morpholino injections. During normal zebrafish vascular

development, as well as in MO-CTRL treated animals, the intersomitic vessels (ISVs) start sprouting from the dorsal aorta (DA) towards the dorsal side of the trunk, where they finally fuse perpendicularly to form the dorsal longitudinal anastomotic vessel (DLAV). Upon injection of MO-Fgfbp1a the normal trunk vascular development looked affected: the number of ISVs that started sprouting from the DA was strongly reduced at all analyzed stages (24, 48 and 72 hpf) ($p<0.001$), and most of them failed to efficiently form connections at the DLAV ($p<0.001$). Conversely, the ISVs sprouting process occurred normally in MO-Fgfbp1b injected animals, but the process of DLAV formation was impaired: indeed, while at 48 hpf there was a higher number of ISVs forming connections at the DLAV compared to age-matched controls ($p<0.025$), this number did not increase at later stages (72 hpf), remaining lower than in MO-CTRl animals ($p<0.05$), indicating that the vascular development was accelerated in the first phases, but then it slowed down and failed to form a completely developed vasculature (Fig. 18).

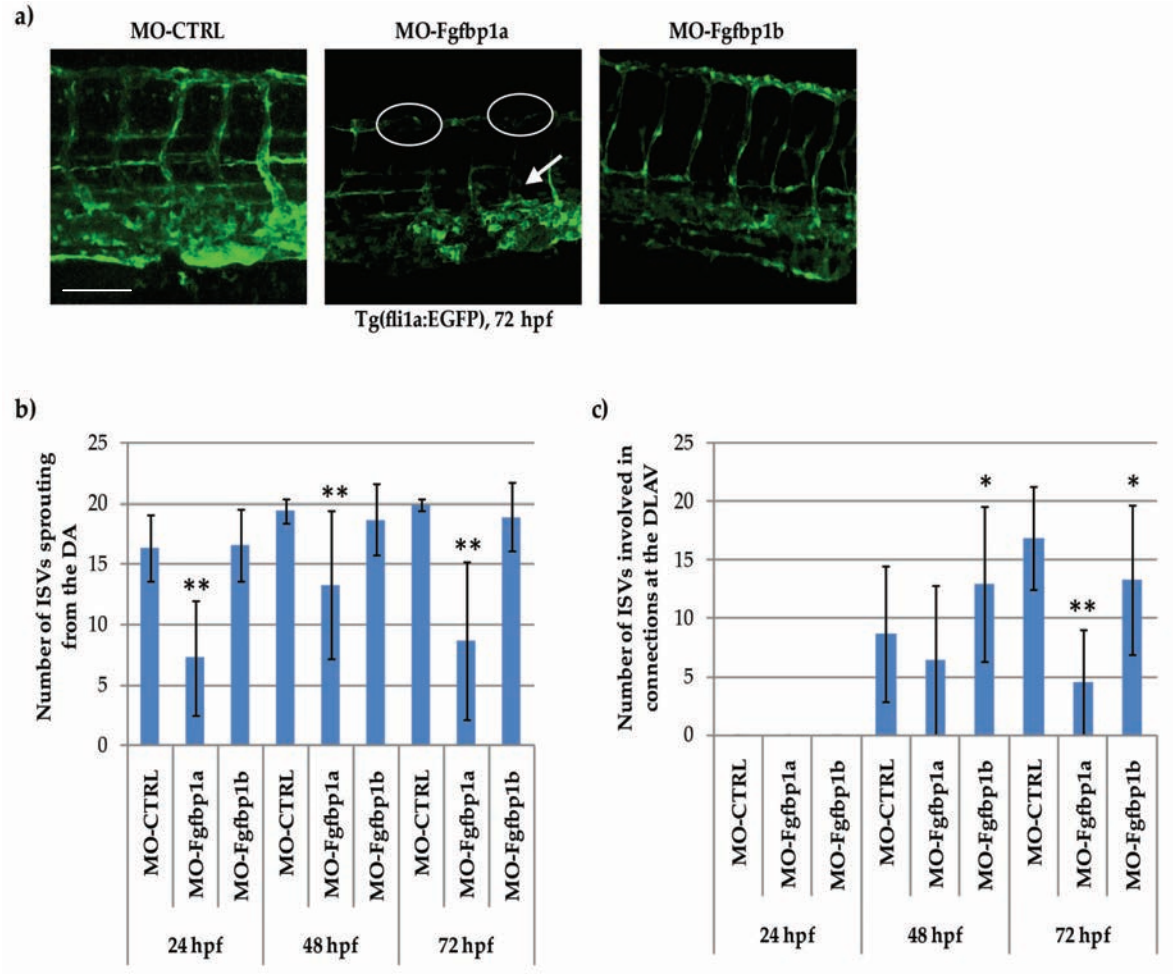

Figure 18. Analysis of the trunk vascular development in zebrafish upon Fgfbp1 knock down

(a) Representative images of confocal Z-stacks of trunk vascular phenotype in Tg(fli1a:EGFP) 72 hpf animals after injection with either MO-Fgfbp1a or MO-Fgfbp1b. Scale bar: 250 μm. **(b)** Quantification of the number of ISVs sprouting from the DA in MO-CTRL, MO-Fgfbp1a and MO-Fgfbp1b animals at 24, 48 and 72 hpf. For each group, at least 30 animals were analyzed. **: $p<0.001$. **(c)** Quantification of the number of ISVs forming connections at the DLAV in MO-CTRL, MO-Fgfbp1a and MO-Fgfbp1b animals at 24, 48 and 72 hpf. For each group, at least 30 animals were analyzed. *: $p<0.05$; **: $p<0.001$.

Besides the defects in the development of the ISVs and of the DLAV, some vascular abnormalities were also found in the head vasculature. Indeed, while control animals had a regular and organized brain vasculature, Fgfbp1a morphants showed the lack of some vessels (Fig. 19, arrows), possibly indicating a defective sprouting activity; conversely, Fgfbp1b morphants showed some

tortuous and irregular vessels (Fig. 19, arrowhead) with hyperbranching events (Fig. 19, asterisk).

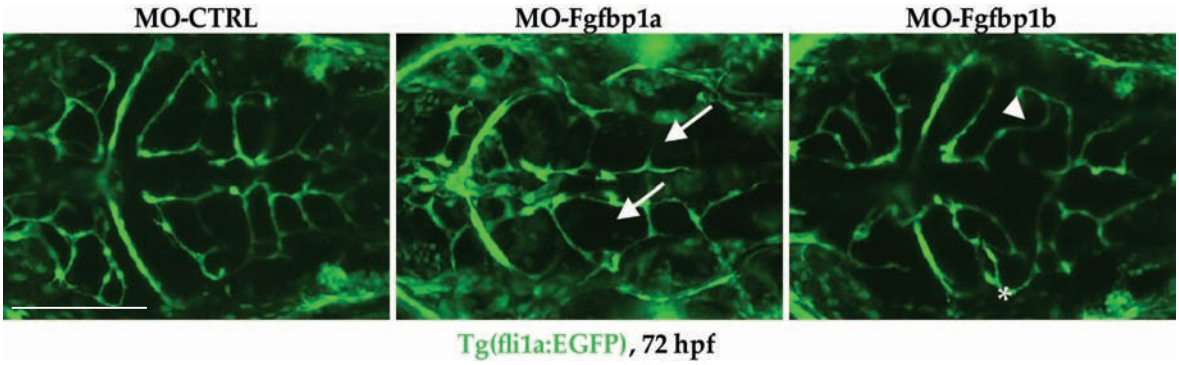

Figure 19. Analysis of the head vascular development in zebrafish upon Fgfbp1 knock down
Representative images of confocal Z-stacks of head vascular phenotype in Tg(fli1a:EGFP) 72 hpf animals after injection with either MO-Fgfbp1a or MO-Fgfbp1b. Scale bar: 250 μm. Arrows: lacking vessels; arrowhead: tortuous vessel; asterisk: extrabranching.

To clarify the dynamics of uprising of the vascular defects in the head, we performed the morpholino injections in the double transgenic strain Tg(fli1a:EGFP)xTg(gata1a:dsRed), in which ECs are highlighted in green by GFP and erythrocytes are highlighted in red by dsRed. We then performed *in vivo* time lapse confocal microscopy of 48 hpf animals to follow the vascular development of the brain for at least 5 hours (see Fig. 20 and movies 1-2-3).

The time lapse of control-injected animals showed a normal vascular development, with the typical sprouting vessel (Fig. 20, circle) that searches the surrounding region, fuses with another proximal vessel and finally opens its lumen allowing the blood flow to start (movie 1).

Conversely, the time lapse on MO-Fgfbp1a animals showed an impairment in the sprouting process, resulting in the inability of the brain vasculature to develop

properly. Moreover, also the arising of the hemorrhagic phenotype was clearly visible as the accumulation of dsRed positive erythrocytes (movie 2; Fig. 20, dotted circle).

Finally, in the Fgfbp1b morphants the time lapse showed that, despite a normal and effective sprouting process, the developing vessels had difficulties in defining their correct growing trajectory. As a result of this impairment in the path-finding, the vessel alternated phases of growth and regression to constantly search for the correct orientation (movie 3 and Fig. 20; the arrow indicates the growing vessels, the dotted lines represent the former trajectories of the vessel).

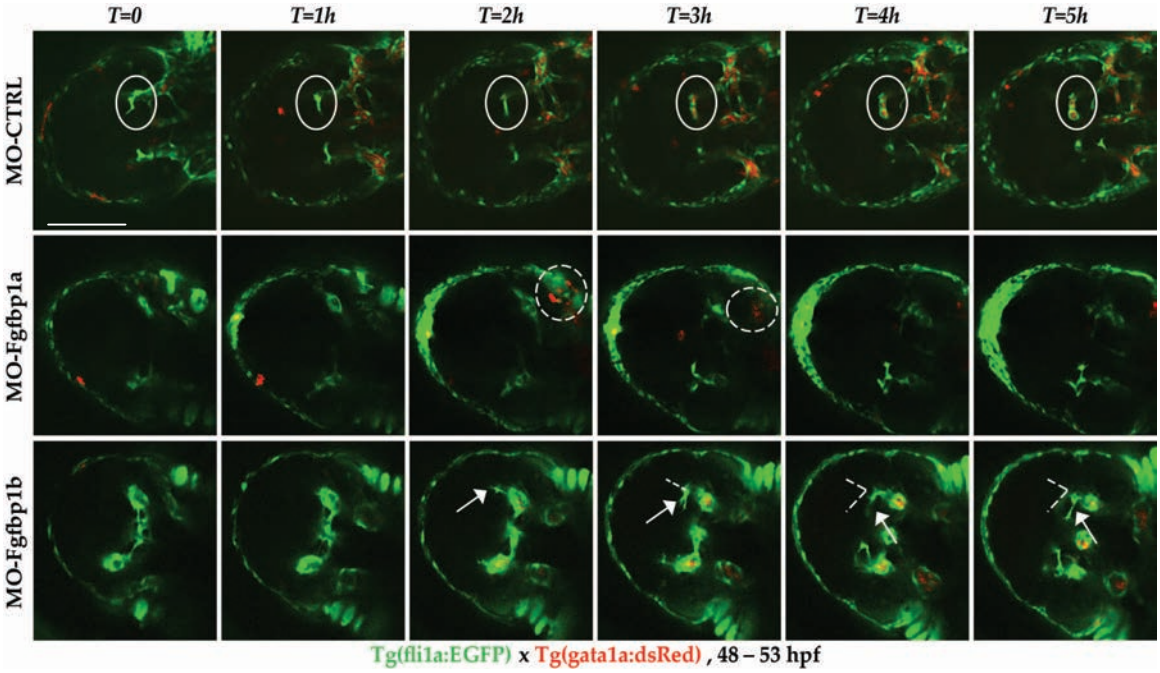

Figure 20. Time lapse confocal microscopy analysis of the brain vascular phenotype of Fgfbp1a and Fgfbp1b morphants

Time lapse microscopy of Tg(Fli1a:EGFP)xTg(gata1a:dsRed) animals injected with MO-CTRL, MO-Fgfbp1a or MO-Fgfbp1b. Anestethized 48 hpf embryos were immobilized in 4% LMP agarose and 12 μm Z-stacks were acquired every 15 minutes for at least 5 hours. Circle: area of sprouting of a new brain vessel; dotted circle: area of hemorrhage; arrow: brain vessel with impaired path-finding capability; dotted lines: different tracks of growth of the vessel. Space bar: 250 μm.

3.2.4 Fgfbp1a knock down in vivo causes increased vascular permeability in zebrafish brains

Finally, to analyze the effect of Fgfbp1 knock down on brain vascular permeability, we performed a functional assay by injecting rhodamine-labeled 10 kDa dextran into the venous sinus of 72 hpf morphants and analyzing them 40 minutes after the injection. We observed that the tracer was retained within the brain vessels both in control animals and in Fgfbp1b morphants, indicating an effective control of permeability; conversely, in Fgfbp1a morphants the vessels were no longer able to retain the tracer, indicating that Fgfbp1a loss causes defects in the control of brain vascular permeability (Fig. 21a). To get quantitative information from this functional assay, we also performed the injection with DAPI, in order to count the number of DAPI positive cells in the brain parenchyma, that is proportional to the amount of dye that leaks out of the vessels. The quantification confirmed a massive increase in brain vascular permeability in Fgfbp1a morphants, while MO-Fgfbp1b injected animals showed a number of DAPI positive brain nuclei comparable to that of control-injected animals (Fig. 21b).

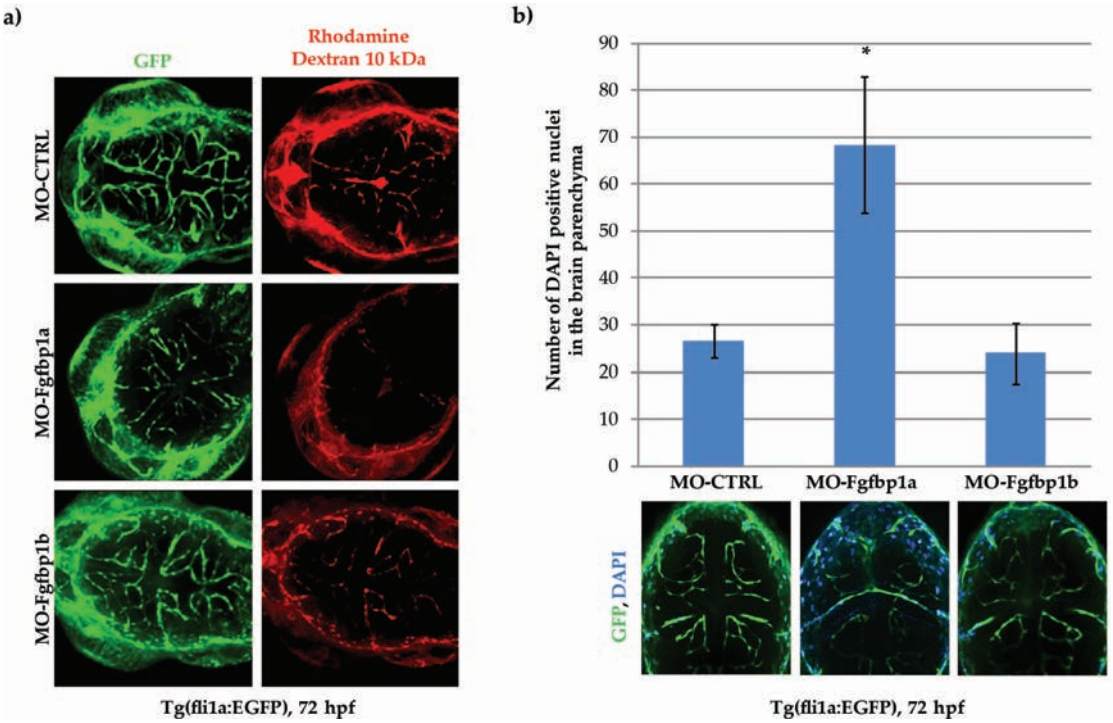

Figure 21. In vivo permeability assay on Tg(fli1a:EGFP) morphants

(a) Representative confocal Z-stack images of the in vivo permeability assay. Rhodamine-labeled 10 kDa dextran was injected in the venous sinus of 72 hpf Tg(fli1a:EGFP) morphants and the animals were fixed in 4% PFA 40 minutes after the injection. At least 10 animals were injected and analyzed per each group. **(b)** Quantification of the in vivo permeability assay. DAPI was injected in the same way as rhodamine-labeled 10 kDa dextran, larvae were fixed 40 minutes after the injection and the number of DAPI positive cells in brain parenchyma was quantified. At least 10 animals were injected and quantified per each group. $p<0.01$.

3.3 Characterization of Fgfbp1 expression and function in the murine brain vasculature

3.3.1 FGFBP1 is expressed age-dependently and is localized perivascularly

Given the vascular phenotype observed in zebrafish when performing the ubiquitous knock down of Fgfbp1, we decided to further investigate whether the mechanism by which FGFBP1 absence causes vascular defects might be attributable to the fraction of the protein that is of endothelial origin. In particular,

we decided to focus our attention on the analysis of the brain since, as already discussed in the introduction and in the previous results sections, Wnt/β-catenin pathway has a particular relevance in the differentiation of the CNS vasculature and Fgfbp1 was shown to have a higher expression in brain-derived ECs compared to lung-derived ECs, both in basal conditions and in β-catenin overactivation conditions (GOF).

For our purpose, we took advantage of the murine transgenic line Fgfbp1$^{flox/flox}$, in which the exon 2 of Fgfbp1 gene is included between two LoxP sites, that are recognized and cleaved by CRE recombinase. We crossed this strain with the transgenic *Cdh5(PAC)-CreERT2* (VEC-PAC) strain to obtain the Fgfbp1$^{flox/flox}$/VEC-PAC line, that allows us to temporally control the knock-out of Fgfbp1 gene to achieve a conditional Fgfbp1 endothelial cell-specific knock-out (ECKO) (Fig. 22).

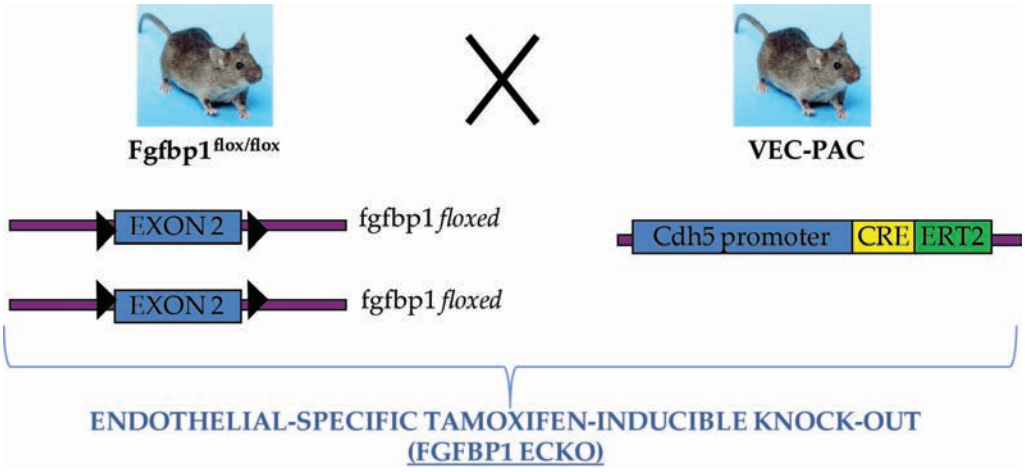

Figure 22. Design of the Fgfbp1$^{flox/flox}$/VEC-PAC transgenic mouse model

Exon 2 of Fgfbp1 gene is surrounded by LoxP sites in Fgfbp1$^{flox/flox}$ mice; after crossing with the VEC-PAC strain, CRE recombinase is expressed only in ECs. When tamoxifen is injected at the desired age, ERT2 tamoxifen-responsive sequence allows to translocate CRE recombinase into the nucleus, where it cleaves the LoxP sequences causing Fgfbp1 loss of function.

To determine the extent of recombination achievable with this system and to establish a time-dependent expression curve of Fgfbp1 mRNA in the brain endothelium, we isolated microvascular fragments from the brain of 1 week old and 3 weeks old mice that received tamoxifen soon after birth (0 dpn). From the qRT-PCR analysis emerged that Fgfbp1 expression levels were significantly different also when comparing brain ECs at different ages: indeed, Fgfbp1 mRNA isolated from brain ECs of 3 weeks old mice was 60% less compared to that isolated from brain ECs of 1 week old mice ($p<0.05$). Moreover, one week after tamoxifen injection in Fgfbp1$^{flox/flox}$/VEC-PAC mice, Fgfbp1 mRNA levels were reduced to 15% of age-matched control mice ($p<0.05$) (Fig. 23).

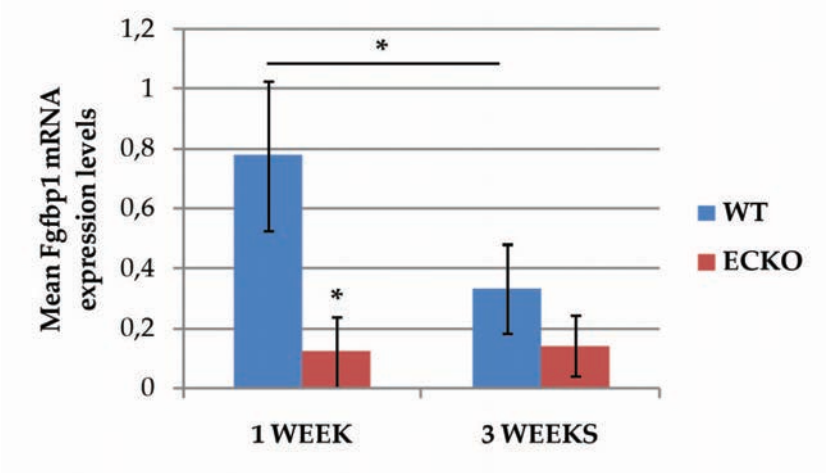

Figure 23. Analysis of Fgfbp1 expression in brain ECs of Fgfbp1 WT and ECKO mice at 1 and 3 weeks of age

qRT-PCR analysis of Fgfbp1expression in ECs freshly isolated from the brain of 1 week old and 3 weeks old Fgfbp1$^{flox/flox}$/VEC-PAC mice injected (ECKO) or not (WT) with tamoxifen. The levels of mRNA are normalized on 18S. Data are presented as mean ± standard deviation of the analyzed samples (1 week WT: n=7, ECKO: n=4; 3 weeks WT: n=4; ECKO: n=6). *: $p<0.05$.

To further evaluate the efficiency of the recombination and to assess the localization of FGFBP1 protein, we performed an immunostaining for FGFBP1 on

brain sections. As expected, the protein was not endothelial-specific, but a strong and intense perivascular staining indicated that a fraction of the protein accumulated around the vessels, detected by PECAM staining, in WT mice. The perivascular staining of FGFBP1 was massively reduced in Fgfbp1 ECKO mice, indicating that the FGFBP1 fraction that resided in the perivascular area was indeed of endothelial origin (Fig. 24).

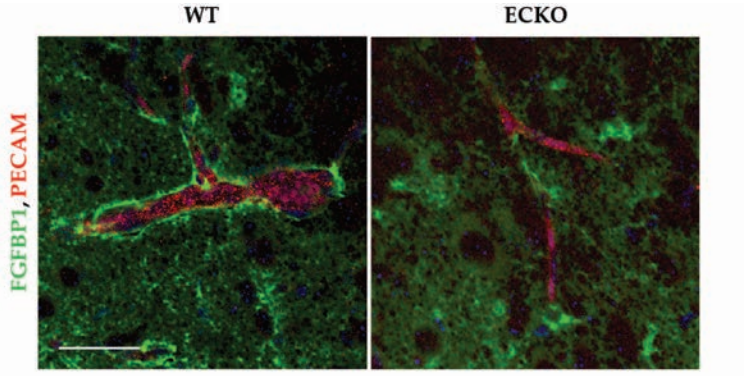

Figure 24. Analysis of FGFBP1 protein localization in brain vasculature

Representative immunostaining of FGFBP1 (green) and PECAM (red) in brain sections from 1 week old animals. Endothelial-derived FGFBP1 protein is localized perivascularly in WT brains, while it is strongly reduced in Fgfbp1 ECKO brains. Scale bar: 100 μm.

Finally, by further crossing Fgfbp1$^{flox/flox}$/VEC-PAC animals with the Rosa 26-Enhanced Yellow Fluorescent Protein (R26-EYFP) reporter strain, that expresses EYFP only after CRE-mediated deletion of a LoxP-flanked stop codon, we verified that in our model system CRE recombinase was homogeneously active in all brain vasculature (Fig. 25), strongly suggesting that also Fgfbp1 deletion might follow the same pattern.

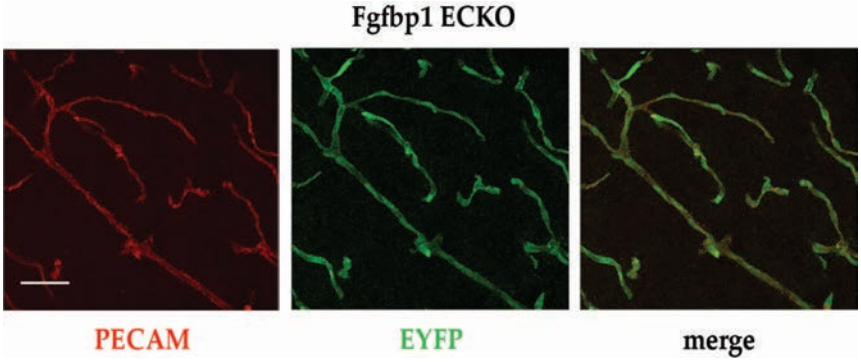

Figure 25. Analysis of EYFP expression in Fgfbp1$^{flox/flox}$/VEC-PAC/R26-EYFP 1 week old mice upon tamoxifen injection

Representative confocal Z-stack images of brain sections of 1 week old Fgfbp1 ECKO mice. Sections were immunostained for EYFP and for the endothelial marker PECAM. Scale bar: 100 μm.

3.3.2 Fgfbp1 endothelial-specific knock out causes vascular abnormalities in brain and retinas

To understand if endothelial FGFBP1 has a role during embryonic vascular development, we crossed a Fgfbp1$^{flox/flox}$/VEC-PAC animal with a Fgfbp1$^{flox/flox}$ animal and intraperitoneally injected tamoxifen in the pregnant female at day 13.5 post coitum (13.5 dpc). The female was then sacrificed at 17.5 dpc, the embryos were fixed and the brains were dissected for immunofluorescence analysis. The immunostaining for the EC marker PECAM showed that the brain vasculature of FGFBP1 ECKO embryos was irregular and disorganized compared to control animals. In particular, in the cortex region vessels were straight and regular in the control animals, while they were shorter, more branched and discontinuous in the ECKO animals; in addition, many vessels appeared to be "curly" and tortuous, resulting in an overall chaotic appearance of the whole brain vasculature (Fig. 26).

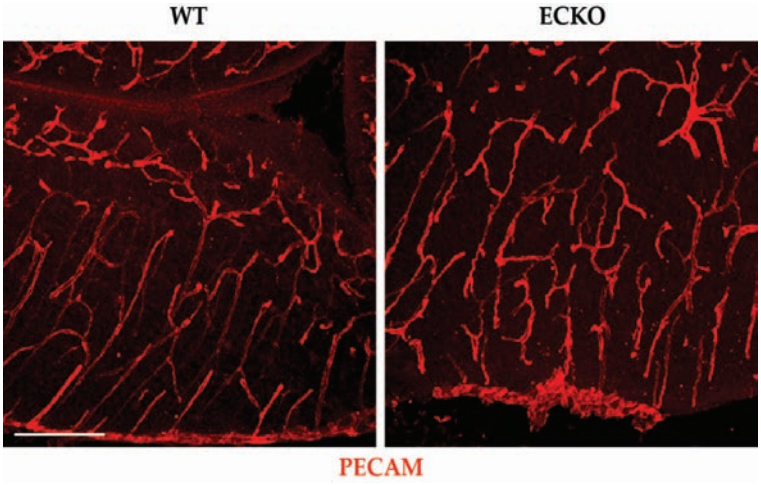

Figure 26. Vascular phenotype of Fgfbp1 WT and ECKO embryos

Representative PECAM immunostainings on brain sections (100 μm thickness) from Fgfbp1 WT and ECKO embryos at 17.5 dpc. Recombination was induced by intraperitoneal tamoxifen injection in the mother at day 13.5 dpc. Scale bar: 200 μm.

We further analysed the vascular phenotype by performing PECAM immunostaining on brain sections from WT and ECKO animals at different postnatal ages: 1 week, 2 weeks and 3 weeks. Again, as already observed in the embryos, many abnormal "curly" vascular structures were present (Fig. 27a). The impairment in the vascular development was clear also from vascular density quantification: while during the first postnatal week ECKO mice show a slightly less dense brain vasculature compared to WT animals, the vascular density tends to increase later on, becoming significantly higher compared to control animals at 3 weeks of age (Fig.27b; $p<0.05$). In addition, as shown by the confocal images and by the related quantifications, brain vessels of ECKO mice showed an higher number of branching points compared to age-matched control animals (Fig. 27c; $p<0.05$).

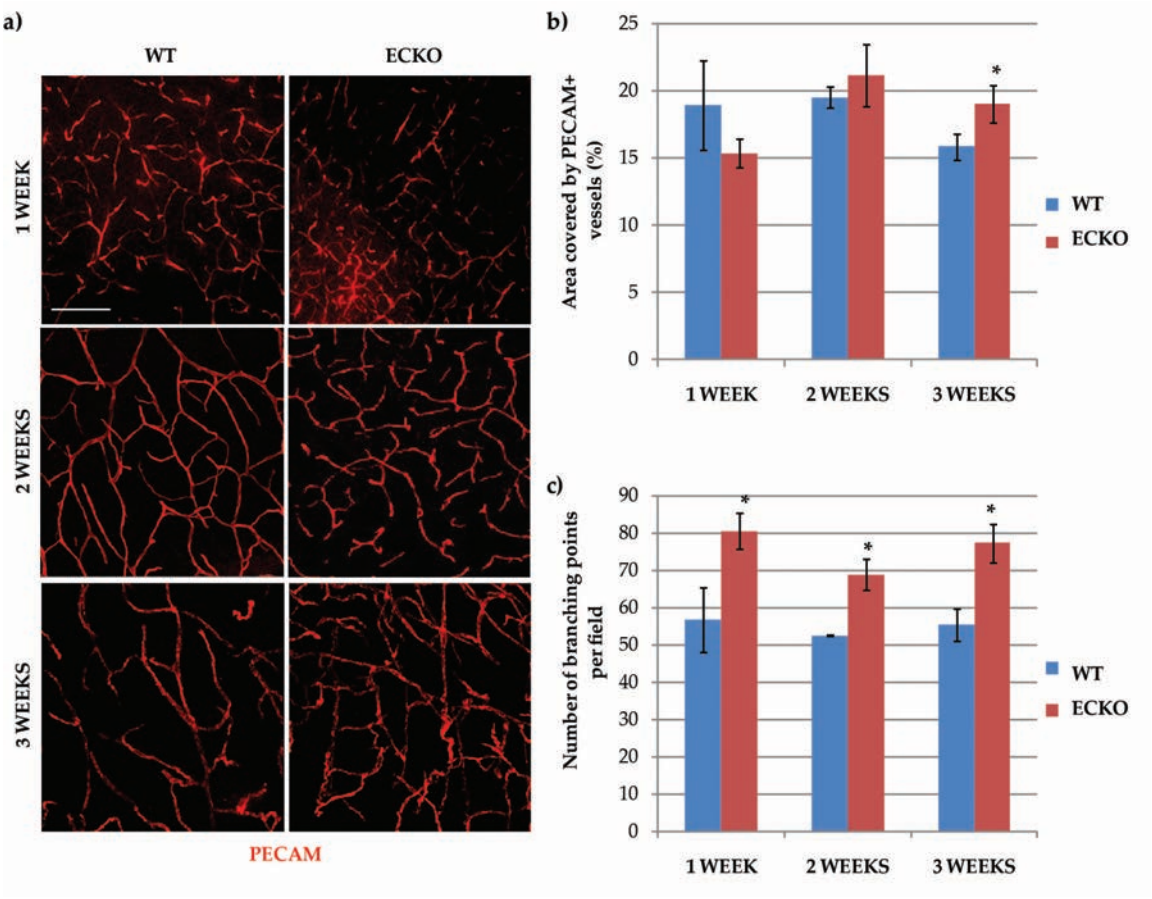

Figure 27. Analysis of brain vasculature in Fgfbp1 WT and ECKO mice at different postnatal ages

(a) Representative images of confocal Z-stacks of brain sections (100 μm thickness) of Fgfbp1 WT and ECKO mice at 1, 2 and 3 weeks of age. Sections were immunostained for the endothelial marker PECAM. Scale bar: 200 μm. **(b)** Quantification of the vascular density (percentage of area covered by PECAM positive vessels) of Fgfbp1 WT and ECKO mice at 1, 2 and 3 weeks of age. For each age group, 2 WT and 3 ECKO mice were analyzed. *: $p<0.05$ **(c)** Quantification of the number of branching points per 20x magnification field of Fgfbp1 WT and ECKO mice at 1, 2 and 3 weeks of age. For each age group, 2 WT and 3 ECKO mice were analyzed. *: $p<0.05$

Finally we investigated retinal vasculature as a model system for BBB vascular development. Whole mount retinas from Fgfbp1 WT and ECKO mice at different ages were immonostained for PECAM and analysed by confocal microscopy (only images corresponding to 1 week old mice are reported in Fig. 28a). The analysis confirmed the same abnormal and atypical features that has been already shown

for both embryonic and postnatal brain vasculature, with the curly phenotype interesting mainly the big vessels (both arteries and veins) departing from the centre of the retina. Although vessel density did not result to be significantly different between WT and ECKO animals at all analysed stages (Fig. 28b), Fgfbp1 ECKO presented an accelerated vascular growth during the initial phases of retina vascularization, as shown by the quantification of the radial growth of angiogenic area from the retina centre towards the periphery (Fig. 28c; newborn: $p<0.05$; 1 week: $p<0.01$). Consistently, the observation of the angiogenic leading front at retina periphery revealed an increased number of filopodia protruding from the tip-cells, the endothelial cells responsible for migration, in 1 week old Fgfbp1 ECKO mice compared to age-matched control animals (Fig. 28a, asterisks). In addition, 1 week after birth also the number of vessel branching points at the periphery was increased in ECKO animals, while the number of branches from the big arteries and veins departing from the centre of the retina remained unchanged (Fig. 28d). Interestingly, both arterial/venous and peripheral branching points tended to decrease at 2 and 3 weeks of age, possibly as a result of a vascular remodeling process; this process mainly seemed to occurr to equal extents both in WT and ECKO animals, except for a significative reduction of branching points from veins in Fgfbp1 ECKO animals at 2 weeks (Fig. 28d; $p<0.05$).

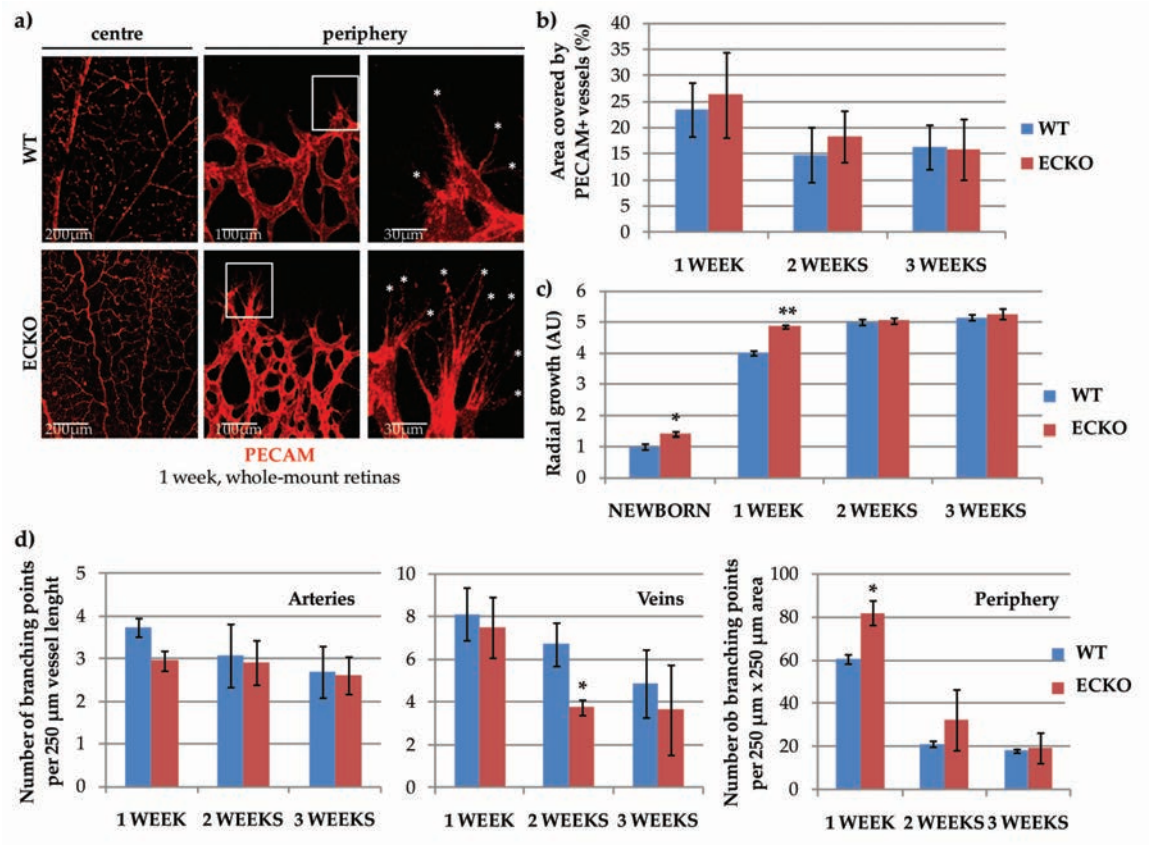

Figure 28. Analysis of retinal vasculature in Fgfbp1 WT and ECKO mice at different postnatal ages

(a) Representative images of confocal Z-stacks of whole mount retinas of Fgfbp1 WT and ECKO mice at 1week of age. Retinas were immunostained for the endothelial marker PECAM. Scale bars: 200 µm, 100 µm and 30 µm. **(b)** Quantification of the vascular density (percentage of area covered by PECAM positive vessels) of Fgfbp1 WT and ECKO mice at 1, 2 and 3 weeks of age. For each age group, 4 WT and 6 ECKO mice were analyzed. **(c)** Quantification of vascular radial growth (measured as distance between retina centre and angiogenic leading front) of Fgfbp1 WT and ECKO mice soon after birth (1 dpn) and at 1, 2 and 3 weeks of age. For each age group, 4 WT and 6 ECKO mice were analyzed. *: $p<0.05$; **: $p<0.01$ **(d)** Quantification of the number of vessel branching points of Fgfbp1 WT and ECKO mice at 1, 2 and 3 weeks of age. For arteries and veins, the number of branching points per 250 µm vessel length is reported; for the peripheral vessels, the number of branching points per field (250 µm x 250 µm area) is indicated. For each age group, 4 WT and 6 ECKO mice were analyzed. *: $p<0.05$

3.3.3 Fgfbp1 ECKO mice show alterations in the ultrastructural organization of the NVU

To deeply investigate the origin of the vascular abnormalities observed in Fgfbp1 ECKO mice and to evaluate the overall organization of the NVU after Fgfbp1 deletion, we performed electron microscopy on brain cortexes of Fgfbp1 WT and ECKO 1 month old mice.

In control animals, blood capillaries in the cortex exhibited typical features: they contained rather few caveolae, their TJs were well developed and almost around each profile it was possible to find the processes of pericytes, that were surrounded by the same BM of endothelial cells (eBM).

Conversely, some obvious alterations were found in the cortex of Fgfbp1 ECKO animal. The section of capillaries was not roundish as in control animals, but mostly oval or oblong, with a reduction in the thickness of the endothelial wall; on the other hand, both the structure of the TJs and the number of caveolae were unchanged.

Not only the endothelial layer was altered in Fgfbp1 ECKO animals, but also the other components of the NVU resulted to be impaired: pericyte processes (Fig. 29, asterisks) around capillary sections were quite rare and the BM (Fig. 29, arrowheads) was much thinner than in control animals; moreover, in many cases the layer of astrocytes surrounding the capillary and adjacent to the BM was swollen (Fig. 29, arrows) and the contacts between neighboring perivascular astrocytes (Fig. 29, boxed area) were tighter compared to WT animals.

Overall, the data collected from the electron microscopy analysis indicate that alterations in the organization of the NVU were present in Fgfbp1 ECKO mice compared to control animals.

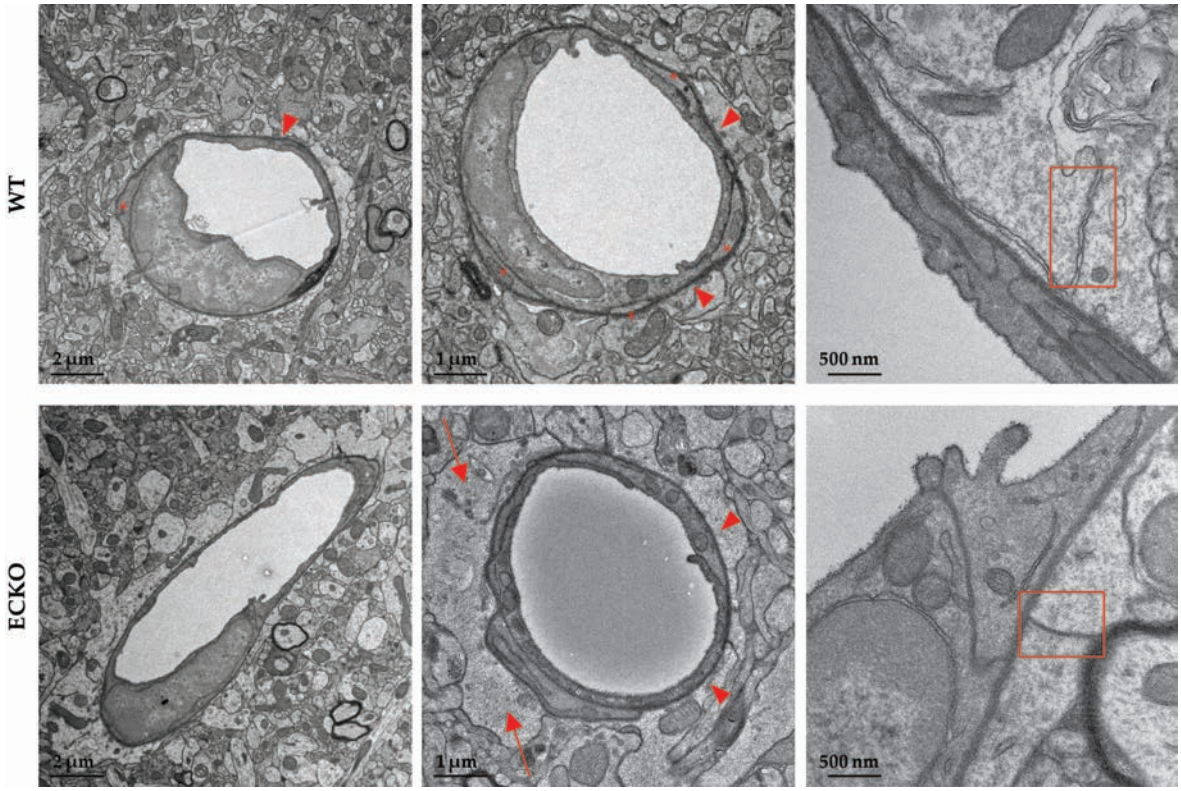

Figure 29. Electron microscopy analysis of ultrastructural organization of the NVU in Fgfbp1 WT and ECKO mice

Representative images of electron microscopy (EM) analysis of the brain cortex of 1 month old Fgfbp1 WT and ECKO mice. 60 nm thick sections from three animals per group were analyzed. Asterisks: pericyte processes; arrowheads: basement membrane; arrows: astrocyte swollening; boxed areas: inter-astrocytic junctions. Scale bars: 2 µm, 1 µm ad 500 nm.

3.3.4 Fgfbp1 ECKO brain vasculature displays defects in pericyte coverage and BM composition

Starting from the information obtained by the electron microscopy experiments, we decided to further investigate the organization of the NVU in Fgfbp1 WT and ECKO mice at different postnatal ages.

The observation that cortex blood capillaries of ECKO animals were rarely associated to pericyte processes suggested the possibility that the number of pericytes might be reduced in ECKO mice compared to control mice. To test this hypothesis we performed an immunostaining for the pericyte marker PDGFRβ on brain sections (Fig. 30a) and quantified the number of PDGFRβ positive pericyte cell bodies; we found that, at all analyzed ages (1, 2 and 3 weeks) the pericytes number was at least 30% lower in Fgfbp1 ECKO mice compared to their age-matched controls (Fig. 30b, $p<0.05$).

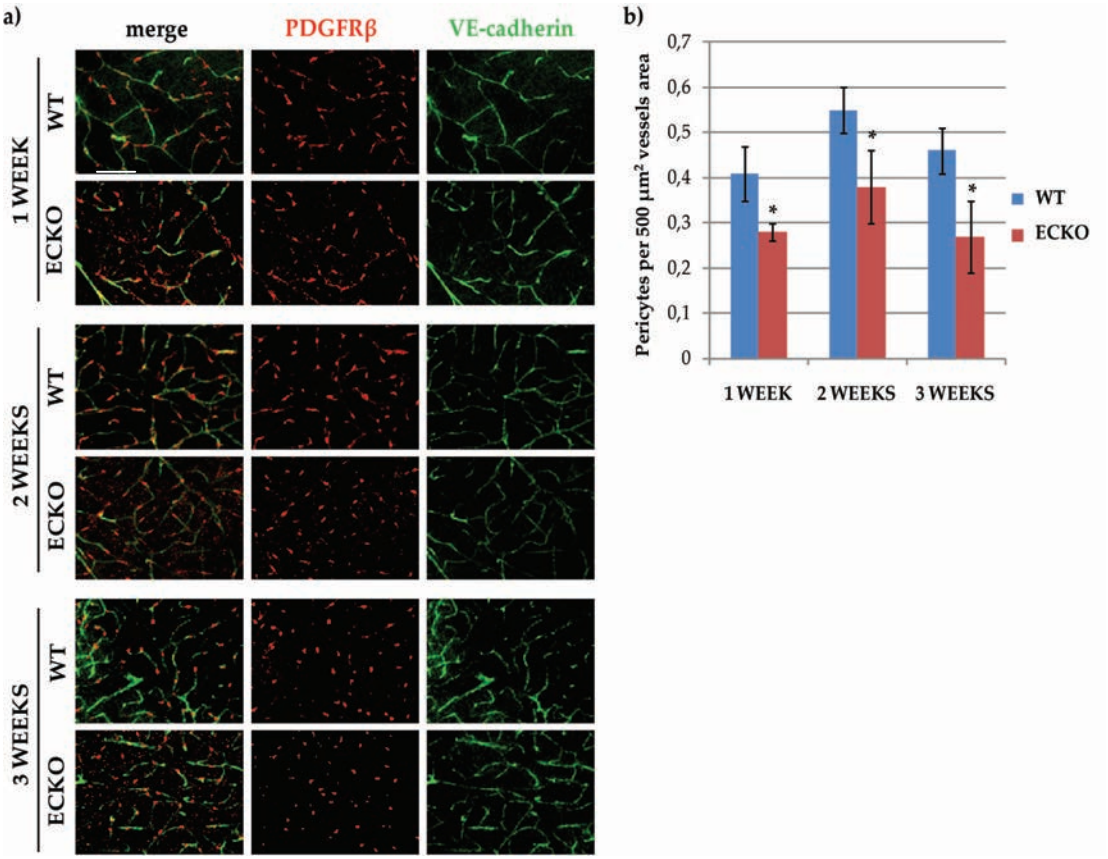

Figure 30. Quantification of pericytes number in Fgfbp1 WT and ECKO mice at different ages

(a) Representative images of confocal Z-stacks of brain sections (100 µm thickness) of Fgfbp1 WT and ECKO mice at 1, 2 and 3 weeks of age. Sections were immunostained for the endothelial marker VE-cadherin and for the pericyte marker PDGFRβ. Scale bar: 200 µm. (b) Quantification of the number of PDGFRβ positive pericytes (measured as number of pericytes per 500 µm² vessel area) of Fgfbp1 WT and ECKO mice at 1, 2 and 3 weeks of age. For each age group, 2 WT and 3 ECKO mice were analyzed. *: $p<0.05$.

To further investigate the pericyte phenotype, we checked also for the expression of two other pericyte markers: NG2, a proteoglycan mainly expressed by pericyte precursors, and desmin, an intermediate filament component commonly expressed by quiescent pericytes [29].

As shown by Fig. 31, 1 week old ECKO mice display an increased expression of NG2 compared to WT controls, suggesting that pericyte precursors are even more recruited to blood capillaries. However at later ages both NG2 and desmin are less expressed in the ECKO mice compared to WT, possibly indicating that the reduction of the number of pericytes might be due to a defect in their capability to maintain their interaction with the endothelium and/or in their maturation rather than to a defect in their recruitment.

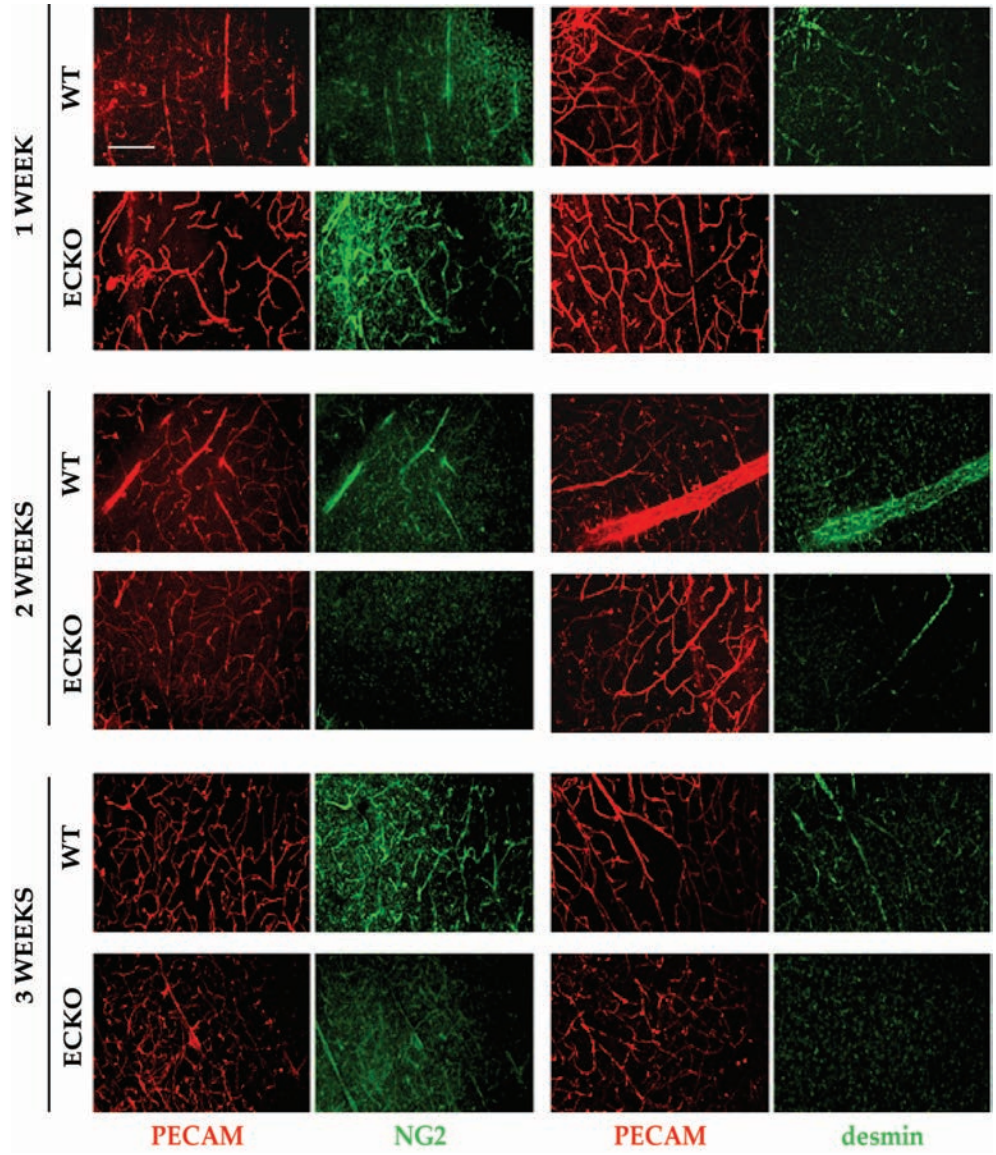

Figure 31. Analysis of the pericyte phenotype in Fgfbp1 WT and ECKO mice at different ages

Representative images of confocal Z-stacks of brain sections (100 μm thickness) of Fgfbp1 WT and ECKO mice at 1, 2 and 3 weeks of age. Sections were immunostained for the endothelial marker PECAM and for the pericyte markers NG2 and desmin. Scale bar: 200 μm.

To investigate possible defects in astrocyte organization and more in particular in astrocyte endfeet polarization, we immunostained the sections for the astrocyte endfeet marker aquaporin IV, that resulted to be equally expressed and correctly polarized in both Fgfbp1 WT and ECKO at all analyzed stages (Fig. 32).

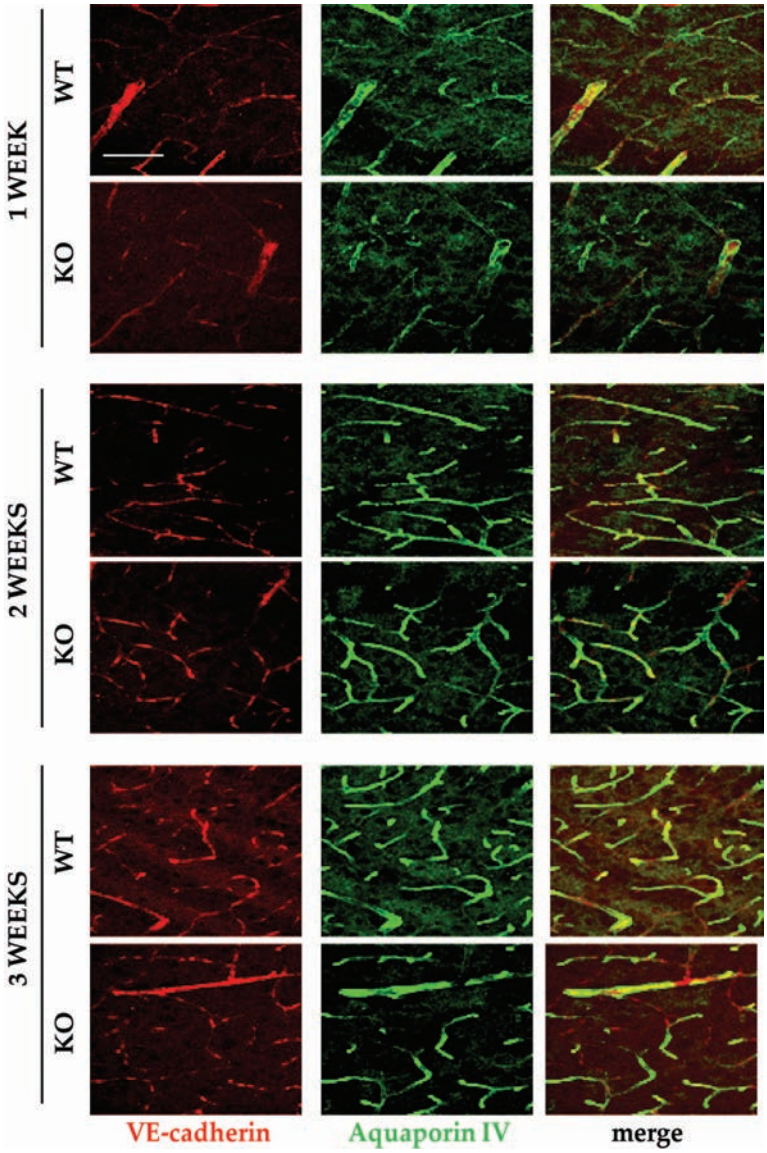

Figure 32. Analysis of astrocyte endfeet polarization by aquaporin IV immunostaining

Representative images of confocal Z-stacks of brain sections (100 μm thickness) of Fgfbp1 WT and ECKO mice at 1, 2 and 3 weeks of age. Sections were immunostained for the endothelial marker VE-cadherin and the astrocyte endfeet marker aquaporin IV. Scale bar: 100 μm.

Finally, taking into account the reduction of the BM thickness detected by EM experiments, we sought to investigate in depth the composition of the BM by analyzing one by one the expression and the vessel coverage of the main BM proteins: Collagen IV, both in the trimeric form and the single chains α1 (Col4a1)

and α2 (Col4a2), and Laminins, both the eBM-specific laminin α4 and α5 and the pBM-specific laminin α2.

By immunostaining analysis, Collagen IV resulted to be decreased in brain sections of Fgfbp1 ECKO mice at 1, 2 and 3 weeks compared to their age-matched controls (Fig. 33a); after quantification of the confocal images we found that both vessel coverage (measured as the percentage of collagen IV positive endothelium) (Fig. 33b) and overall expression levels (measured as mean fluorescence intensity) (Fig. 33c) were reduced, even though the reduction in overall expression levels resulted to be statistically significative only in 3 weeks old mice (Fig. 33c; $p<0.05$).

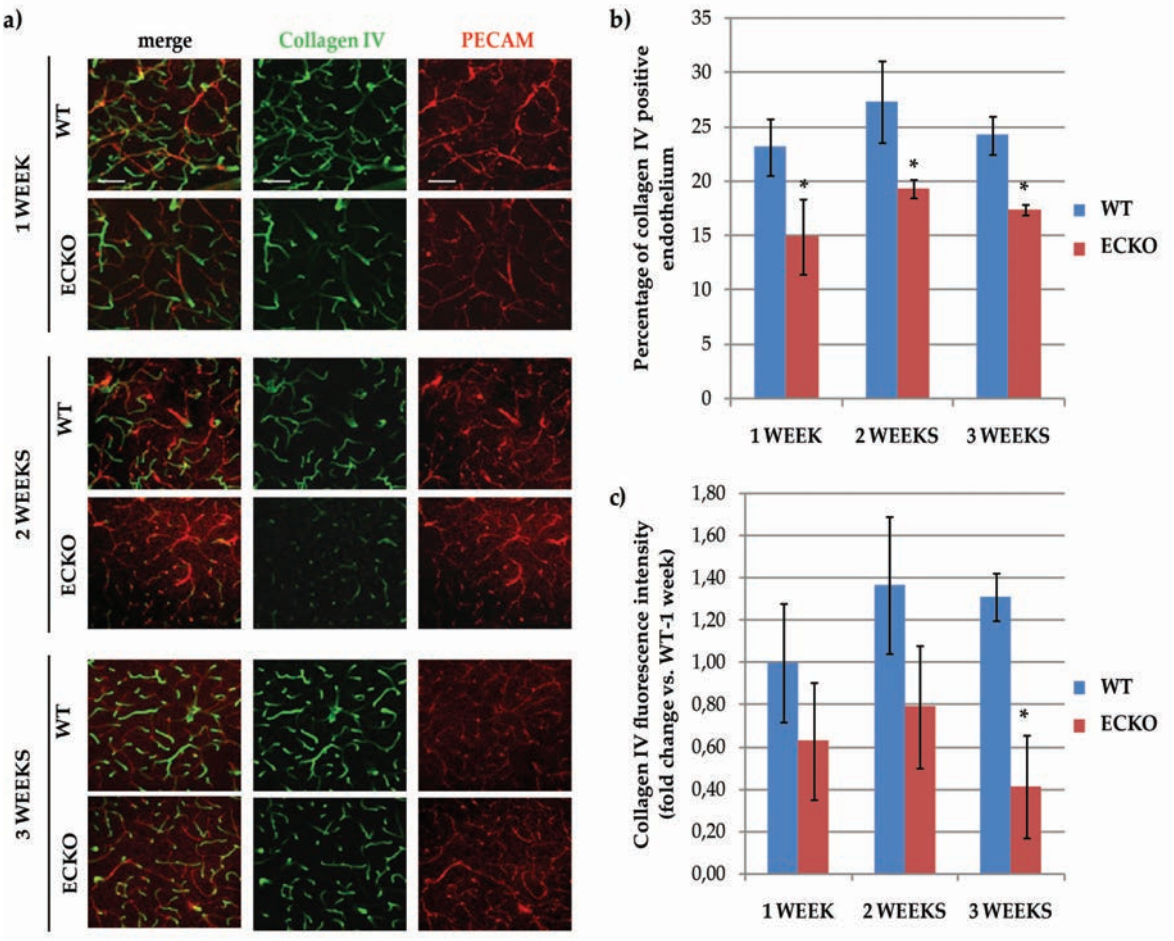

Figure 33. Analysis of collagen IV expression and coverage in Fgfbp1 WT and ECKO mice at different ages

(a) Representative images of confocal Z-stacks of brain sections (100 μm thickness) of Fgfbp1 WT and ECKO mice at 1, 2 and 3 weeks of age. Sections were immunostained for the endothelial marker PECAM and the BM protein collagen IV. Scale bar: 100 μm. **(b)** Quantification of collagen IV vessel coverage (measured as percentage of collagen IV positive endothelium) in Fgfbp1 WT and ECKO mice at 1, 2 and 3 weeks of age. For each age group, 2 WT and 3 ECKO mice were analyzed. *: $p<0.05$. **(c)** Quantification of collagen IV expression (measured as mean collagen IV fluorescence intensity) in Fgfbp1 WT and ECKO mice at 1, 2 and 3 weeks of age. For each age group, 2 WT and 3 ECKO mice were analyzed. *: $p<0.05$.

Given the alterations in Collagen IV expression and coverage, we went on analyzing the single collagen IV chains, $\alpha 1$ and $\alpha 2$, that are known from the literature to be produced and secreted by ECs.

Collagen IV α1 chain (Col4a1) staining revealed some small differences between Fgfbp1 WT and ECKO at different stages (Fig. 34a); however by quantification none of these differences resulted to be statistically significant, neither in terms of vessel coverage nor expression levels (Fig. 34b-c).

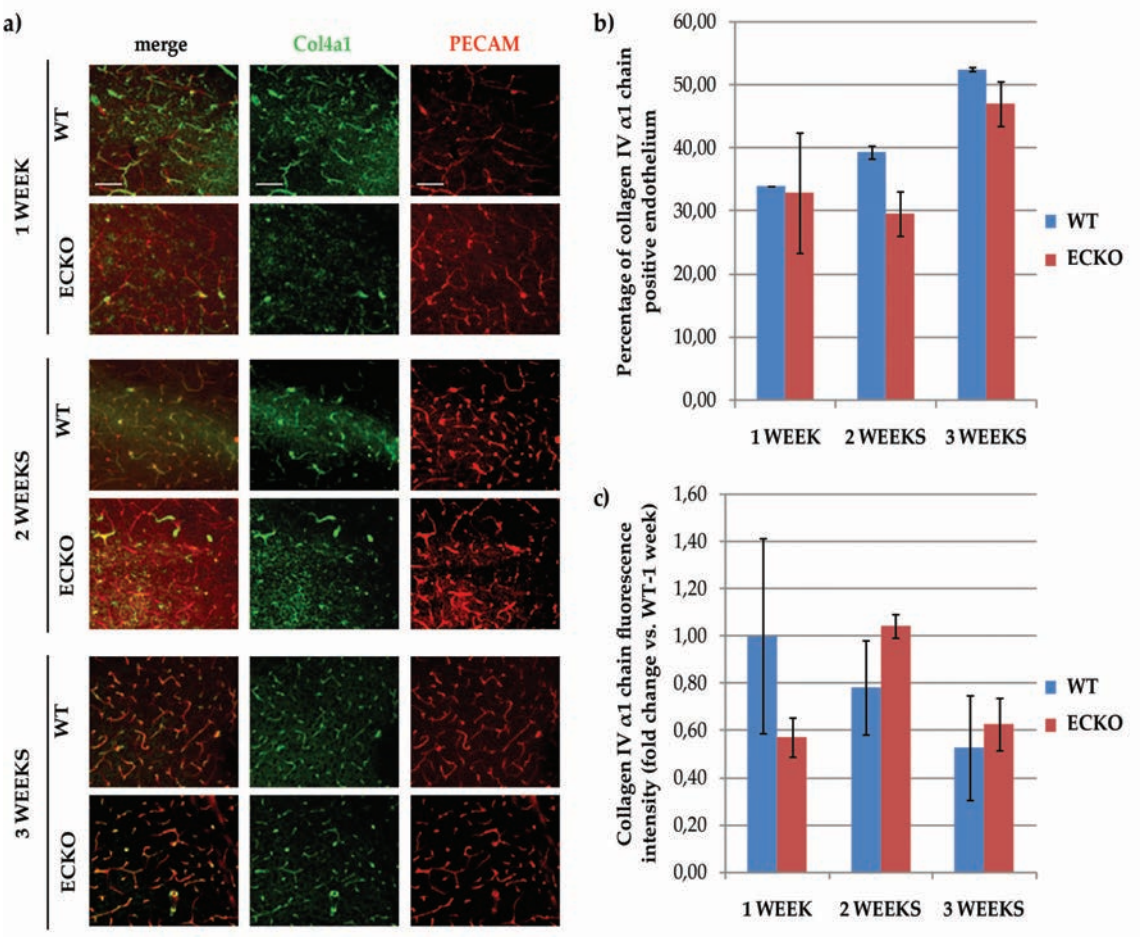

Figure 34. Analysis of collagen IV α1 chain (Col4a1) expression and coverage in Fgfbp1 WT and ECKO mice at different ages

(a) Representative images of confocal Z-stacks of brain sections (100 μm thickness) of Fgfbp1 WT and ECKO mice at 1, 2 and 3 weeks of age. Sections were immunostained for the endothelial marker PECAM and the BM protein Col4a1. Scale bar: 100 μm. **(b)** Quantification of Col4a1 vessel coverage (measured as percentage of Col4a1 positive endothelium) in Fgfbp1 WT and ECKO mice at 1, 2 and 3 weeks of age. For each age group, 2 WT and 3 ECKO mice were analyzed. **(c)** Quantification of Col4a1 expression (measured as mean Col4a1 fluorescence intensity) in Fgfbp1 WT and ECKO mice at 1, 2 and 3 weeks of age. For each age group, 2 WT and 3 ECKO mice were analyzed.

Regarding collagen IV α2 chain (Col4a2) (Fig. 35a), no major differences were detectable except a small and non statistically significant decrease in vessel coverage in Fgfbp1 ECKO mice at 3 weeks (Fig. 35b), and a substantial increase in expression in ECKO animals at 1 week (Fig. 35c; $p<0.05$).

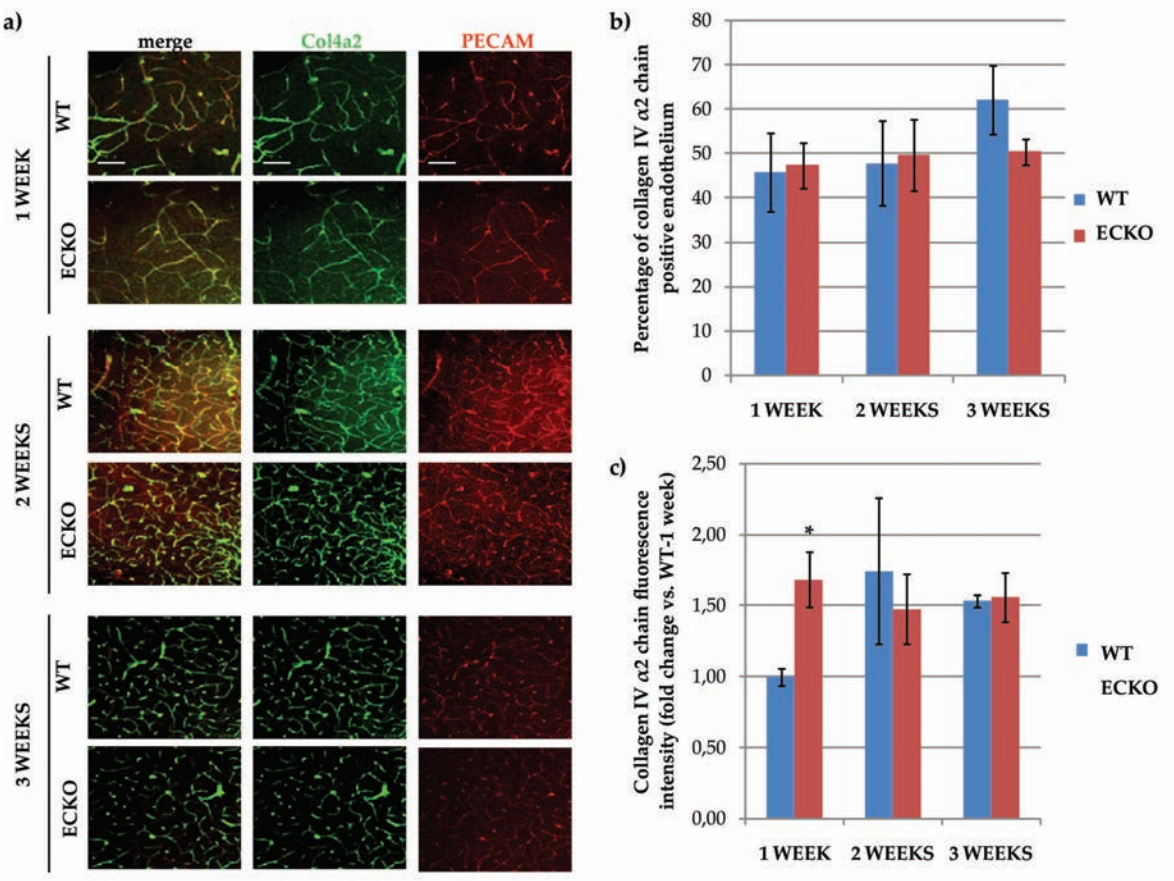

Figure 35. Analysis of collagen IV α2 chain (Col4a2) expression and coverage in Fgfbp1 WT and ECKO mice at different ages

(a) Representative images of confocal Z-stacks of brain sections (100 µm thickness) of Fgfbp1 WT and ECKO mice at 1, 2 and 3 weeks of age. Sections were immunostained for the endothelial marker PECAM and the BM protein Col4a2. Scale bar: 100 µm. **(b)** Quantification of Col4a2 vessel coverage (measured as percentage of collagen IV α2 chain positive endothelium) in Fgfbp1 WT and ECKO mice at 1, 2 and 3 weeks of age. For each age group, 2 WT and 3 ECKO mice were analyzed. **(c)** Quantification Col4a2 expression (measured as mean collagen IV α2 chain fluorescence intensity) in Fgfbp1 WT and ECKO mice at 1, 2 and 3 weeks of age. For each age group, 2 WT and 3 ECKO mice were analyzed. *: $p<0.05$.

The analysis of laminins started from the characterization of the components of the eBM laminin α4 and laminin α5.

Laminin α4 was found to be expressed more or less equally, both in terms of vessel coverage and expression levels, in Fgfbp1 WT and ECKO mice at 2 and 3 weeks, with a slightly lower expression in 1 week old ECKO mice compared to age-matched controls (Fig. 36).

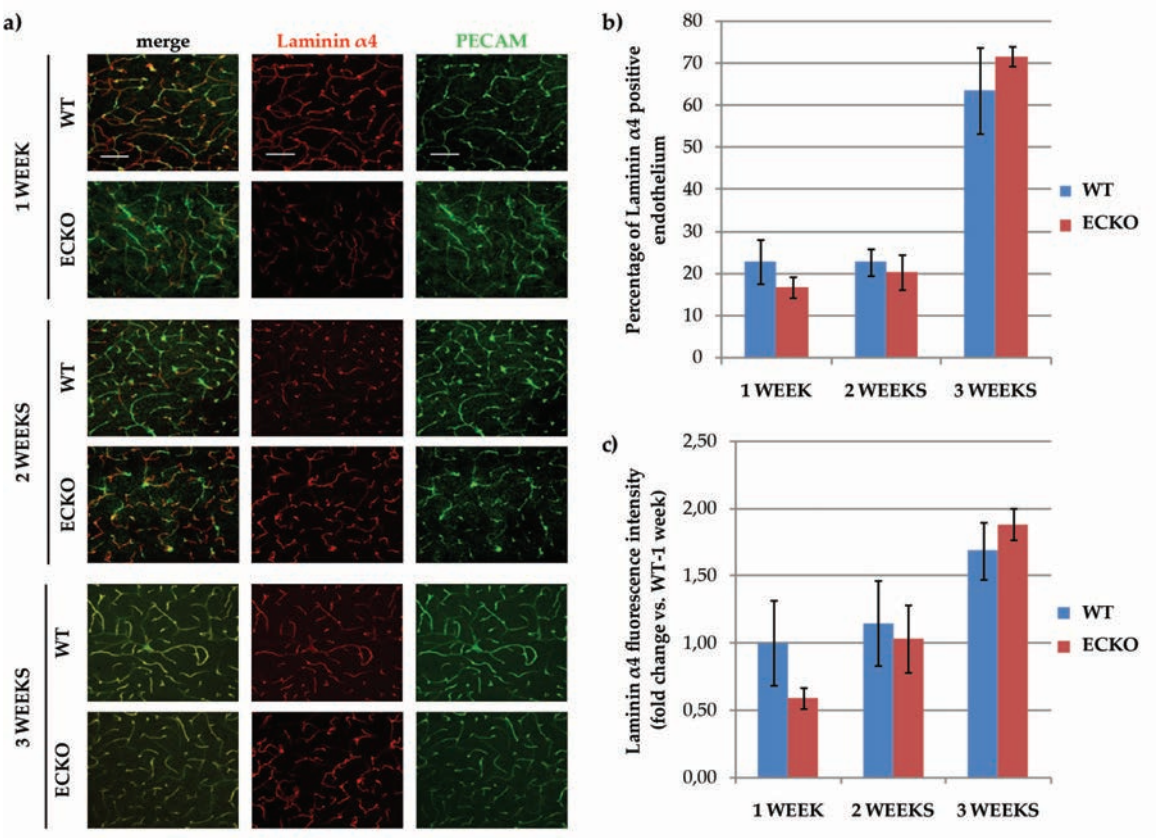

Figure 36. Analysis of laminin α4 expression and coverage in Fgfbp1 WT and ECKO mice at different ages

(a) Representative images of confocal Z-stacks of brain sections (100 μm thickness) of Fgfbp1 WT and ECKO mice at 1, 2 and 3 weeks of age. Sections were immunostained for the endothelial marker PECAM and the BM protein laminin α4. Scale bar: 100 μm. **(b)** Quantification of laminin α4 vessel coverage (measured as percentage of laminin α4 positive endothelium) in Fgfbp1 WT and ECKO mice at 1, 2 and 3 weeks of age. For each age group, 2 WT and 3 ECKO mice were analyzed. **(c)** Quantification of laminin α4 expression (measured as mean laminin α4 chain fluorescence intensity) in Fgfbp1 WT and ECKO mice at 1, 2 and 3 weeks of age. For each age group, 2 WT and 3 ECKO mice were analyzed.

Conversely, regarding laminin α5, the immonostaining analysis (Fig. 37a) and its related quantifications (Fig. 37b-c) revealed a higher vessel coverage ($p<0.05$) and expression level of laminin α5 in Fgfbp1 ECKO mice compared to control animals; however, while at later stages (2 and 3 weeks) both the coverage and the expression tended to increase time-dependently in WT animals, they remained roughly unchanged in ECKO mice, finally resulting in an overall decrease in both vessel coverage and expression of laminin α5 in Fgfbp1 ECKO mice compared to controls.

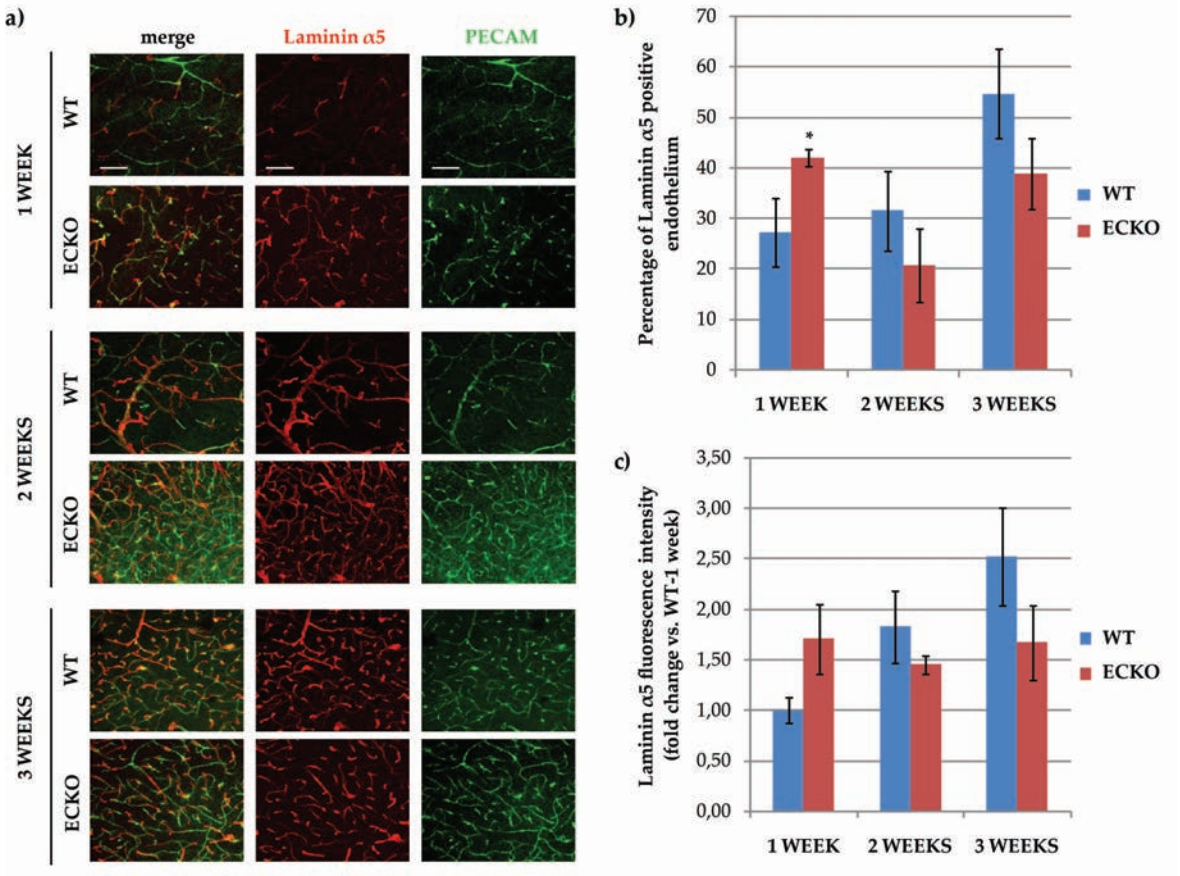

Figure 37. Analysis of laminin α5 expression and coverage in Fgfbp1 WT and ECKO mice at different ages

(a) Representative images of confocal Z-stacks of brain sections (100 μm thickness) of Fgfbp1 WT and ECKO mice at 1, 2 and 3 weeks of age. Sections were immunostained for the endothelial marker PECAM and the BM protein laminin α5. Scale bar: 100 μm. **(b)** Quantification of laminin α5 vessel coverage (measured as percentage of laminin α5 positive endothelium) in Fgfbp1 WT and ECKO mice at 1, 2 and 3 weeks of age. For each age group, 2 WT and 3 ECKO mice were analyzed. *: $p<0.05$ **(c)** Quantification of laminin α5 expression (measured as mean laminin α5 chain fluorescence intensity) in Fgfbp1 WT and ECKO mice at 1, 2 and 3 weeks of age. For each age group, 2 WT and 3 ECKO mice were analyzed.

Finally, we analyzed the pBM component laminin α2, that did not result to vary remarkably between Fgfbp1 WT and ECKO animals, except for a slight increase in coverage in 2 weeks old ECKO mice and a slight, not statistically significant, decrease in expression in the same mice at 1 week (Fig. 38).

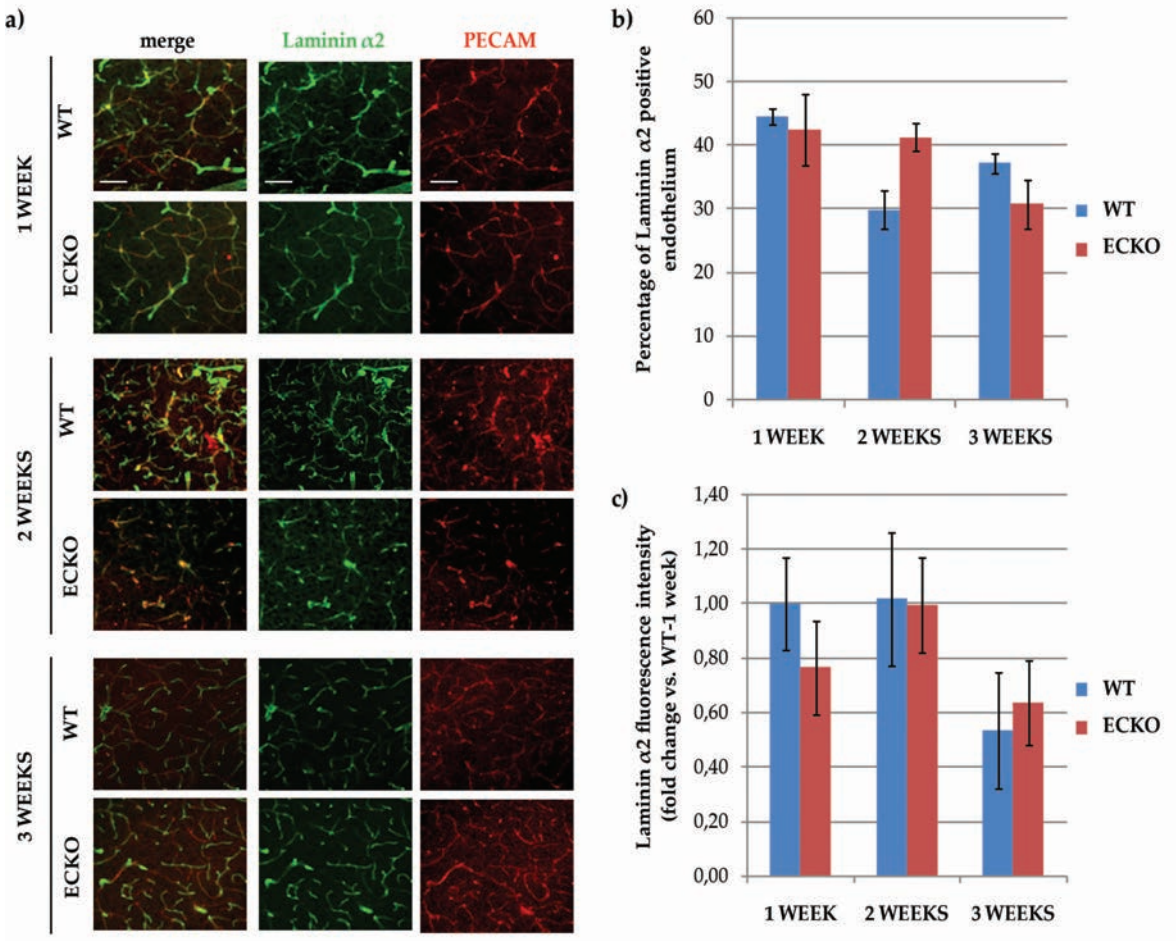

Figure 38. Analysis of laminin α2 expression and coverage in Fgfbp1 WT and ECKO mice at different ages

(a) Representative images of confocal Z-stacks of brain sections (100 µm thickness) of Fgfbp1 WT and ECKO mice at 1, 2 and 3 weeks of age. Sections were immunostained for the endothelial marker PECAM and the BM protein laminin α2. Scale bar: 100 µm. **(b)** Quantification of laminin α2 vessel coverage (measured as percentage of laminin α2 positive endothelium) in Fgfbp1 WT and ECKO mice at 1, 2 and 3 weeks of age. For each age group, 2 WT and 3 ECKO mice were analyzed. **(c)** Quantification of laminin α2 expression (measured as mean laminin α2 chain fluorescence intensity) in Fgfbp1 WT and ECKO mice at 1, 2 and 3 weeks of age. For each age group, 2 WT and 3 ECKO mice were analyzed.

The overmentioned immunostaining results were obtained by performing an initial unmasking with pepsin (see "Materials and methods") to exclude the possibility that the observed differences might be due to the presence of other

molecules masking the antigen of interest; importantly, however, the same differences were detectable also in non-pepsin treated samples (data not shown). Overall, as shown by the analysis of the BM composition (summarized in Table 6), the results point out to the possibility that endothelial-specific deletion of Fgfbp1 gene might cause a collective rearrangement of the BM, due to changes (sometimes also rather subtle) in the balance of the single BM components.

	Fgfbp1 ECKO vs. WT					
	Coverage			Expression		
	1 week	*2 weeks*	*3 weeks*	*1 week*	*2 weeks*	*3 weeks*
Collagen IV (trimeric)	--	--	--	-	-	--
Collagen IV α1 chain (Col4a1)	=	-	-	-	+	=
Collagen IV α2 chain (Col4a2)	=	=	-	++	=	=
Laminin α4	-	=	=	-	=	=
Laminin α5	++	-	-	+	-	-
Laminin α2	=	++	-	-	=	=

Table 6. Summary table of the modification detected in the BM of Fgfbp1 ECKO mice

++: increase (statistically significant);

+: increase (not statistically significant);

--: decrease (statistically significant);

-: decrease (not statistically significant);

=: unchanged.

To determine whether the modifications in the BM composition were due to alterations in the production by the ECs, we isolated brain microvascular fragments from 1 week old and 3 weeks old Fgfbp1 WT and ECKO mice and checked, by qRT-PCR, the expression of genes encoding for the endothelial-derived BM components Col4a1, Col4a2, laminin α4 and laminin α5.

The analysis showed that, except for a reduction in laminin α4 expression in the endothelium of 1 week old Fgfbp1 ECKO mice, neither collagen IV chains nor laminin α5 were significantly modified, indicating that the alterations in BM deposition were not attributable to a defective production by brain ECs (Fig. 39).

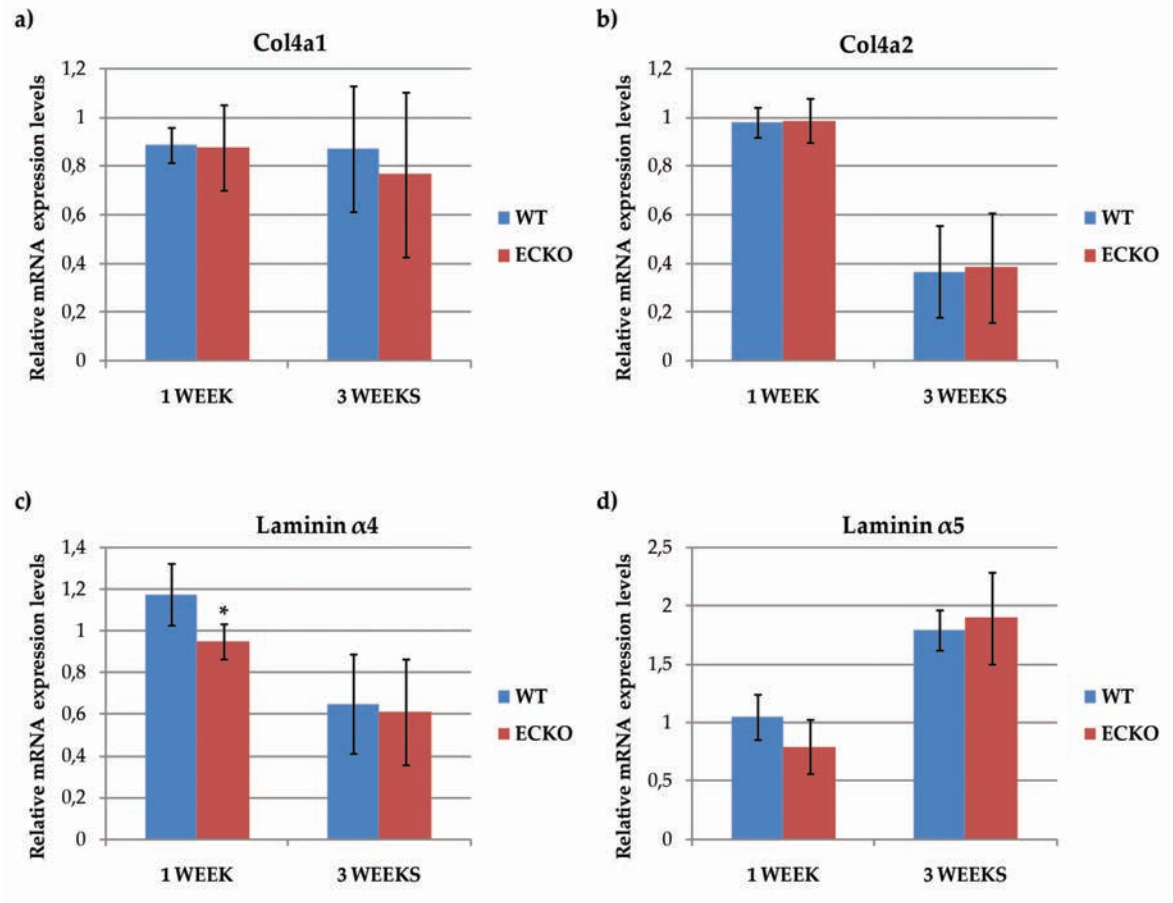

Figure 39. Analysis of expression of endothelial-derived BM components in 1 week old and 3 weeks old Fgfbp1 WT and ECKO mice

qRT-PCR analysis of the endothelial-derived BM components **(a)** Col4a1, **(b)** Col4a2, **(c)** laminin α4 and **(d)** laminin α5 in ECs freshly isolated from the brain of 1 week old and 3 weeks old Fgfbp1$^{flox/flox}$/VEC-PAC mice injected (ECKO) or not (WT) with tamoxifen. The levels of mRNA are normalized on 18S. Data are presented as mean ± standard deviation of the analyzed samples (1 week WT: n=7, ECKO: n=4; 3 weeks WT: n=4; ECKO: n=6). *: $p<0.05$

These data, together with the observation that Fgfbp1 ECKO animals show a decreased number of vessel-associated pericytes, suggest that endothelial-derived

FGFBP1 might be involved in the regulation of the cell-cell and cell-BM interactions within the NVU.

3.3.5 Fgfbp1 ECKO mice present increased BBB permeability

To functionally characterize the phenotype of Fgfbp1 ECKO animals, we investigated the status of BBB permeability by injecting 10 dpn mice with Alexa555-labeled cadaverine (molecular weight: ~950 Dalton) and searching for areas of tracer extravasation within the brain.

Since after extravasation Alexa555-cadaverine is intercepted by neurons, that absorb it acquiring a red staining (example in Fig. 40a) [61], we quantified the number of Alexa555-cadaverine positive neurons per field as a measure of the amount of dye that extravasated and found out a strong increase in BBB vessel permeability in Fgfbp1 ECKO animals compared to controls (Fig. 40b; $p<0.05$).

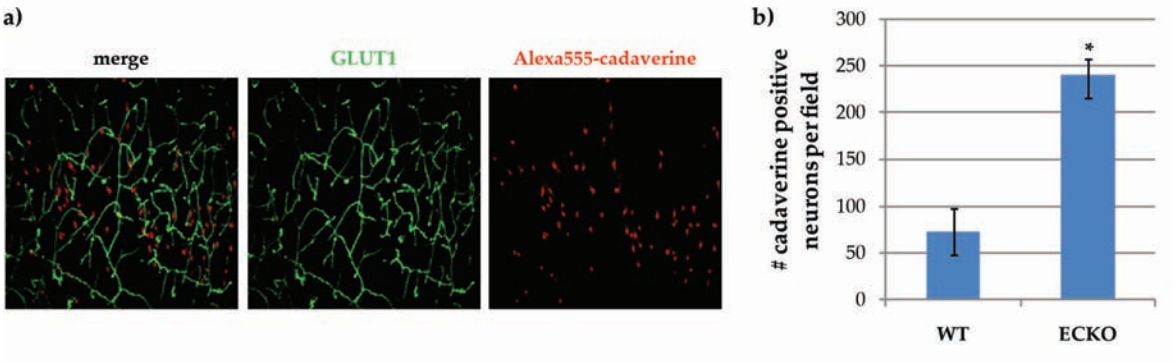

Figure 40. Analysis of BBB permeability by quantification of Alexa555-cadaverine leakage

(a) Representative image of a brain section were Alexa555-cadaverine leakage is detected. Sections (100 µm thickness) were immunostained for the BBB marker GLUT1. **(b)** Quantification of Alexa555-cadaverine leakage (measured as number of cadaverine positive neurons per 20x magnification field) in Fgfbp1 WT and ECKO mice at 10 dpn. *: $p<0.05$.

To determine whether this increase in permeability was due to alterations in the organization of TJs, we performed an immunostaining for claudin-5; however from this analysis we could not detect any sign of junctional disorganization, leading us to exclude the possibility that the impairment in the control of BBB permeability in Fgfbp1 ECKO might be due to TJs dismantling (Fig. 41).

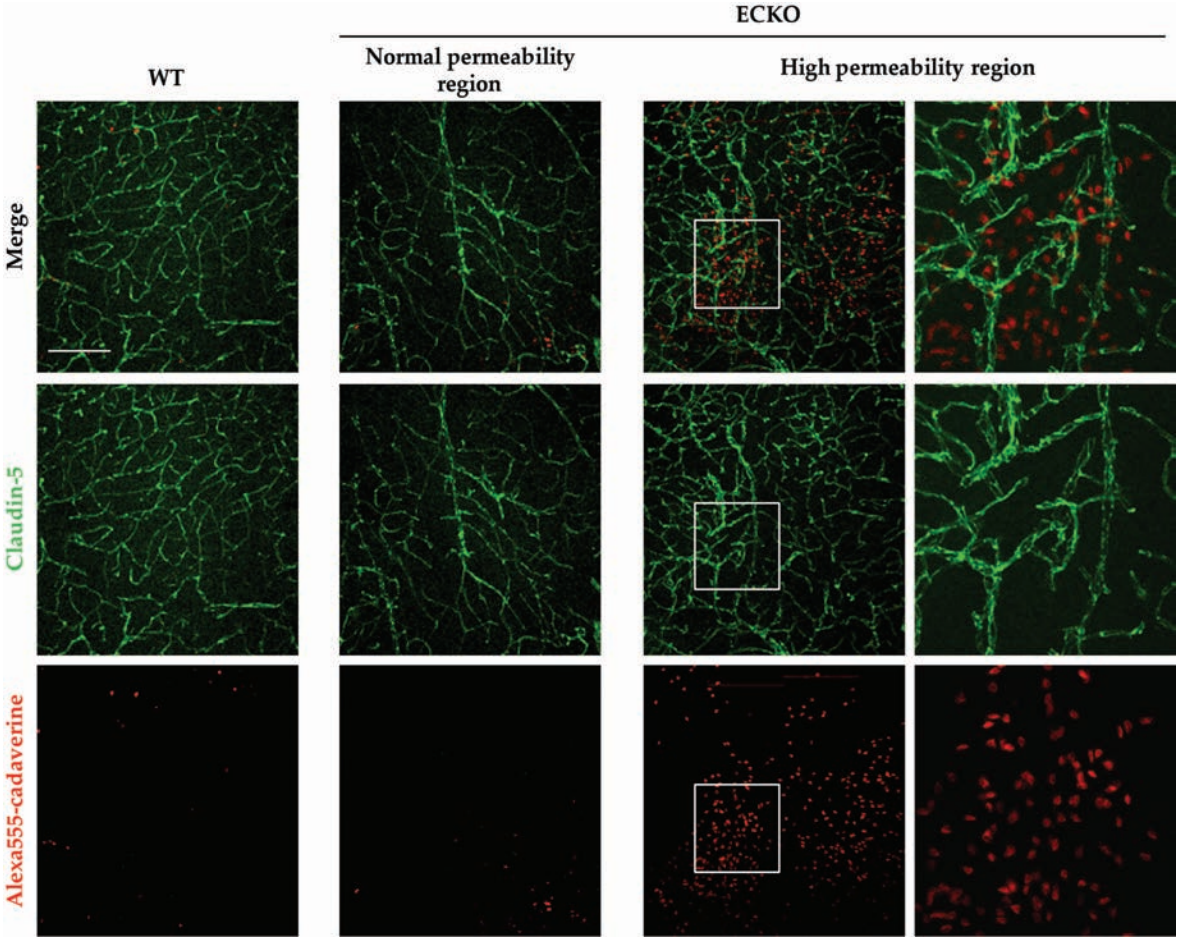

Figure 41. Analysis of correlation between increased BBB permeability and TJs organization
Representative images of confocal Z-stack images of brain sections (100 μm thickness) of Fgfbp1 WT and ECKO mice at 10 dpn after Alexa555-cadaverine injection. Sections were immunostained for the TJ marker claudin-5. Scale bar: 200 μm.

Opposite to what we observed regarding claudin-5, we found a correlation between the increased BBB permeability and the already described reduction in

collagen IV coverage. Indeed we detected a strong reduction in collagen IV coverage in the areas of increased vessel permeability were Alexa555-cadaverine extravasation occurred, while collagen IV coverage was normal in both control animals and ECKO animals in the areas with a normal permeability (no Alexa555-cadaverine extravasation) (Fig. 42).

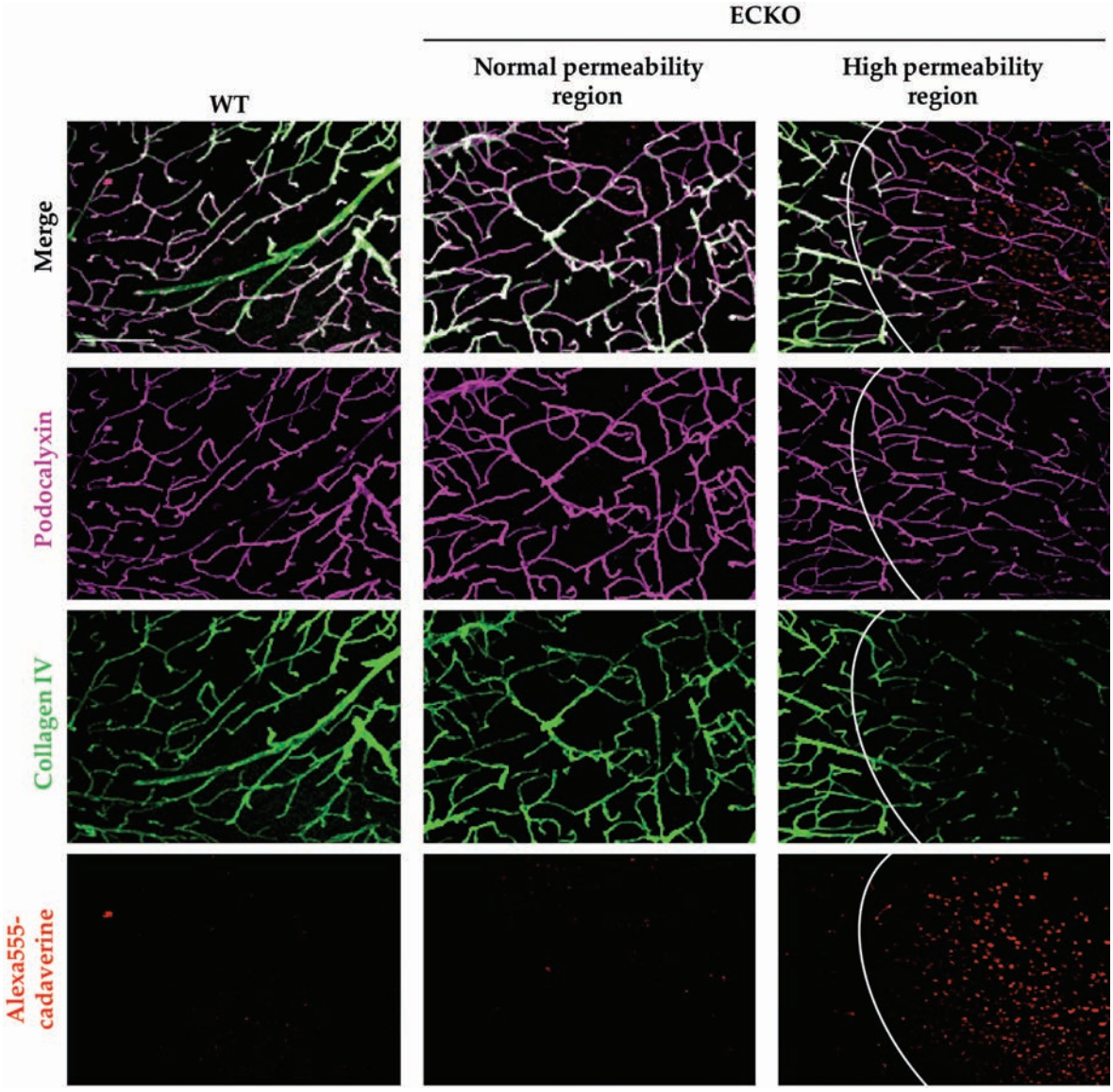

Figure 42. Analysis of correlation between increased BBB permeability and TJs organization

Representative images of confocal Z-stack images of brain sections (100 μm thickness) of Fgfbp1 WT and ECKO mice at 10 dpn after Alexa555-cadaverine injection. Sections were immunostained for the endothelial marker podocalyxin and for the BM protein collagen IV. Scale bar: 200 μm.

To further characterize the phenotype of Fgfbp1 ECKO animals, we investigated the status of the BBB permeability by checking for the leakage of high molecular weight molecules. To this purpose, we performed an immunostaining for IgG on brain sections of Fgfbp1 WT and ECKO mice at 1, 2 and 3 weeks of age and adult mice (4 months) and then quantified the number of IgG leakage areas per brain sagittal section.

As for Alexa555-cadaverine, we could not detect massive IgG leakage all over the brain sections, but only small areas of IgG extravasation (Fig. 43a). The quantifications of these "IgG spots" displayed a significant increase in the number of IgG leakage areas at 2 and 3 weeks in Fgfbp1 ECKO mice compared to age-matched controls ($p<0.05$); in addition, this phenotype resulted to be exacerbated in adult Fgfbp1 ECKO mice, even though some IgG spots were detectable also in WT mice of the same age ($p<0.01$) (Fig. 43b).

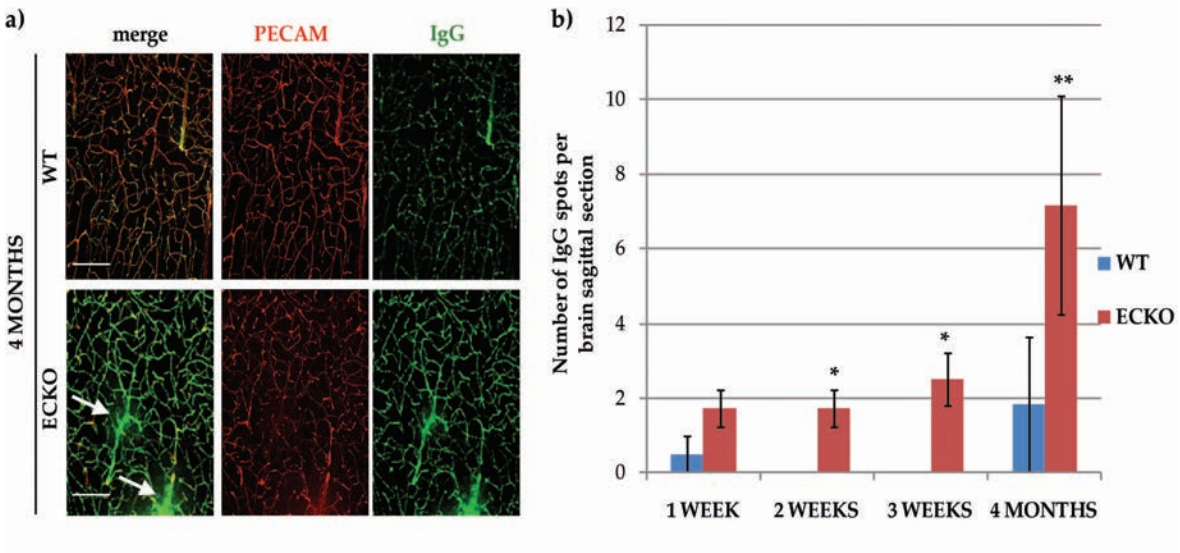

Figure 43. Analysis of IgG leakage in Fgfbp1 WT and ECKO brains

(a) Representative confocal Z-.stacks and (b) quantifications of IgG leakake spots in sagittal brain sections (100 μm thickness) from Fgfbp1 WT and ECKO mice at 1, 2 and 3 weeks and adult mice (4 months). Sections were immunostained for the endothelial marker PECAM and for IgG. At least 2 WT and 3 ECKO animals were analyzed per each stage. *: $p<0.05$; **: $p<0.01$.

With the intention of clarifying the mechanism responsible for the increase in permeability, we decided to analyze the expression of Plvap, a protein known to be downregulated in brain ECs by Wnt signaling activation during the establishment of the BBB and already reported to be associated to poor BBB differentiation [139].

From Plvap immunostaining (Fig. 44a) and its related quantification (Fig. 44b), we detected an increase in Plvap protein levels in Fgfbp1 ECKO mice compared to controls at all analyzed stages, reflecting a defect in protein downregulation at later stages of development in comparison to WT animals. Moreover, we also found that Plvap overexpression could justify the increase in IgG permeability,

since we observed a correlation between the areas of high Plvap expression and the presence of extravasated IgG (Fig. 44a).

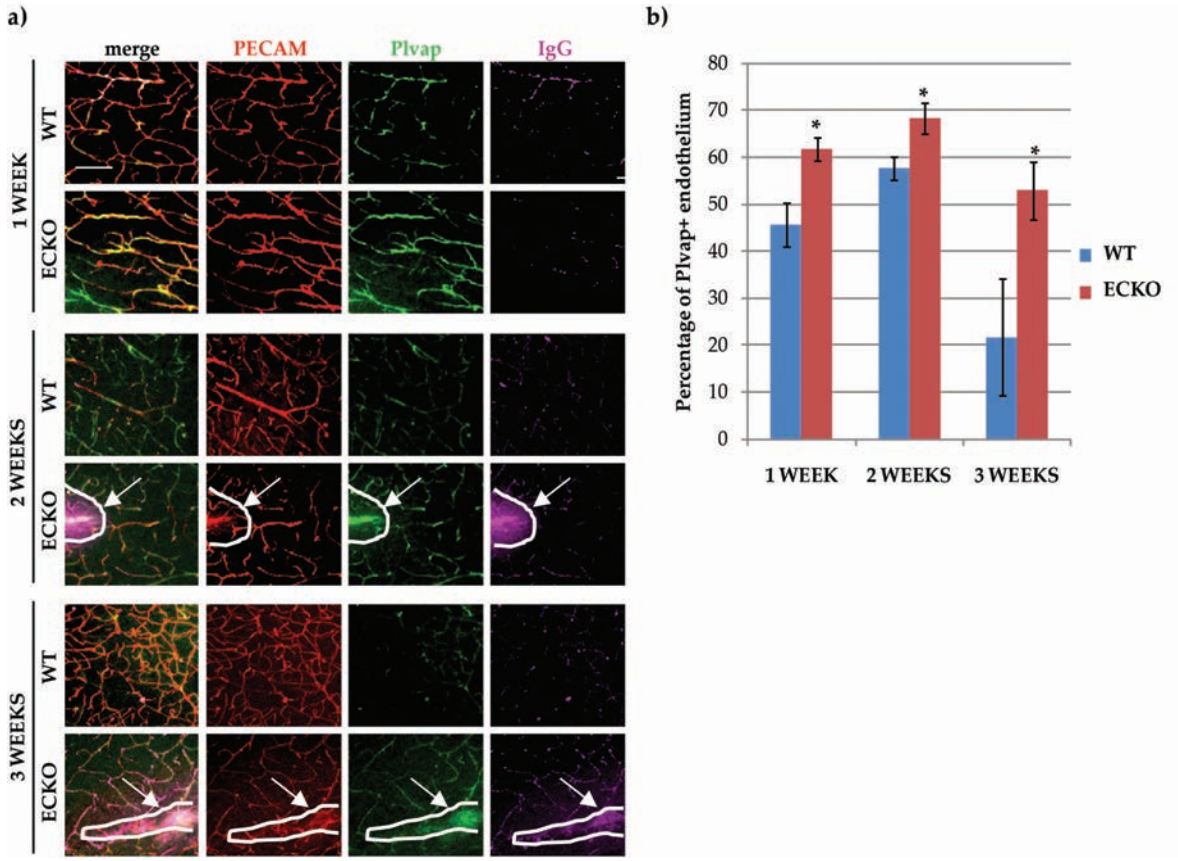

Figure 44. Correlation between IgG leakage and Plvap expression in Fgfbp1 ECKO mice

(a) Representative images of confocal Z-stack images of brain sections (100 μm thickness) of Fgfbp1 WT and ECKO mice at 1, 2 and 3 weeks of age. Sections were immunostained for the endothelial marker PECAM, for IgGs and for Plvap. Scale bar: 100 μm. **(b)** Quantification of the expression of Plvap in the brain endothelium of Fgfbp1 WT and ECKO mice at 1, 2 and 3 weeks of age. *: $p<0.05$.

3.3.6 Endothelial Fgfbp1 knock out does not alter BBB molecular signature

To determine whether endothelial-specific deletion of FGFBP1 could affect the expression of other typical molecular components of ECs at the BBB besides the NVU components reported in the previous sections, we isolated brain microvascular fragments from 1 week old and 3 weeks old Fgfbp1 WT and ECKO mice; we then checked, by qRT-PCR, the expression of genes encoding for

endothelial-specific BBB transporters and markers, as well as for junctional components.

The analysis showed that neither 1 week old (Fig. 45a) nor 3 weeks old (Fig. 45b) Fgfbp1 ECKO mice presented a molecular signature significantly different from the one of age-matched control animals, indicating that FGFBP1 deletion does not affect in general the transcriptional profile of the endothelial components of the BBB.

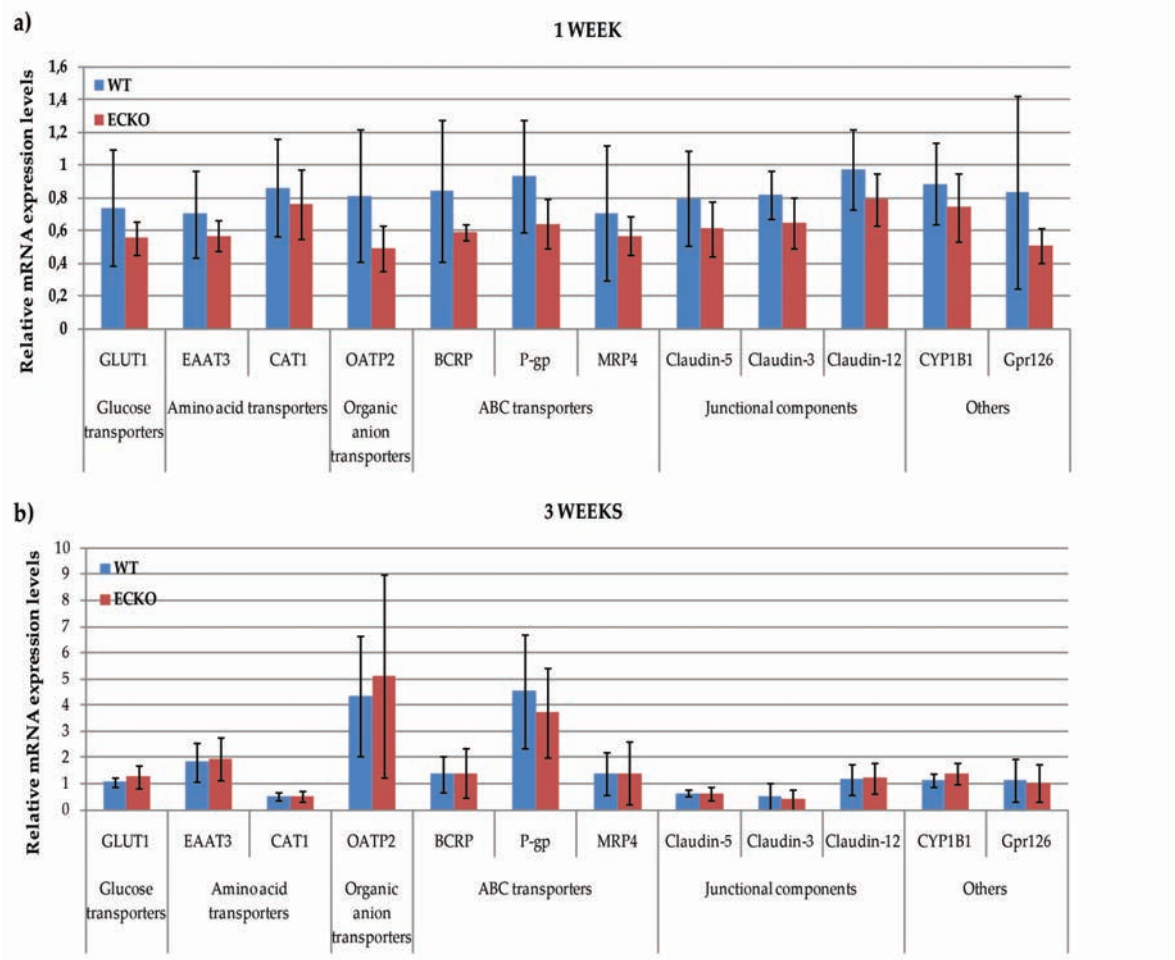

Figure 45. Analysis of BBB molecular signature in 1 week old and 3 weeks old Fgfbp1 WT and ECKO mice

qRT-PCR analysis of BBB molecular components in ECs freshly isolated from the brain of 1 week old and 3 weeks old Fgfbp1$^{flox/flox}$/VEC-PAC mice injected (ECKO) or not (WT) with tamoxifen. The levels of mRNA are normalized on 18S. Data are presented as mean ± standard deviation of the analyzed samples (1 week WT: n=7, ECKO: n=4; 3 weeks WT: n=4; ECKO: n=6).

3.4 Characterization of FGFBP1 expression and function in murine primary brain ECs (bMECs)

3.4.1 FGFBP1 is effectively downregulated *in vitro* by siRNA

The analysis of the phenotype arising from both the global (zebrafish) and the endothelial-specific (mouse) ablation of FGFBP1 highlighted the possibility that the responses mediated by FGFBP1 could be either directed towards the endothelium itself, to regulate cell-autonomous activities, or to different cell types interacting with endothelium, namely the components of the NVU.

To discriminate between these two types of responses, and in particular to identify the endothelial-cell autonomous activities of FGFBP1, we started taking advantage of the *in vitro* cultures of primary ECs isolated from murine brains (bMECs). To study the effect of FGFBP1 absence in this *in vitro* model, we designed three different siRNAs and tested their efficacy by checking for Fgfbp1 mRNA expression by Real Time PCR. All the three siRNA tested (siFGFBP1#1, #2 and #3) resulted to be effective in this *in vitro* setting, but the strongest Fgfbp1 mRNA downregulation was achieved by siFGFBP1#2 (Fig. 46; $p<0.01$), that was therefore selected for the following studies.

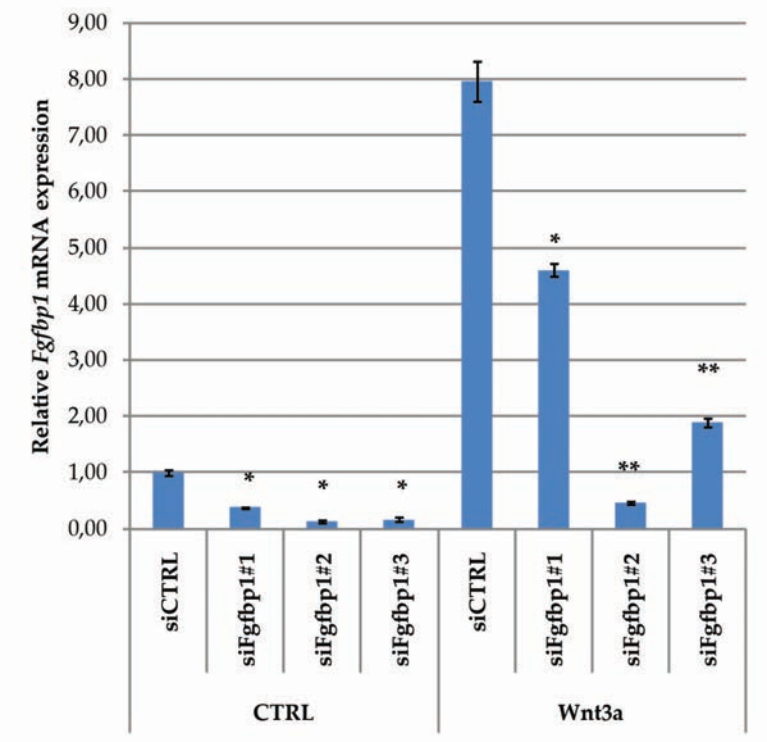

Figure 46. Analysis of Fgfbp1 expression in bMECs upon transfection with three different siRNAs

qRT-PCR analysis of Fgfbp1 expression in bMECs treated or non-treated with Wnt3a upon transfection with three different siRNAs targeting Fgfbp1 mRNA (siFGFBP1#1, #2 and #3). The levels of mRNA are normalized on 18S. Data are presented as mean ± standard deviation of replicates of a representative expreriment (n=3). *: $p<0.05$; **: $p<0.01$.

The downregulation of FGFBP1 was effective not only at mRNA level, but also at protein level. Indeed, as shown by IF analysis, FGFBP1 protein. that is localized at EC membrane, is upregulated upon treatment with Wnt3a and is strongly reduced upon transfection with siFGFBP1#2 (Fig. 47).

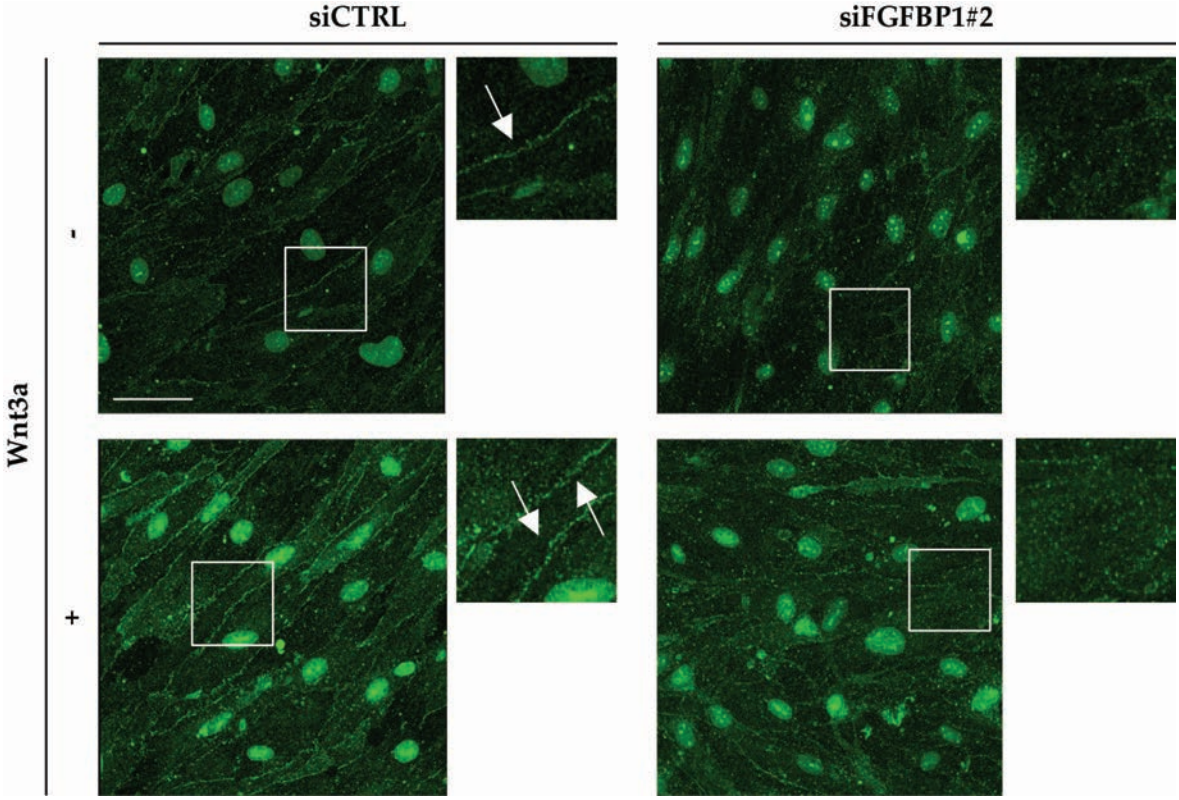

Figure 47. Analysis of FGFBP1 protein expression and localization in bMECs upon transfection with siFGFBP1#2

Representative confocal images of FGFBP1 immunostaining on bMECs. Cells were treated with Wnt3a and with siFGFBP1#2. Scale bar: 50 μm.

3.4.2 Fgfbp1 knockdown does not affect the autocrine activity of FGF-2

Since it has been reported that FGFBP1 has a role in presenting FGF-2 to its receptor, facilitating its signaling, we decided to test whether Fgfbp1 knockdown could modify the signaling pathway downstream of FGF receptor activation. To this purpose, besides the treatment with Wnt3a and with siFGFBP1#2, we also added a treatment with FGF-2 to assess the impact of FGFBP1 absence on FGF-2 activity; then, we checked by western blot (WB) for the expression and phosphorylation of p42/p44 MAP kinases (MAPK), that are downstream of most signaling routes activated by FGF-2. The WB (Fig. 48a) and its quantification (Fig. 48b) showed that p42/p44 MAPK phosphorylation was increased upon FGF-2

treatment, as expected, but was not affected by the presence or absence of FGFBP1, indicating that FGFBP1 is not able to influence the autocrine activity of FGF-2 on ECs in this *in vitro* setting.

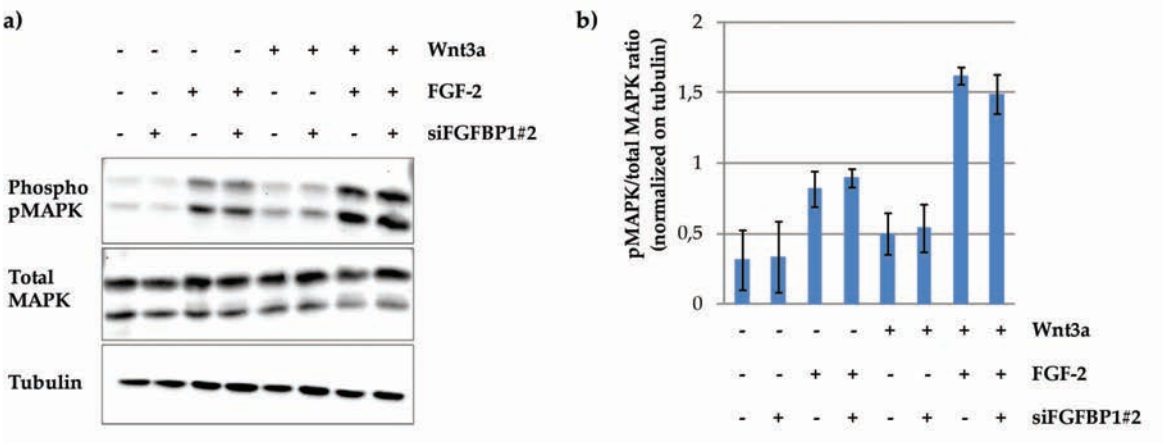

Figure 48. Analysis of FGF-2- induced p42/p44 MAPK phosphorylation in bMECs after Fgfbp1 siRNA treatment

(a) Western blot analysis of FGF-2 induced phosphorylation of p42/p44 MAPK in bMECs treated or non treated with Fgfbp1 siRNA and (b) its related quantification. Both total and phosphorylated p42/p44 were normalized on tubulin, then the ratio of the two was calculated. The data are presented as mean ± standard deviation of replicates of a representative experiment (n=2).

3.4.3 Fgfbp1 knockdown induces a tip cell-like phenotype *in vitro*

Given the *in vivo* observations that the brain vasculature of Fgfbp1 ECKO animals is more branched and dense than the one of control animals and that in the retina of ECKO animals an increased number of tip cells is present, we checked *in vitro*, by RT-PCR analysis, for the expression of some tip-cell markers, such as Dll4, VEGFR2 and Neuropilin 1 (Nrp1). The RT-PCR data (Fig. 49) showed an upregulation of the mRNAs of all these molecules in Fgfbp1 siRNA-treated cells compared to control cells; moreover, this upregulation was not dependent on the

treatment with Wnt3a and FGF-2, indicating that FGFBP1 absence is sufficient to induce the expression of these tip-cell markers *in vitro*.

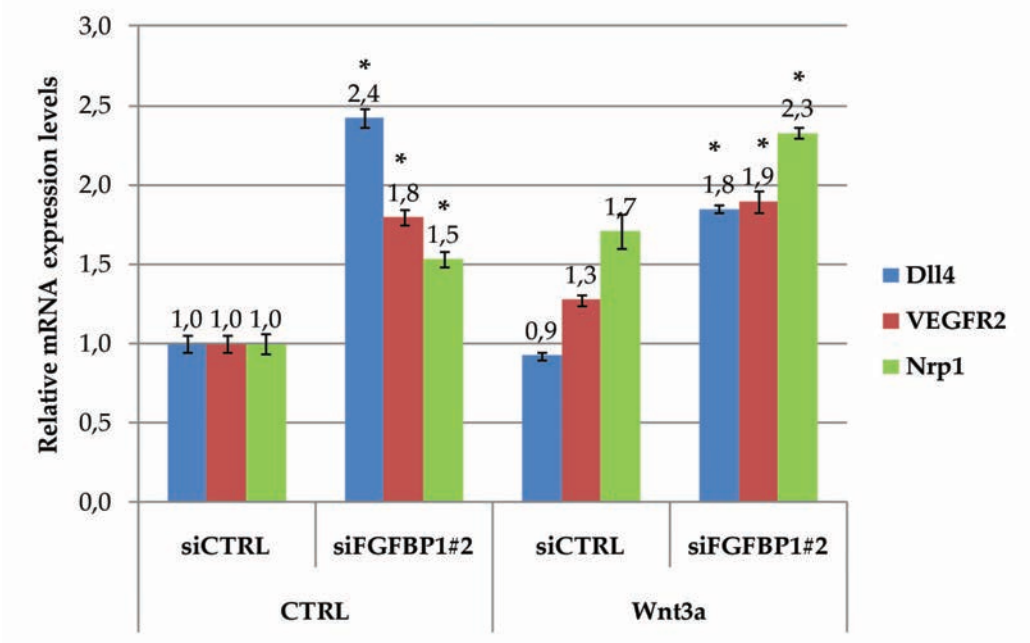

Figure 49. Analysis of tip-cell markers expression in bMECs upon transfection with Fgfbp1 siRNA

qRT-PCR analysis of Dll4, VEGFR2 and Nrp1 expression in bMECs treated or non-treated with Wnt3a upon transfection with Fgfbp1 siRNA. The levels of mRNA are normalized on 18S. Data are presented as mean ± standard deviation of replicates of a representative expreriment (n=3). *: $p<0.05$.

To validate this observation, we also performed a wound-healing assay on Wnt3a-treated bMECs upon transfection with either a control siRNA or Fgfbp1 siRNA to see if FGFBP1 ablation induced a morphological change in the cells towards a tip-like phenotype. The assay showed that the cells, after Fgfbp1 knockdown, were more oriented towards the wound area; moreover, an increased number of cellular protrusions was present, indicating that, in the absence of FGFBP1, cells were more prone to migrate compared to control cells (Fig. 50).

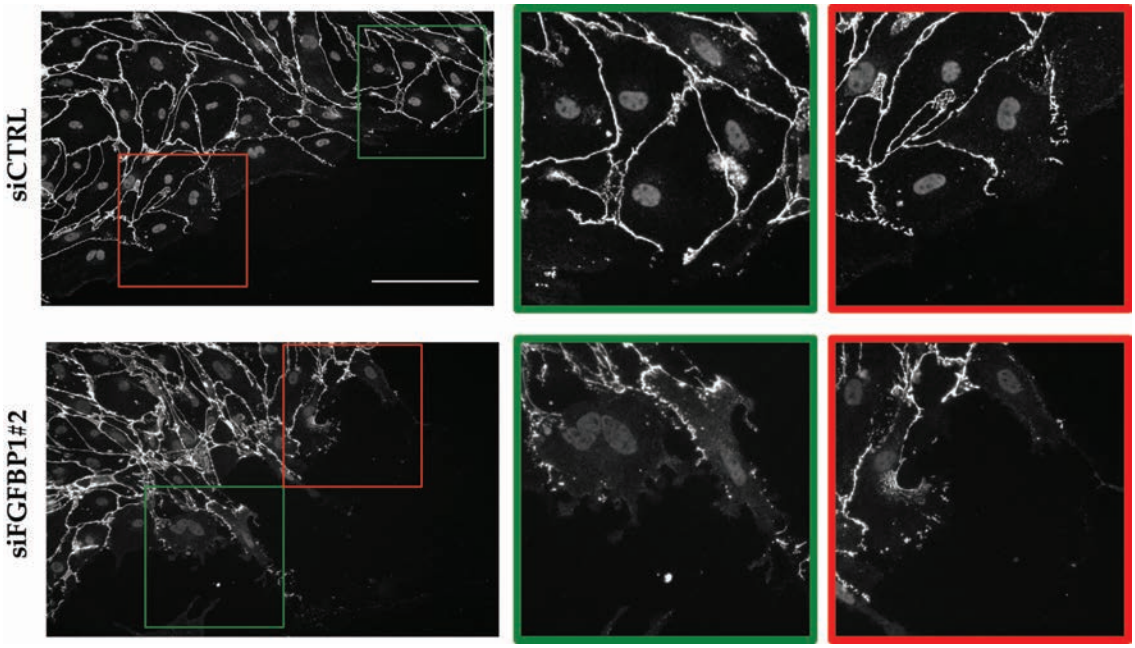

Figure 50. Analysis of Wnt3a-treated bMECs morphology in a wound-healing assay upon Fgfbp1 siRNA

Representative confocal images of a wound healing assay on Wnt3a-treated bMECs upon transfection with either a control siRNA or Fgfbp1 siRNA. Cells were immunostained for the endothelial marker VE-cadherin. Scale bar: 50 μm

3.4.4 Fgfbp1 knockdown causes the upregulation of Plvap *in vitro*

Starting from the *in vivo* observation that increased BBB permeability correlated with a higher expression of Plvap, we decided to test whether the upregulation of this protein following Fgfbp1 gene deletion in the endothelium was cell-autonomous or not; together with this, we also wanted confirm that the increased permeability was not due to TJ dismantling. To answer these questions, we analyzed *in vitro* the expression of Plvap, Claudin-5 and the BBB-selective Claudin-3, both at mRNA level by qRT-PCR and at protein level by IF.

The qRT-PCR analysis (Fig. 51a) showed a significant 30% increase of Plvap mRNA expression in Fgfbp1 siRNA-treated cells ($p<0.05$) already in basal

conditions (i.e. non Wnt3a-treated); however, while Plvap expression decreased, as expected, in presence of Wnt3a in siCTRL-treated cells (30% decrease, $p<0.05$), Wnt-mediated downregulation of Plvap was milder (15%) in siFGFBP1#2-treated cells ($p<0.05$). Consistently to what observed in vivo, the increase of Plvap, both at mRNA and protein level, is not coupled to a reduction in Claudin-5, that resulted to be unchanged in control and siRNA-treated cells both in terms of expression (Fig. 51a) and junctional localization (Fig. 51b). Finally, Claudin-3 showed a slight increase in mRNA expression levels in Fgfbp1 siRNA-treated bMECs (Fig. 51a, $p<0.05$), but the protein levels and its localization were not modified (Fig. 51b).

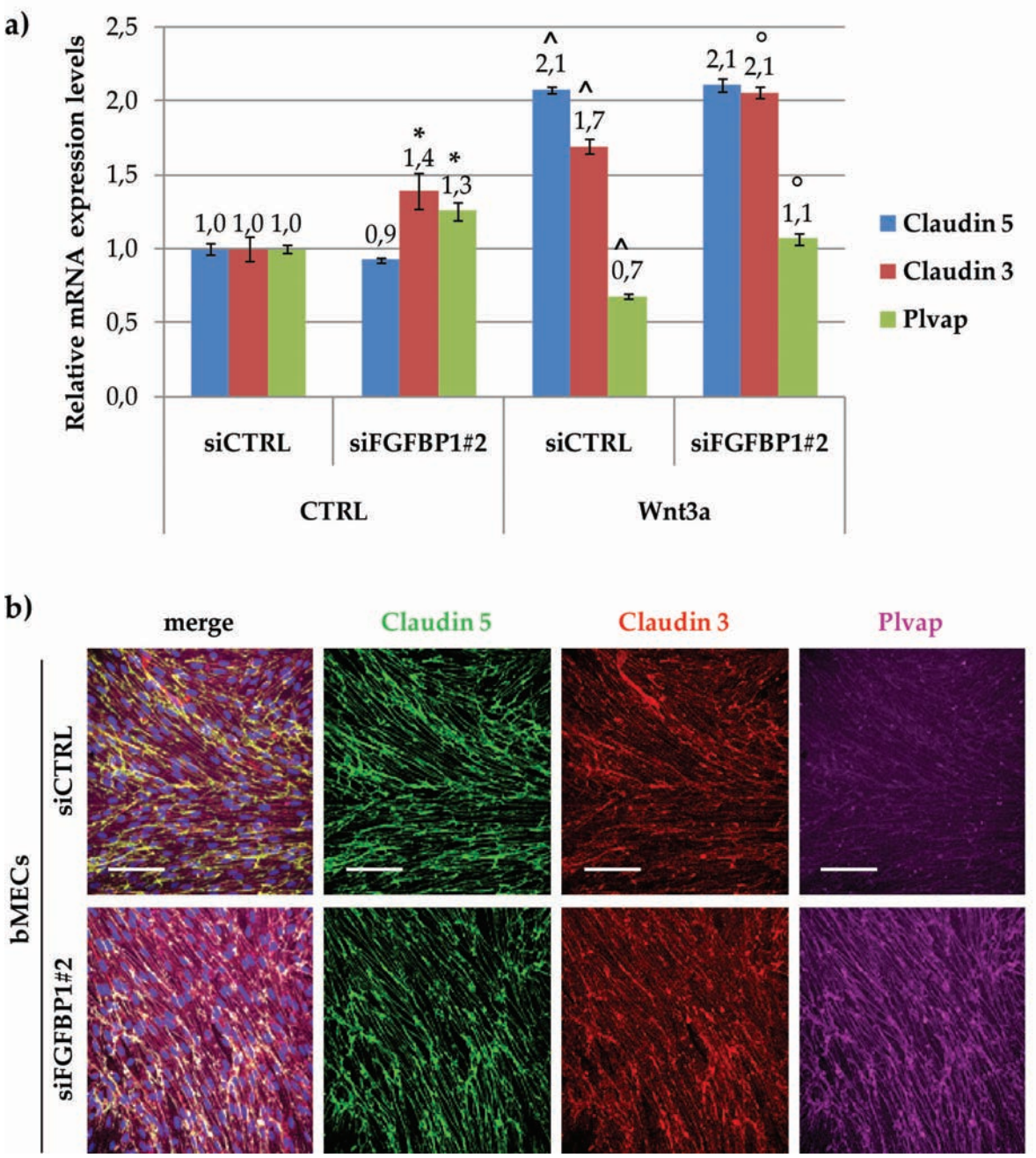

Figure 51. Analysis of claudin-5, claudin-3 and Plvap expression and localization in bMECs upon Fgfbp1 siRNA transfection

(a) qRT-PCR analysis of claudin-5, claudin-3 and Plvap expression in bMECs treated or non-treated with Wnt3a upon transfection with Fgfbp1 siRNA. The levels of mRNA are normalized on 18S. Data are presented as mean ± standard deviation of replicates of a representative expreriment (n=3). *: CTRL siFGFBP1#2 vs. siCTRL: $p<0.05$. ^: siCTRL Wnt3a vs. CTRL: $p<0.05$. °: Wnt3a siFGFBP1#2 vs. siCTRL: $p<0.05$. **(b)** Representative confocal images of a IF analysis on bMECs upon transfection with either a control siRNA or Fgfbp1 siRNA. Cells were immunostained for claudin-5, claudin-3 and Plvap. Scale bar: 50 µm

3.4.5 Fgfbp1 knock down in bMECs causes alterations in the response to Wnt3a treatment

The observation that Plvap, a gene known to be downregulated by canonical Wnt pathway, is more effectively downregulated by Wnt3a in siCTRL-treated bMECs than in siFgfbp1#2-treated cells (Fig. 51a) raised the hypothesis that FGFBP1 absence might change the overall response of brain ECs to Wnt3a treatment.

To test this possibility we analyzed the Affymetrix data by comparing the list of genes that were modulated (either upregulated or downregulated) by Wnt3a treatment either in control cells or in interfered cells (i.e. "Upregulated by Wnt3a in siCTRL vs. upregulated by Wnt3a in siFgfbp1#2" and "Downregulated by Wnt3a in siCTRL vs. downregulated by Wnt3a in siFgfbp1#2").

The analysis showed that, within the group of genes that were upregulated by Wnt3a treatment, 37 of them showed this upregulation only in control cells, 51 only in interfered cells and 117 in both conditions. In parallel, within the group of genes that were downregulated by Wnt3a treatment, 31 genes were downregulated only in control cells, 39 only in siFgfbp1#2-treated cells and 52 in both (Fig. 52).

Moreover, within the group of genes that were modulated by Wnt3a in both control and interfered cells, some genes presented differences in the extent of the upregulation/downregulation, including some canonical Wnt targets: in particular, Axin-2 upregulation upon Wnt3a stimulation was more than 40% lower in siFgfbp1#2-treated cells compared to control, while Plvap downregulation was

more that 15% lower in interfered cells compared to control cells, confirming our previous observations (see Tables 7 and 8).

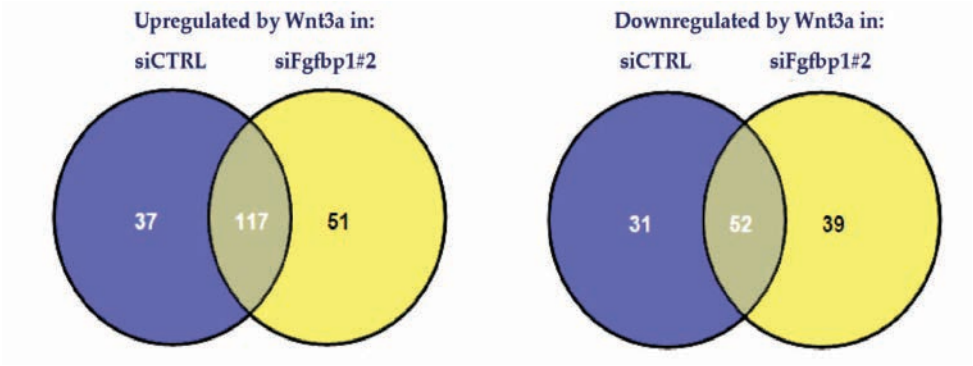

Figure 52. Graphical representation of the differential response to Wnt3a treatment in siCTRL-treated cells and siFgfbp1#2-treated cells

Diagram of the number of genes whose transcription is modulated (upregulated or downregulated) upon Wnt3a stimulation in siCTRL-treated cells and siFgfb1#2-treated cells.

To determine whether the differentially modulated transcripts might account for some specific biological process, we performed a Gene Ontology scan to classify them according to the biological functions in which they are involved. We observed that most of the genes that were upregulated specifically in siFgfbp1#2-treated cells and most of those who were specifically downregulated in siCTRL-treated cells were genes that participate in the processes of vascular development, vessel morphogenesis and tissue remodeling (Table 7).

Biological function	GO term annotation	Number of entries	p value
Vasculature development	GO: 0001944	13	6.085e-08
Blood vessel development	GO:0001568	11	3.699e-06
Blood vessel morphogenesis	GO:0048514	10	4.991e-06
Cardiovascular system development	GO:0072358	13	1.351e-05

Table 7. Gene Ontology analysis of the most enriched biological processes in which differentially Wnt-modulated genes are involved

The observation that these genes were specifically downregulated by Wnt3a in presence of FGFBP1 and specifically upregulated by Wnt3a in absence of FGFBP1, suggests that FGFBP1 might act, through a mechanism that is still to be investigated, as a molecular mediator of Wnt activity.

Upregulated by Wnt3a			
Only in siCTRL	*Only in siFgfbp1#2*	*Both*	
			% of siCTRL
ACP6	ADRB2	2610019F03RIK	87.91
ADM	AHRR	4933409K07RIK	97.50
ALAS1	ANGPT2	5730469M10RIK	101.73
ARL4A	ANGPTL4	A130022J15RIK	100.32
ATP10A	ASB4	ABHD2	92.42
BSG	B930036N10RIK	ACER2	99.69
CACHD1	BC028528	ADH1	72.31
CTLA2A	BGN	APCDD1	78.98
DISP2	CCDC85A	APOD	80.10
ERN1	CTHRC1	AQP11	95.09
FBLN1	ELOVL7	AXIN2	57.88
FGFBP1	GM6020	BEX1	66.20
GPER	GM8174	BMP2	99.74
GPM6A	GNAS	CACNA1E	91.37
IFITM1	HMCN1	CADM1	106.48
JAG1	KANK4	CAR2	85.87
JUB	LCE1H	CCDC141	84.33
LPCAT3	MAOB	CCL2	92.82
LRG1	MCOLN2	CD24A	102.74
LRP8	MRPS21	CDH2	93.63
NGFRAP1	MT2	CHRM3	103.99
NOMO1	PCDH7	CLDN5	98.04
NRGN	PHLDA1	COL10A1	111.31
ODC1	PTGS2	CRCT1	118.10
PLAT	RAMP3	CSF1	96.70
RET	RECK	CTSC	104.32
RGS16	RERG	CTXN1	106.70
RYBP	RNU2	CYP1B1	86.88
SLC16A12	RNU73B	DARC	109.68
SLC7A5	RNY1	DPP4	100.58
SPRY1	RPL13	EDN1	107.81
SUSD4	SCARNA17	EFEMP1	93.35
SWAP70	SFRP1	ENPP2	106.34
TMEM37	SLAIN2	ENTPD1	104.45
TTYH2	SLC44A1	FAM102A	111.13
ZFP703	SNHG1	FAM13A	90.00
ZNRF3	SNORD32A	FAM163A	91.88
	SNORD34	FHL1	101.82
	SNORD35A	FLRT2	89.78
	SNORD49B	FOXF2	107.42
	SNORD82	FOXQ1	87.05
	SRGN	FRZB	106.11

Upregulated by Wnt3a			
Only in siCTRL	*Only in siFgfbp1#2*	*Both*	
			% of siCTRL
	ST3GAL6	GATM	89.87
	STXBP4	GKN3	69.95
	TIPARP	GLDN	107.42
	TRP53I11	GLI3	98.44
	UCP2	GM12824	110.49
	USP46	GPR126	109.09
	VAULTRC5	GSTA4	97.21
	ZFP36L1	HTR2A	115.72
	ZFP51	INSR	109.83
		ISM1	101.30
		ISYNA1	80.02
		ITGA4	110.12
		KBTBD11	95.80
		KCNIP3	80.83
		KCNJ2	106.21
		LAMA1	83.28
		LCN2	121.37
		LEF1	107.84
		LIPA	105.34
		LPHN3	93.52
		LRRC7	82.19
		LSR	91.62
		MAL	108.15
		MAOA	98.34
		MEIS2	108.51
		MFSD7C	98.46
		MMRN1	91.45
		MOGAT2	90.44
		MYH10	93.07
		MYL4	99.71
		NEFL	95.11
		NOSTRIN	135.25
		NPNT	105.91
		NTS	96.21
		OLFML2A	112.98
		PARM1	97.05
		PDE7B	107.22
		PGLYRP1	100.77
		PKNOX2	108.69
		PLXNB1	90.05
		RASSF9	119.32
		REEP1	113.31

Upregulated by Wnt3a			
Only in siCTRL	*Only in siFgfbp1#2*	*Both*	
			% of siCTRL
		RGS2	97.13
		RHOBTB1	107.37
		RNF183	97.77
		SCN3B	96.01
		SERPINB6B	87.27
		SESN3	93.45
		SLC16A4	96.67
		SLC16A6	94.10
		SLC19A3	88.57
		SLC22A14	102.48
		SLC22A8	90.46
		SLC2A1	99.15
		SLC35F2	100.96
		SLC38A3	84.03
		SLC38A5	87.92
		SLC39A8	97.57
		SLC40A1	110.66
		SLCO1A4	107.91
		SLCO1A5	113.59
		SLCO1C1	75.69
		SLCO2B1	119.62
		SRPX2	102.82
		ST3GAL5	106.18
		STC2	102.16
		TBX1	94.21
		TCF7	103.86
		TGFB2	100.69
		TNFRSF19	100.52
		TRF	99.07
		VIL1	83.47
		VWF	98.31
		ZIC2	107.01
		ZIC3	99.77

Table 8. List of genes differentially upregulated by Wnt3a treatment in siCTRL-treated cells and siFgfbp1#2 cells. Color code: Red = genes whose decrease in upregulation in siFgfbp1#2 vs. siCTRL cells is higher that 15%. Green = genes whose increase in upregulation in siFgfbp1#2 vs. siCTRL cells is higher that 15%.

Downregulated by Wnt3a			
Only in siCTRL	*Only in siFgfbp1#2*	*Both*	
			% of siCTRL
4930523C07RIK	APOL9B	8430408G22RIK	90.514448
ACVR1B	CBS	ABLIM3	96.49760224
AHR	CDA	ACE	101.9551747
ATP2B4	CMPK2	ADAM12	99.53873793
CXCR7	CPNE7	ADAM19	105.5553718
EDNRB	CX3CL1	ADARB1	97.14657243
ENPP6	D8ERTD82E	APLNR	104.6585372
ESM1	DDX60	CCDC88C	119.0786689
FAM36A	FBXL7	CDC42EP2	100.7548998
FAM70A	GM10081	CLIC6	98.0041672
GDA	GM5970	COL15A1	110.8416429
GJA1	GPR21	COL8A1	100.4271954
IGF1	GPRIN3	CXCL10	87.85400738
IGFBP3	GRP	CYP1A1	94.06044091
ITGA8	HEY1	D4BWG0951E	96.06248269
LRRC55	I830012O16RIK	DEPDC6	96.6991424
MGP	IFI203	DOCK8	100.281119
NPTX1	IFIT1	EFNB2	103.2398535
NUDT4	IFIT2	EGFL8	121.4628394
P2RY2	IRF7	EMP2	88.98598257
PAPSS2	MTX2	ENPP3	86.19583113
PIK3R3	MYH9	EPHB1	125.3020484
PLXNA4	OASL1	F8	82.35482031
RAPH1	OASL2	FBLN2	89.60710288
RASA4	PHXR4	FMO2	105.7758295
SELP	PRKCH	GALNTL2	99.54529267
SNCG	PRRG3	GJA4	120.482616
SYT15	RSAD2	GJA5	78.54220467
TINAGL1	RTP3	GPC4	101.0745654
TNFSF18	S100A10	GPIHBP1	106.1044379
VMN2R22	SERPINA1C	GRIN2A	87.34396929
	SLC43A3	KCNE3	105.0921566
	TGTP1	LAMA3	98.33180291
	TRDN	LIFR	88.79805612
	TSPAN33	LTBP4	96.70383439
	UBE2L6	MCAM	99.57117086
	UBE2V1	MEST	105.1719514
	USP18	MET	86.38603422
	XAF1	MMP15	91.94703767
		NOS2	108.5699614
		NT5E	107.322681
		PLAU	100.1977422

Downregulated by Wnt3a			
Only in siCTRL	*Only in siFgfbp1#2*	*Both*	
			% of siCTRL
		PLVAP	84.51621127
		PRKCC	105.322232
		PTP4A3	101.9703698
		RNF125	98.54878571
		SEMA3G	111.6749029
		SH3GLB2	101.5577262
		SLC45A4	98.58567937
		SULT5A1	104.2227336
		TRPC3	95.56836222
		UPP1	106.1423209

Table 9. List of genes differentially downregulated by Wnt3a treatment in siCTRL-treated cells and siFgfbp1#2 cells. Color code: Red = genes whose decrease in downregulation in siFgfbp1#2 vs. siCTRL cells is higher that 15%. Green = genes whose increase in downregulation in siFgfbp1#2 vs. siCTRL cells is higher that 15%.

4. DISCUSSION

The BBB has a critical role in accurately maintaining the stringent homeostasis of the CNS that is strictly required to allow a proper neuronal function. For this reason, a perfectly functional BBB is needed to supply nutrients and ions to the brain parenchyma and to block any possible assault by toxins and pathogens coming from the environment [140].

Many groups have already demonstrated that the BBB breakdown is an event often related to many neurological disorders, including stroke, brain trauma, multiple sclerosis (MS) and Alzheimer's disease (AD) [141-143], for which a resolving therapy is still to be found.

On the other hand, the BBB also represents the main obstacle to the pharmaceutical treatment of cerebral pathologies, for example brain tumors, since it can prevent the entrance of drugs into the brain parenchyma.

In this perspective, defining the molecular mechanisms that regulate the development and the function of the BBB assumes a great medical relevance, since it would allow to search for specific therapeutic tools able to restore the proper functional activity of the BBB, in the cases of BBB breakdown, or to selectively and transiently open it in order to allow the entrance of specific pharmacological compounds, in the cases in which an enhanced drug delivery to the brain is required.

In this study, we aimed at determining the role of FGFBP1 in the regulation of the BBB properties. Indeed, FGFBP1 is an appealing candidate for a function in BBB

development, since we found that its expression is much higher in ECs isolated from the brain compared to other ECs and that its expression is strongly upregulated by the activation of canonical Wnt/β-catenin pathway, a well-known molecular determinant of the BBB phenotype [11, 17, 18].

In order to clarify FGFBP1 function, we took advantage of different *in vivo* and *in vitro* systems:

- an ubiquitous Fgfbp1 knock down zebrafish model, to investigate the effect of Fgfbp1 ablation in the whole organism;
- a conditional endothelial-specific Fgfbp1 knock-out murine model, to specifically determine the role of endothelial-derived FGFBP1;
- cultures of primary brain-derived murine ECs (bMECs) treated with a specific siRNA targeting Fgfbp1, to characterize the endothelial cell-autonomous responses of brain ECs to FGFBP1 absence.

4.1 Fgfbp1a and b expression and function in zebrafish: different specializations after the evolutionary divergence of the two paralogues

In zebrafish, FGFBP1 is present as two different paralogues, FGFBP1a and FGFBP1b, being the latter the paralogue with the highest homology with the murine protein. Both proteins show a low (23-25%) total sequence identity with the murine sequence, but with the presence of two highly conserved regions, corresponding to the functional domains of the protein: an internal heparin-binding domain and a C-terminal FGF-binding domain.

In this study, we analyzed the expression of the two paralogues, their function and their capability to be induced by Wnt pathway activation: our data strongly underlined that many differences (summarized in Table 10) exist between the two proteins, both in terms of regulation and activity.

	Fgfbp1a	***Fgfbp1b***
Peak of expression	24 hpf	72 hpf
Cell specificity	Mostly ECs	Mostly non-ECs
Hemorrhages	Many and large	Few and small
Vascular defects	Brain and trunk; lack of vessels	Brain; hyperbranching and misorientation
Brain vascular permeability	Increased	Normal
Induction by Wnt	ECs and non-ECs	ECs

Table 10. Schematic summary of the differences between Fgfbp1a and Fgfbp1b

The results obtained clearly indicate the involvement of FGFBP1a and b in the development of the zebrafish vasculature; however, the above mentioned differences suggest that the two paralogues could have acquired different functions during evolution.

Fgfbp1a is likely to be involved in the overall vascular development. Its expression is mostly endothelial-specific, and its peak of expression is around 24 hpf, a time when active angiogenic processes are ongoing both in the trunk and in the head [144]. Consistently with a role in the regulation of the angiogenic sprouting, the kind of vascular defects arising from Fgfbp1 knock down (i.e. the lack of some

cerebral and intersomitic vessels) resemble the phenotype reported for zebrafish VEGFR-2 mutants [145], as well as for other mutants affecting VEGF downstream signaling, that result all in defects in ISVs and cranial vessels formation [146-148]. Although in our work we did not analyze the structure and the composition of AJs and TJs in zebrafish morphants, it is possible that the hemorrhages and the increased vascular permeability observed in MO-Fgfbp1a animals might be due to endothelial junctional alterations, since defects in the cranial vasculature associated to hemorrhagic phenomena were also reported by our group after injection of a morpholino targeting VE-cadherin [149].

On the other side, we reported that Fgfbp1b is mainly expressed by non-ECs but, differently from the other paralogue, its expression is not very high at 24 hpf. However, Fgfbp1b mRNA levels tend to increase during later stages: in particular at 72 hpf, that is the last time point we considered in our analysis, its expression is strongly enhanced compared to earlier stages. The kinetics and the cell specificity of this paralogue do not make it a good candidate for the regulation of angiogenic development, but they rather suggest that it might be involved in the later process of BBB specification. Indeed, although still limited knowledge is available on the BBB in zebrafish from either a developmental, structural or functional point of view, it was recently reported that, even if the TJ proteins ZO-1 and claudin-5 in zebrafish brain vessels appear by 48-72 hpf, the size-dependent exclusion of molecules from the brain is a feature that is acquired only later on [150]. Moreover, it is also reported that, as for mammals, also in zebrafish the brain vasculature is associated to perivascular cells like pericytes and astrocytes, even though their

role in the control of BBB function and permeability in this model is still to be clarified [150, 151]. In this context, Fgfbp1b might represent a molecular mediator of the interactions between endothelium and perivascular cells. Moreover, given the observation that our murine transgenic model presents a reduction in the number of pericytes, it would be interesting to exploit the mural-cell reporter animal developed by the group of Dr. Childs [151] to investigate whether Fgfbp1b knockdown can influence pericyte recruitment and/or maturation.

4.2 The glial barrier: an astrocyte reaction to endothelial barrier impairment

One of the most intriguing and puzzling data obtained in this work is the observation, in the EM ultrastructural analysis, that perivascular astrocytes in Fgfbp1 ECKO animals were characterized by the presence of swelling and by intercellular junctions that appeared tighter than in WT animals. Taking in consideration the numerous other defects observed in Fgfbp1 ECKO mice, including the reduction in the number of pericytes, the BM remodeling and its reduction in thickness and the increased permeability to both low and high molecular weight molecules, the abnormal appearance of the astrocyte might be considered as a sort of compensatory reaction to the impairment in the endothelial barrier function.

This possibility is not surprising, since in nature many animal species exist in which the brain endothelial layer is incomplete or leaky, but the barrier properties are took on by perivascular glial cells [152]. Also, it has been proposed that the ancestral vertebrate had a glial BBB, while the endothelial BBB would have

appeared later on during evolution, indicating that it confers a strong selective advantage in certain environments [153].

As a further confirmation of this hypothesis, other groups reported that in some pathologies of the CNS involving BBB dysfunction, such as tumors and epilepsy, compensatory changes in astrocytes and glial cells are present [154, 155], indicating that astrocyte layer "tightening" might indeed represent a second line of defense in case of endothelial BBB disruption.

4.3 Pericyte decrease and BM rearrangements: a "chicken or egg" situation

The phenotype detected in our Fgfbp1 ECKO model includes modifications in the number and maturation state of pericytes and a reshaping of BM composition, mainly represented by a decrease in collagen IV coverage and expression. As already discussed in the introduction, in recent years many groups have focused their attention on how these two entities can influence the BBB functional properties and how they synergically interact with the endothelium to establish these properties, but very less is known about the intercommunication between pericytes and BM and the ways in which alterations of one of the two can affect the other.

In the context of this project, two possible scenarios emerge to provide explanations to our experimental phenotype.

The first scenario presupposes that Fgfbp1 ECKO directly affects the recruitment and maturation of pericytes; then, as a consequence of their reduction, the production and secretion of collagen IV and other BM components is altered. This

hypothesis is supported by the observation of Dr. Jeon and colleagues that pericytes in culture can produce the major structural components of the BM, including collagen IV and multiple laminin chains [85]. Complementary to this observation, also Dr. Stratman and coworkers reported that, in *in vitro* cocultures of ECs and pericytes, the recruitment of pericytes to vascular tubes and their heterotypic interaction with the ECs triggers the production and deposition of collagen IV, laminins and other BM components, such as nidogens and perlecan [83, 87]. Also, it was recently shown that the pericyte-specific ablation of NG2 proteoglycan was able to reduce collagen IV coverage of B16F10 melanoma vessels [156]. On the contrary, this hypothesis is refuted by the work of the group of Prof. Betsholtz, that demonstrated some years ago, in a murine model showing a decreased number of pericytes, that the BM composition was not altered by pericyte reduction; in this work, the only BM protein that results modified by pericyte lack is the pBM component laminin α2, but this change is accompanied by modifications in aquaporin IV expression and localization, indicating that the observed laminin α2 alterations are likely due to defects in the astrocytic compartment rather than to defects in BM protein deposition [61].

Conversely, the second scenario contemplates the possibility that an initial impairment in BM deposition might affect the recruitment of pericytes. This hypothesis is sustained by the observation that the BM composition, in particular the proper N-sulfation of HSPGs, is critical for the binding and the activation of the heparin-binding growth factor PDGF-B and subsequent pericyte recruitment, as shown by the fact that mice mutant for Ndst-1 (Ndst-1$^{-/-}$), the enzyme

responsible for heparan-sulfates N-sulfation, show decreased pericyte coverage [38].

Importantly, these two hypotheses are not mutually exclusive. It is likely that the phenotype observed in Fgfbp1 ECKO mice might depend on the influence of both pericytes on BM and BM on pericytes. Indeed, based on the data we obtained, we can postulate a model (schematized in Fig. 53) in which FGFBP1 ablation in brain ECs directly causes cell-autonomous responses involving the acquisition of a tip-like phenotype and the overexpression of tip-cell markers, such as Dll4, VEGFR2 and Nrp1. As shown by Dr. del Toro and coworkers in 2010 [157], tip-cells transcriptome is enriched for proteases, such as ADAM-TS (A Disintegrin-Like and Metalloproteinase with Thrombospondin motif) family members, which are known to degrade the BM facilitating cell migration; this might explain the reduced BM thickness and the modifications in BM composition observed in Fgfbp1 ECKO mice. At the same time, while it is known that tip-cells also produce soluble factors, such as PDGF-B, to recruit pericytes, the latter are known to preferentially associate to stalk cells [30]; in the cellular context created by FGFBP1 deletion, where ECs "act" as tip-cells, this might account for a defective pericyte association to the vasculature and subsequent pericyte number decrease. Further modifications in the BM might occur as a consequence of the impaired EC-pericyte association, that in turn might cause ulterior defects in pericyte physiology. All these phenomena might contribute in establishing a "vicious circle" in which defects in the BM affect the pericytic compartment and, vice versa, pericytes affect the BM.

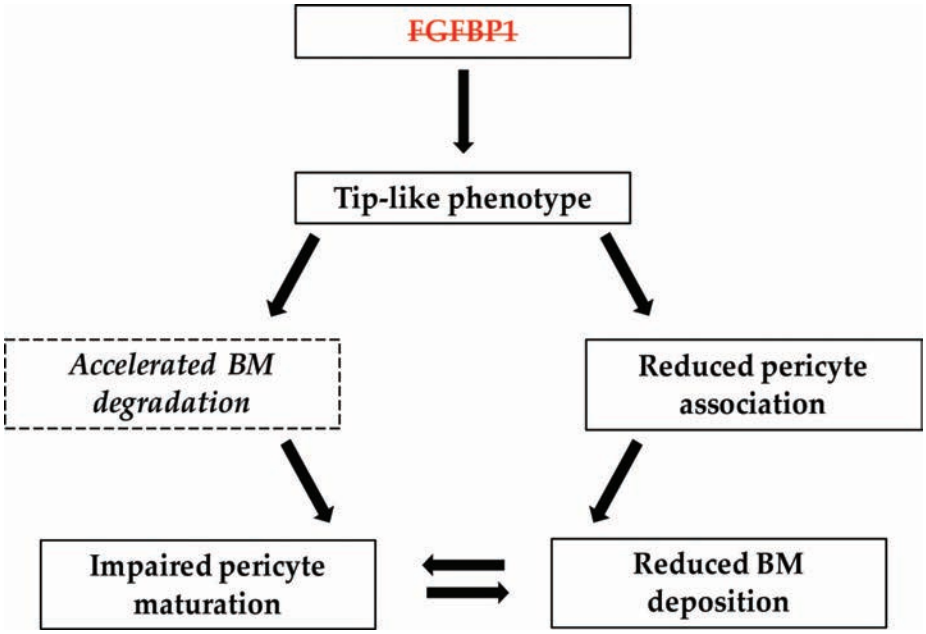

Figure 53. Proposed model for pericyte deficiency and BM impairment in brain vasculature of Fgfbp1 ECKO mice

Schematic representation of the possible mechanisms accounting for the defects in pericyte number and BM deposition in the brain vasculature of Fgfbp1 ECKO mice. The ablation of FGFBP1 in the endothelium originates a cell-autonomous switch of ECs to a tip-like phenotype, with a subsequent acceleration in BM degradation and an impairment in EC-pericyte association. In turn, these two phenomena are responsible for further defects in BM deposition and pericyte maturation. The italic within the dotted box represents literature-based assumptions whose experimental confirmation is still pending.

4.5 Small vessel disease (SVD): a link between FGFBP1, Collagen IV and increased cerebral hemorrhage susceptibility

In our work, we reported that increased brain vessel permeability in Fgfbp1 ECKO mice is associated to decreased collagen IV vessel coverage. Collagen IV is already known to be the major BM component responsible for vessel stabilization, and it has been shown to have a fundamental role also in the maintenance of BM integrity under mechanical stress conditions, although it is dispensable for BM assembly during development [79]. Moreover, mutations in Col4a1 and Col4a2 are

reported to be associated to hemorrhagic events: in particular, it has been shown that these mutations do not affect the production and the trimerization of collagen IV chains, but they impair the secretion of collagen IV trimer, that is therefore retained within the endoplasmic reticulum [80, 81, 158]. As shown by our data, also in Fgfbp1 ECKO mice the transcription of Col4a1 and Col4a2 is not altered, possibly indicating that the decreased collagen IV vessel coverage might be ascribed to a defect in its secretion.

Mutations in Col4a1 have also been shown to be one of the genetic determinants of small vessel disease (SVD), a group of multifactorial diseases characterized by vessel tortuosity, vascular hyperbranching, BM focal disruption and increase susceptibility to cerebral hemorrhages [159]. Given the similarities between these clinical manifestations and the phenotype observed in our zebrafish and mouse *in vivo* models, and given the multiplicity of genes interested by genetic mutations causing a SVD phenotype, it would be interesting to further investigate whether *Fgfbp1* might be a candidate gene for mutations causing this disease. Indeed, single nucleotide polymorhisms (SNPs) in *Fgfbp1* gene have been already associated not only to bone mineral density regulation [160], but notably also to hypertension [161], that is reported to be a risk factor for cerebral hemorrhages and strokes [81].

4.6 FGFBP1: a novel regulator of Wnt activity?

The observation that Plvap expression is differently downregulated by Wnt3a in control and siFgfbp1#2-treated cells prompted us to investigate more in depth

whether the absence of FGFBP1 could influence more generally the response of brain ECs to Wnt. A first confirmation of this hypothesis came from the expression of Axin-2, a canonical Wnt target gene, whose upregulation upon Wnt3a treatment was lower in siRNA-treated bMECs compared to control cells. In addition, by Affymetrix analysis, we managed to detect strong differences in the transcriptome of Fgfbp1 WT and knock down cells in response to Wnt3a stimulation: indeed, we found that some genes were specifically modulated in WT cells, some other specifically in interfered cells and some other in both cell types, but to different extents. These data clearly indicate that FGFBP1 is somehow able to influence the cellular response to Wnt, at least in our experimental setting. The mechanism through which FGFBP1 can modulate Wnt activity is still to be defined: we aim at clarifying this point in the next future by analyzing the expression of known Wnt signaling inhibitors, such as Dkk1, and the expression and phosphorylation of Frizzled and LRP5/6 receptors.

Interestingly, the genes that resulted to be affected by FGFBP1 presence in their response to Wnt activation are mostly genes involved in the regulation of vascularization. More specifically, these genes have been found to be upregulated by Wnt3a in FGFBP1-deficient cells and downregulated by Wnt3a in FGFBP1-proficient cells, possibly indicating that the role of FGFBP1 in this conditions might be to negatively modulate Wnt action in promoting cerebral vascularization. If this hypothesis is true, we could start considering FGFBP1 expression as a sort of "protective mechanism" to avoid uncontrolled angiogenesis in the CNS, that would occur in absence of a proper fine-tuning of Wnt activity. In

this perspective, the upregulation of FGFBP1 that other groups have reported in pathological angiogenic conditions [128] might not be causative of these conditions but rather a "defense response" to them.

Finally we found that, among the genes that are specifically upregulated by Wnt in absence of FGFBP1, some might be of particular relevance for the explanation of FGFBP1 ECKO mice phenotype: Ang-2, whose overexpression has been shown to cause pericyte loss [49]; ESM-1 (endothelial specific molecule 1) and IGFBP-3 (insulin growth factor binding protein 3), that have been shown to enhance VEGF-induced signaling in ECs and to regulate the interaction with astrocytes, pericytes and microglial cells [157, 162-164]. Since these genes have been also reported to be particularly enriched in tip-cells [157], their further study could provide a link between the differential response to Wnt, the tip-like phenotype and the NVU alterations that we reported to occur in the absence of FGFBP1.

4.7 Concluding remarks

In conclusion, our work showed that FGFBP1 is upregulated by Wnt/β-catenin pathway specifically in brain ECs, where it controls the interaction between the endothelial compartment and the other components of the NVU, possibly by modulating Wnt responses. Although the underlying molecular mechanisms governing FGFBP1 action still need to be clarified, we believe that our work contributed in identifying a novel regulator of BBB physiology, with potential future applications in the therapeutic field.

BIBLIOGRAPHY

1. Kann, O., *The energy demand of fast neuronal network oscillations: insights from brain slice preparations.* Front Pharmacol, 2011. **2**: p. 90.
2. Abbott, N.J., *Blood-brain barrier structure and function and the challenges for CNS drug delivery.* J Inherit Metab Dis, 2013. **36**(3): p. 437-49.
3. Abbott, N.J., *Evidence for bulk flow of brain interstitial fluid: significance for physiology and pathology.* Neurochem Int, 2004. **45**(4): p. 545-52.
4. Abbott, N.J., et al., *Structure and function of the blood-brain barrier.* Neurobiol Dis, 2010. **37**(1): p. 13-25.
5. Paolinelli, R., et al., *The molecular basis of the blood brain barrier differentiation and maintenance. Is it still a mystery?* Pharmacol Res, 2011. **63**(3): p. 165-71.
6. Siegenthaler, J.A., F. Sohet, and R. Daneman, *'Sealing off the CNS': cellular and molecular regulation of blood-brain barriergenesis.* Curr Opin Neurobiol, 2013. **23**(6): p. 1057-64.
7. Dejana, E., E. Tournier-Lasserve, and B.M. Weinstein, *The control of vascular integrity by endothelial cell junctions: molecular basis and pathological implications.* Dev Cell, 2009. **16**(2): p. 209-21.
8. Anderson, J.M. and C.M. Van Itallie, *Physiology and function of the tight junction.* Cold Spring Harb Perspect Biol, 2009. **1**(2): p. a002584.
9. Nitta, T., et al., *Size-selective loosening of the blood-brain barrier in claudin-5-deficient mice.* J Cell Biol, 2003. **161**(3): p. 653-60.
10. Daneman, R., et al., *The mouse blood-brain barrier transcriptome: a new resource for understanding the development and function of brain endothelial cells.* PLoS One, 2010. **5**(10): p. e13741.
11. Liebner, S., et al., *Wnt/beta-catenin signaling controls development of the blood-brain barrier.* J Cell Biol, 2008. **183**(3): p. 409-17.
12. Wallez, Y. and P. Huber, *Endothelial adherens and tight junctions in vascular homeostasis, inflammation and angiogenesis.* Biochim Biophys Acta, 2008. **1778**(3): p. 794-809.

13. Furuse, M., *Molecular basis of the core structure of tight junctions.* Cold Spring Harb Perspect Biol, 2010. **2**(1): p. a002907.

14. Li, F., et al., *Endothelial Smad4 maintains cerebrovascular integrity by activating N-cadherin through cooperation with Notch.* Dev Cell, 2011. **20**(3): p. 291-302.

15. Taddei, A., et al., *Endothelial adherens junctions control tight junctions by VE-cadherin-mediated upregulation of claudin-5.* Nat Cell Biol, 2008. **10**(8): p. 923-34.

16. Ohtsuki, S. and T. Terasaki, *Contribution of carrier-mediated transport systems to the blood-brain barrier as a supporting and protecting interface for the brain; importance for CNS drug discovery and development.* Pharm Res, 2007. **24**(9): p. 1745-58.

17. Daneman, R., et al., *Wnt/beta-catenin signaling is required for CNS, but not non-CNS, angiogenesis.* Proc Natl Acad Sci U S A, 2009. **106**(2): p. 641-6.

18. Stenman, J.M., et al., *Canonical Wnt signaling regulates organ-specific assembly and differentiation of CNS vasculature.* Science, 2008. **322**(5905): p. 1247-50.

19. De Vivo, D.C., et al., *Defective glucose transport across the blood-brain barrier as a cause of persistent hypoglycorrhachia, seizures, and developmental delay.* N Engl J Med, 1991. **325**(10): p. 703-9.

20. Dutheil, F., et al., *ABC transporters and cytochromes P450 in the human central nervous system: influence on brain pharmacokinetics and contribution to neurodegenerative disorders.* Expert Opin Drug Metab Toxicol, 2010. **6**(10): p. 1161-74.

21. Huang, J., U.M. Upadhyay, and R.J. Tamargo, *Inflammation in stroke and focal cerebral ischemia.* Surg Neurol, 2006. **66**(3): p. 232-45.

22. Engelhardt, B., *Immune cell entry into the central nervous system: involvement of adhesion molecules and chemokines.* J Neurol Sci, 2008. **274**(1-2): p. 23-6.

23. Keuschnigg, J., et al., *The prototype endothelial marker PAL-E is a leukocyte trafficking molecule.* Blood, 2009. **114**(2): p. 478-84.

24. Ioannidou, S., et al., *An in vitro assay reveals a role for the diaphragm protein PV-1 in endothelial fenestra morphogenesis.* Proc Natl Acad Sci U S A, 2006. **103**(45): p. 16770-5.

25. Shue, E.H., et al., *Plasmalemmal vesicle associated protein-1 (PV-1) is a marker of blood-brain barrier disruption in rodent models.* BMC Neurosci, 2008. **9**: p. 29.

26. Obermeier, B., R. Daneman, and R.M. Ransohoff, *Development, maintenance and disruption of the blood-brain barrier.* Nat Med, 2013. **19**(12): p. 1584-96.

27. Muoio, V., P.B. Persson, and M.M. Sendeski, *The neurovascular unit - concept review.* Acta Physiol (Oxf), 2014. **210**(4): p. 790-8.

28. Sims, D.E., *The pericyte--a review.* Tissue Cell, 1986. **18**(2): p. 153-74.

29. Armulik, A., G. Genove, and C. Betsholtz, *Pericytes: developmental, physiological, and pathological perspectives, problems, and promises.* Dev Cell, 2011. **21**(2): p. 193-215.

30. Gerhardt, H. and C. Betsholtz, *Endothelial-pericyte interactions in angiogenesis.* Cell Tissue Res, 2003. **314**(1): p. 15-23.

31. Gerhardt, H., H. Wolburg, and C. Redies, *N-cadherin mediates pericytic-endothelial interaction during brain angiogenesis in the chicken.* Dev Dyn, 2000. **218**(3): p. 472-9.

32. Diaz-Flores, L., et al., *Pericytes. Morphofunction, interactions and pathology in a quiescent and activated mesenchymal cell niche.* Histol Histopathol, 2009. **24**(7): p. 909-69.

33. Mathiisen, T.M., et al., *The perivascular astroglial sheath provides a complete covering of the brain microvessels: an electron microscopic 3D reconstruction.* Glia, 2010. **58**(9): p. 1094-103.

34. Armulik, A., A. Abramsson, and C. Betsholtz, *Endothelial/pericyte interactions.* Circ Res, 2005. **97**(6): p. 512-23.

35. Soriano, P., *Abnormal kidney development and hematological disorders in PDGF beta-receptor mutant mice.* Genes Dev, 1994. **8**(16): p. 1888-96.

36. Leveen, P., et al., *Mice deficient for PDGF B show renal, cardiovascular, and hematological abnormalities.* Genes Dev, 1994. **8**(16): p. 1875-87.

37. Ostman, A., et al., *Identification of a cell retention signal in the B-chain of platelet-derived growth factor and in the long splice version of the A-chain.* Cell Regul, 1991. **2**(7): p. 503-12.
38. Abramsson, A., et al., *Defective N-sulfation of heparan sulfate proteoglycans limits PDGF-BB binding and pericyte recruitment in vascular development.* Genes Dev, 2007. **21**(3): p. 316-31.
39. Kurup, S., et al., *Heparan sulphate requirement in platelet-derived growth factor B-mediated pericyte recruitment.* Biochem Soc Trans, 2006. **34**(Pt 3): p. 454-5.
40. Lindblom, P., et al., *Endothelial PDGF-B retention is required for proper investment of pericytes in the microvessel wall.* Genes Dev, 2003. **17**(15): p. 1835-40.
41. Stenzel, D., et al., *Peripheral mural cell recruitment requires cell-autonomous heparan sulfate.* Blood, 2009. **114**(4): p. 915-24.
42. Gaengel, K., et al., *Endothelial-mural cell signaling in vascular development and angiogenesis.* Arterioscler Thromb Vasc Biol, 2009. **29**(5): p. 630-8.
43. Falcon, B.L., et al., *Contrasting actions of selective inhibitors of angiopoietin-1 and angiopoietin-2 on the normalization of tumor blood vessels.* Am J Pathol, 2009. **175**(5): p. 2159-70.
44. Sundberg, C., et al., *Stable expression of angiopoietin-1 and other markers by cultured pericytes: phenotypic similarities to a subpopulation of cells in maturing vessels during later stages of angiogenesis in vivo.* Lab Invest, 2002. **82**(4): p. 387-401.
45. Dumont, D.J., et al., *The endothelial-specific receptor tyrosine kinase, tek, is a member of a new subfamily of receptors.* Oncogene, 1993. **8**(5): p. 1293-301.
46. Patan, S., *TIE1 and TIE2 receptor tyrosine kinases inversely regulate embryonic angiogenesis by the mechanism of intussusceptive microvascular growth.* Microvasc Res, 1998. **56**(1): p. 1-21.
47. Suri, C., et al., *Requisite role of angiopoietin-1, a ligand for the TIE2 receptor, during embryonic angiogenesis.* Cell, 1996. **87**(7): p. 1171-80.

48. Dumont, D.J., et al., *Dominant-negative and targeted null mutations in the endothelial receptor tyrosine kinase, tek, reveal a critical role in vasculogenesis of the embryo.* Genes Dev, 1994. **8**(16): p. 1897-909.

49. Hammes, H.P., et al., *Angiopoietin-2 causes pericyte dropout in the normal retina: evidence for involvement in diabetic retinopathy.* Diabetes, 2004. **53**(4): p. 1104-10.

50. Jeansson, M., et al., *Angiopoietin-1 is essential in mouse vasculature during development and in response to injury.* J Clin Invest, 2011. **121**(6): p. 2278-89.

51. Jones, N., et al., *Rescue of the early vascular defects in Tek/Tie2 null mice reveals an essential survival function.* EMBO Rep, 2001. **2**(5): p. 438-45.

52. Sato, Y. and D.B. Rifkin, *Inhibition of endothelial cell movement by pericytes and smooth muscle cells: activation of a latent transforming growth factor-beta 1-like molecule by plasmin during co-culture.* J Cell Biol, 1989. **109**(1): p. 309-15.

53. Chen, S., M. Kulik, and R.J. Lechleider, *Smad proteins regulate transcriptional induction of the SM22alpha gene by TGF-beta.* Nucleic Acids Res, 2003. **31**(4): p. 1302-10.

54. Ota, T., et al., *Targets of transcriptional regulation by two distinct type I receptors for transforming growth factor-beta in human umbilical vein endothelial cells.* J Cell Physiol, 2002. **193**(3): p. 299-318.

55. Goumans, M.J., et al., *Balancing the activation state of the endothelium via two distinct TGF-beta type I receptors.* EMBO J, 2002. **21**(7): p. 1743-53.

56. Goumans, M.J., et al., *Activin receptor-like kinase (ALK)1 is an antagonistic mediator of lateral TGFbeta/ALK5 signaling.* Mol Cell, 2003. **12**(4): p. 817-28.

57. Al Ahmad, A., M. Gassmann, and O.O. Ogunshola, *Maintaining blood-brain barrier integrity: pericytes perform better than astrocytes during prolonged oxygen deprivation.* J Cell Physiol, 2009. **218**(3): p. 612-22.

58. Dohgu, S., et al., *Brain pericytes contribute to the induction and up-regulation of blood-brain barrier functions through transforming growth factor-beta production.* Brain Res, 2005. **1038**(2): p. 208-15.

59. Hori, S., et al., *A pericyte-derived angiopoietin-1 multimeric complex induces occludin gene expression in brain capillary endothelial cells through Tie-2 activation in vitro.* J Neurochem, 2004. **89**(2): p. 503-13.

60. Hayashi, K., et al., *Effects of hypoxia on endothelial/pericytic co-culture model of the blood-brain barrier.* Regul Pept, 2004. **123**(1-3): p. 77-83.

61. Armulik, A., et al., *Pericytes regulate the blood-brain barrier.* Nature, 2010. **468**(7323): p. 557-61.

62. Wolburg, H., et al., *Brain endothelial cells and the glio-vascular complex.* Cell Tissue Res, 2009. **335**(1): p. 75-96.

63. Molofsky, A.V., et al., *Astrocytes and disease: a neurodevelopmental perspective.* Genes Dev, 2012. **26**(9): p. 891-907.

64. Landis, D.M. and T.S. Reese, *Membrane structure in mammalian astrocytes: a review of freeze-fracture studies on adult, developing, reactive and cultured astrocytes.* J Exp Biol, 1981. **95**: p. 35-48.

65. Janzer, R.C. and M.C. Raff, *Astrocytes induce blood-brain barrier properties in endothelial cells.* Nature, 1987. **325**(6101): p. 253-7.

66. Araya, R., et al., *BMP signaling through BMPRIA in astrocytes is essential for proper cerebral angiogenesis and formation of the blood-brain-barrier.* Mol Cell Neurosci, 2008. **38**(3): p. 417-30.

67. Alvarez, J.I., et al., *The Hedgehog pathway promotes blood-brain barrier integrity and CNS immune quiescence.* Science, 2011. **334**(6063): p. 1727-31.

68. Iliff, J.J., et al., *A paravascular pathway facilitates CSF flow through the brain parenchyma and the clearance of interstitial solutes, including amyloid beta.* Sci Transl Med, 2012. **4**(147): p. 147ra111.

69. Bechmann, I., et al., *Immune surveillance of mouse brain perivascular spaces by blood-borne macrophages.* Eur J Neurosci, 2001. **14**(10): p. 1651-8.

70. Prinz, M., et al., *Heterogeneity of CNS myeloid cells and their roles in neurodegeneration.* Nat Neurosci, 2011. **14**(10): p. 1227-35.

71. Kim, W.K., et al., *CD163 identifies perivascular macrophages in normal and viral encephalitic brains and potential precursors to perivascular macrophages in blood.* Am J Pathol, 2006. **168**(3): p. 822-34.

72. Wynn, T.A., A. Chawla, and J.W. Pollard, *Macrophage biology in development, homeostasis and disease.* Nature, 2013. **496**(7446): p. 445-55.

73. Nimmerjahn, A., F. Kirchhoff, and F. Helmchen, *Resting microglial cells are highly dynamic surveillants of brain parenchyma in vivo.* Science, 2005. **308**(5726): p. 1314-8.

74. Daneman, R., *The blood-brain barrier in health and disease.* Ann Neurol, 2012. **72**(5): p. 648-72.

75. Keller, A., *Breaking and building the wall: the biology of the blood-brain barrier in health and disease.* Swiss Med Wkly, 2013. **143**: p. w13892.

76. Yurchenco, P.D., *Basement membranes: cell scaffoldings and signaling platforms.* Cold Spring Harb Perspect Biol, 2011. **3**(2).

77. Yousif, L.F., J. Di Russo, and L. Sorokin, *Laminin isoforms in endothelial and perivascular basement membranes.* Cell Adh Migr, 2013. **7**(1): p. 101-10.

78. Miner, J.H., *Laminins and their roles in mammals.* Microsc Res Tech, 2008. **71**(5): p. 349-56.

79. Poschl, E., et al., *Collagen IV is essential for basement membrane stability but dispensable for initiation of its assembly during early development.* Development, 2004. **131**(7): p. 1619-28.

80. Gould, D.B., et al., *Mutations in Col4a1 cause perinatal cerebral hemorrhage and porencephaly.* Science, 2005. **308**(5725): p. 1167-71.

81. Jeanne, M., et al., *COL4A2 mutations impair COL4A1 and COL4A2 secretion and cause hemorrhagic stroke.* Am J Hum Genet, 2012. **90**(1): p. 91-101.

82. Engelhardt, B. and L. Sorokin, *The blood-brain and the blood-cerebrospinal fluid barriers: function and dysfunction.* Semin Immunopathol, 2009. **31**(4): p. 497-511.

83. Stratman, A.N. and G.E. Davis, *Endothelial cell-pericyte interactions stimulate basement membrane matrix assembly: influence on vascular tube remodeling, maturation, and stabilization.* Microsc Microanal, 2012. **18**(1): p. 68-80.

84. Brachvogel, B., et al., *Isolated Anxa5+/Sca-1+ perivascular cells from mouse meningeal vasculature retain their perivascular phenotype in vitro and in vivo.* Exp Cell Res, 2007. **313**(12): p. 2730-43.

85. Jeon, H., et al., *Pericytes from microvessel fragment produce type IV collagen and multiple laminin isoforms.* Biosci Biotechnol Biochem, 1996. **60**(5): p. 856-61.

86. Miner, J.H. and P.D. Yurchenco, *Laminin functions in tissue morphogenesis.* Annu Rev Cell Dev Biol, 2004. **20**: p. 255-84.

87. Stratman, A.N., et al., *Pericyte recruitment during vasculogenic tube assembly stimulates endothelial basement membrane matrix formation.* Blood, 2009. **114**(24): p. 5091-101.

88. Yurchenco, P.D., P.S. Amenta, and B.L. Patton, *Basement membrane assembly, stability and activities observed through a developmental lens.* Matrix Biol, 2004. **22**(7): p. 521-38.

89. Sudhakar, Y.A., R.K. Verma, and S.C. Pawar, *Type IV collagen alpha1-chain noncollagenous domain blocks MMP-2 activation both in-vitro and in-vivo.* Sci Rep, 2014. **4**: p. 4136.

90. Stenzel, D., et al., *Endothelial basement membrane limits tip cell formation by inducing Dll4/Notch signalling in vivo.* EMBO Rep, 2011. **12**(11): p. 1135-43.

91. Yao, Y., et al., *Astrocytic laminin regulates pericyte differentiation and maintains blood brain barrier integrity.* Nat Commun, 2014. **5**: p. 3413.

92. Breier, G. and W. Risau, *The role of vascular endothelial growth factor in blood vessel formation.* Trends Cell Biol, 1996. **6**(12): p. 454-6.

93. Hogan, K.A., et al., *The neural tube patterns vessels developmentally using the VEGF signaling pathway.* Development, 2004. **131**(7): p. 1503-13.

94. Daneman, R., et al., *Pericytes are required for blood-brain barrier integrity during embryogenesis.* Nature, 2010. **468**(7323): p. 562-6.

95. Nakao, T., A. Ishizawa, and R. Ogawa, *Observations of vascularization in the spinal cord of mouse embryos, with special reference to development of boundary membranes and perivascular spaces.* Anat Rec, 1988. **221**(2): p. 663-77.

96. Risau, W., et al., *Brain induces the expression of an early cell surface marker for blood-brain barrier-specific endothelium.* EMBO J, 1986. **5**(12): p. 3179-83.

97. Wakai, S. and N. Hirokawa, *Development of the blood-brain barrier to horseradish peroxidase in the chick embryo.* Cell Tissue Res, 1978. **195**(2): p. 195-203.

98. Kniesel, U., W. Risau, and H. Wolburg, *Development of blood-brain barrier tight junctions in the rat cortex.* Brain Res Dev Brain Res, 1996. **96**(1-2): p. 229-40.

99. Vallon, M., et al., *Developmental and pathological angiogenesis in the central nervous system.* Cell Mol Life Sci, 2014. **71**(18): p. 3489-506.

100. Carmeliet, P., et al., *Abnormal blood vessel development and lethality in embryos lacking a single VEGF allele.* Nature, 1996. **380**(6573): p. 435-9.

101. Shalaby, F., et al., *Failure of blood-island formation and vasculogenesis in Flk-1-deficient mice.* Nature, 1995. **376**(6535): p. 62-6.

102. Raab, S., et al., *Impaired brain angiogenesis and neuronal apoptosis induced by conditional homozygous inactivation of vascular endothelial growth factor.* Thromb Haemost, 2004. **91**(3): p. 595-605.

103. Haigh, J.J., et al., *Cortical and retinal defects caused by dosage-dependent reductions in VEGF-A paracrine signaling.* Dev Biol, 2003. **262**(2): p. 225-41.

104. Cadigan, K.M. and R. Nusse, *Wnt signaling: a common theme in animal development.* Genes Dev, 1997. **11**(24): p. 3286-305.

105. Lustig, B. and J. Behrens, *The Wnt signaling pathway and its role in tumor development.* J Cancer Res Clin Oncol, 2003. **129**(4): p. 199-221.

106. Liu, T., et al., *G protein signaling from activated rat frizzled-1 to the beta-catenin-Lef-Tcf pathway.* Science, 2001. **292**(5522): p. 1718-22.

107. Malbon, C.C., H. Wang, and R.T. Moon, *Wnt signaling and heterotrimeric G-proteins: strange bedfellows or a classic romance?* Biochem Biophys Res Commun, 2001. **287**(3): p. 589-93.

108. Mao, J., et al., *Low-density lipoprotein receptor-related protein-5 binds to Axin and regulates the canonical Wnt signaling pathway.* Mol Cell, 2001. **7**(4): p. 801-9.

109. Tamai, K., et al., *LDL-receptor-related proteins in Wnt signal transduction.* Nature, 2000. **407**(6803): p. 530-5.

110. Wehrli, M., et al., *arrow encodes an LDL-receptor-related protein essential for Wingless signalling.* Nature, 2000. **407**(6803): p. 527-30.

111. Mao, B., et al., *LDL-receptor-related protein 6 is a receptor for Dickkopf proteins.* Nature, 2001. **411**(6835): p. 321-5.

112. Miller, J.R., *The Wnts.* Genome Biol, 2002. **3**(1): p. REVIEWS3001.

113. Rao, T.P. and M. Kuhl, *An updated overview on Wnt signaling pathways: a prelude for more.* Circ Res, 2010. **106**(12): p. 1798-806.

114. Liu, C., et al., *Control of beta-catenin phosphorylation/degradation by a dual-kinase mechanism.* Cell, 2002. **108**(6): p. 837-47.

115. Griffiths-Jones, S., et al., *miRBase: microRNA sequences, targets and gene nomenclature.* Nucleic Acids Res, 2006. **34**(Database issue): p. D140-4.

116. Reis, M., et al., *Endothelial Wnt/beta-catenin signaling inhibits glioma angiogenesis and normalizes tumor blood vessels by inducing PDGF-B expression.* J Exp Med, 2012. **209**(9): p. 1611-27.

117. Abuharbeid, S., F. Czubayko, and A. Aigner, *The fibroblast growth factor-binding protein FGF-BP.* Int J Biochem Cell Biol, 2006. **38**(9): p. 1463-8.

118. Aigner, A., et al., *An FGF-binding protein (FGF-BP) exerts its biological function by parallel paracrine stimulation of tumor cell and endothelial cell proliferation through FGF-2 release.* Int J Cancer, 2001. **92**(4): p. 510-7.

119. Wu, D.Q., et al., *Characterization and molecular cloning of a putative binding protein for heparin-binding growth factors.* J Biol Chem, 1991. **266**(25): p. 16778-85.

120. Kurtz, A., et al., *Expression of a binding protein for FGF is associated with epithelial development and skin carcinogenesis.* Oncogene, 1997. **14**(22): p. 2671-81.

121. Lametsch, R., et al., *Structural characterization of the fibroblast growth factor-binding protein purified from bovine prepartum mammary gland secretion.* J Biol Chem, 2000. **275**(26): p. 19469-74.

122. Wang, X.C., et al., *Purification of heparin-binding protein HBp17 and identification of HBp17 heparin binding site.* Biochem Mol Biol Int, 1998. **46**(1): p. 81-7.

123. Mongiat, M., et al., *Fibroblast growth factor-binding protein is a novel partner for perlecan protein core.* J Biol Chem, 2001. **276**(13): p. 10263-71.

124. Xie, B., et al., *Identification of the fibroblast growth factor (FGF)-interacting domain in a secreted FGF-binding protein by phage display.* J Biol Chem, 2006. **281**(2): p. 1137-44.

125. Aigner, A., et al., *Immunolocalization of an FGF-binding protein reveals a widespread expression pattern during different stages of mouse embryo development.* Histochem Cell Biol, 2002. **117**(1): p. 1-11.

126. Czubayko, F., et al., *Tumor growth and angiogenesis induced by a secreted binding protein for fibroblast growth factors.* J Biol Chem, 1994. **269**(45): p. 28243-8.

127. Kagan, B.L., et al., *Complex regulation of the fibroblast growth factor-binding protein in MDA- MB-468 breast cancer cells by CCAAT/enhancer-binding protein beta.* Cancer Res, 2003. **63**(7): p. 1696-705.

128. Czubayko, F., et al., *A secreted FGF-binding protein can serve as the angiogenic switch in human cancer.* Nat Med, 1997. **3**(10): p. 1137-40.

129. Aigner, A., et al., *Ribozyme-targeting of a secreted FGF-binding protein (FGF-BP) inhibits proliferation of prostate cancer cells in vitro and in vivo.* Oncogene, 2002. **21**(37): p. 5733-42.

130. Tassi, E., et al., *Enhancement of fibroblast growth factor (FGF) activity by an FGF-binding protein.* J Biol Chem, 2001. **276**(43): p. 40247-53.

131. Gibby, K.A., et al., *A distinct role for secreted fibroblast growth factor-binding proteins in development.* Proc Natl Acad Sci U S A, 2009. **106**(21): p. 8585-90.

132. Corada, M., et al., *The Wnt/beta-catenin pathway modulates vascular remodeling and specification by upregulating Dll4/Notch signaling.* Dev Cell, 2010. **18**(6): p. 938-49.

133. Soriano, P., *Generalized lacZ expression with the ROSA26 Cre reporter strain.* Nat Genet, 1999. **21**(1): p. 70-1.

134. Harada, N., et al., *Intestinal polyposis in mice with a dominant stable mutation of the beta-catenin gene.* EMBO J, 1999. **18**(21): p. 5931-42.

135. Maretto, S., et al., *Mapping Wnt/beta-catenin signaling during mouse development and in colorectal tumors.* Proc Natl Acad Sci U S A, 2003. **100**(6): p. 3299-304.

136. Calabria, A.R., et al., *Puromycin-purified rat brain microvascular endothelial cell cultures exhibit improved barrier properties in response to glucocorticoid induction.* J Neurochem, 2006. **97**(4): p. 922-33.

137. Liebner, S., et al., *Correlation of tight junction morphology with the expression of tight junction proteins in blood-brain barrier endothelial cells.* Eur J Cell Biol, 2000. **79**(10): p. 707-17.

138. Santoro, M.M., G. Pesce, and D.Y. Stainier, *Characterization of vascular mural cells during zebrafish development.* Mech Dev, 2009. **126**(8-9): p. 638-49.

139. Zhou, Y., et al., *Canonical WNT signaling components in vascular development and barrier formation.* J Clin Invest, 2014. **124**(9): p. 3825-46.

140. Engelhardt, B., *Development of the blood-brain barrier.* Cell Tissue Res, 2003. **314**(1): p. 119-29.

141. Alvarez, J.I., R. Cayrol, and A. Prat, *Disruption of central nervous system barriers in multiple sclerosis.* Biochim Biophys Acta, 2011. **1812**(2): p. 252-64.

142. Sandoval, K.E. and K.A. Witt, *Blood-brain barrier tight junction permeability and ischemic stroke.* Neurobiol Dis, 2008. **32**(2): p. 200-19.

143. Zlokovic, B.V., *The blood-brain barrier in health and chronic neurodegenerative disorders.* Neuron, 2008. **57**(2): p. 178-201.

144. Gore, A.V., et al., *Vascular development in the zebrafish.* Cold Spring Harb Perspect Med, 2012. **2**(5): p. a006684.

145. Habeck, H., et al., *Analysis of a zebrafish VEGF receptor mutant reveals specific disruption of angiogenesis.* Curr Biol, 2002. **12**(16): p. 1405-12.

146. Covassin, L.D., et al., *Distinct genetic interactions between multiple Vegf receptors are required for development of different blood vessel types in zebrafish.* Proc Natl Acad Sci U S A, 2006. **103**(17): p. 6554-9.

147. Lawson, N.D., et al., *phospholipase C gamma-1 is required downstream of vascular endothelial growth factor during arterial development.* Genes Dev, 2003. **17**(11): p. 1346-51.

148. Pham, V.N., et al., *Combinatorial function of ETS transcription factors in the developing vasculature.* Dev Biol, 2007. **303**(2): p. 772-83.

149. Montero-Balaguer, M., et al., *Stable vascular connections and remodeling require full expression of VE-cadherin in zebrafish embryos.* PLoS One, 2009. **4**(6): p. e5772.

150. Fleming, A., H. Diekmann, and P. Goldsmith, *Functional characterisation of the maturation of the blood-brain barrier in larval zebrafish.* PLoS One, 2013. **8**(10): p. e77548.

151. Whitesell, T.R., et al., *An alpha-smooth muscle actin (acta2/alphasma) zebrafish transgenic line marking vascular mural cells and visceral smooth muscle cells.* PLoS One, 2014. **9**(3): p. e90590.

152. Bundgaard, M. and H. Cserr, *A glial blood-brain barrier in elasmobranchs.* Brain Res, 1981. **226**(1-2): p. 61-73.

153. Bundgaard, M. and N.J. Abbott, *All vertebrates started out with a glial blood-brain barrier 4-500 million years ago.* Glia, 2008. **56**(7): p. 699-708.

154. Bronger, H., et al., *ABCC drug efflux pumps and organic anion uptake transporters in human gliomas and the blood-tumor barrier.* Cancer Res, 2005. **65**(24): p. 11419-28.

155. Marroni, M., et al., *Vascular and parenchymal mechanisms in multiple drug resistance: a lesson from human epilepsy.* Curr Drug Targets, 2003. **4**(4): p. 297-304.

156. You, W.K., et al., *NG2 proteoglycan promotes tumor vascularization via integrin-dependent effects on pericyte function.* Angiogenesis, 2014. **17**(1): p. 61-76.

157. del Toro, R., et al., *Identification and functional analysis of endothelial tip cell-enriched genes.* Blood, 2010. **116**(19): p. 4025-33.

158. Gunda, B., et al., *COL4A2 mutation causing adult onset recurrent intracerebral hemorrhage and leukoencephalopathy.* J Neurol, 2014. **261**(3): p. 500-3.

159. Gould, D.B., et al., *Role of COL4A1 in small-vessel disease and hemorrhagic stroke.* N Engl J Med, 2006. **354**(14): p. 1489-96.

160. Hoppman, N., et al., *A common variant in fibroblast growth factor binding protein 1 (FGFBP1) is associated with bone mineral density and influences gene expression in vitro.* Bone, 2010. **47**(2): p. 272-80.

161. Tomaszewski, M., et al., *Pathway analysis shows association between FGFBP1 and hypertension.* J Am Soc Nephrol, 2011. **22**(5): p. 947-55.

162. Hudson, N., et al., *Differential apicobasal VEGF signaling at vascular blood-neural barriers.* Dev Cell, 2014. **30**(5): p. 541-52.

163. Jarajapu, Y.P., et al., *Protection of blood retinal barrier and systemic vasculature by insulin-like growth factor binding protein-3.* PLoS One, 2012. **7**(7): p. e39398.

164. Shin, J.W., R. Huggenberger, and M. Detmar, *Transcriptional profiling of VEGF-A and VEGF-C target genes in lymphatic endothelium reveals endothelial-specific molecule-1 as a novel mediator of lymphangiogenesis.* Blood, 2008. **112**(6): p. 2318-26.

ACKNOWLEDGEMENTS

Fifty candidates are waiting for the results of their PhD selection while I'm writing this acknowledgements, and this makes me feel quite nostalgic: four strange, intense, tough, joyful years have passed since I was a PhD candidate, too. I would like to be able to find the right words to describe this experience and to give the right merit to all the people that happened to cross my path and somehow change it, but I will use someone else's words, instead, since they managed to give voice to most of my feelings during this adventure.

"Luck is truly where preparation meets opportunity". Many people told me I was lucky to get this position, but the truth is that I would not have been so lucky if my boss, Elisabetta Dejana, had not decided to give me this opportunity, believing in me since the very beginning. Good mentors are those who stay passionate about their job and make you feel passionate too, and I have no doubt that she was the best mentor I could have found.

"Experience is what you get when you didn't get what you wanted". Thanks to all the people that helped and supported me, especially when the experiments didn't give us what we wanted: my PhD advisors, Lydia Sorokin and Giuliana Pelicci, for their many suggestions; Gianluca Deflorian e Federica Pezzimenti for teaching me all they could about zebrafish; Alexandre Mironov and Galina Beznusenko for their support with the electron microscopy; Matteo, Monica and Ganesh for their precious help and useful discussion. A special "thank you" to Maria Grazia

Lampugnani for following me in every step of this project, for listening to my ideas and sharing hers and for being always an excellent guide and advisor.

"Wait long enough and people will surprise and impress you." Thanks to all the present and past members of our team: all of them shared with me a piece of their life and filled me with precious memories worth telling to my grandchildren-to-be. Thanks especially to Luca for having turned from a labmate to a good friend.

"The brick walls are there for a reason. The brick walls are not there to keep us out; the brick walls are there to give us a chance to show how badly we want something. The brick walls are there to stop the people who don't want it badly enough." Thanks to all the people that constantly reminded me what's on the other side of my brick walls: to my friends Marina, Nunzia and Caterina for their comforting smiles, helping hands and long chatters; to "Pro-Test Italia" team for believing in me more than I do; to Seb because, although he has seen the best and the worst of me, he has decided to spend the rest of his life "walking beside me" anyway; to my amazing family because, besides fighting all my battles enthusiastically, they keep encouraging my dreams and ambitions, no matter how far they will take me. And thanks for all the people that, during my life, have tried and will try again to discourage me: they keep giving me the strength to kick all my brick walls, because after four years I "want it badly" more than ever!